Investigation of Tensile Strength of Carbon Fabric-Reinforced Cementitious Matrix (FRCM) at High Temperatures

Hamidreza Asgharigharakheili

A thesis submitted in partial fulfilment of the requirements for the
Master's degree in Applied Science

Department of Civil Engineering
Faculty of Engineering
University of Ottawa

ACKNOWLEDGEMENTS

First and foremost, I would like to express my special thanks of gratitude to my supervisors" Martin Noel and Hamzeh Hajiloo" for their help and support in pursuing my project. They guided me professionally and academically and let me be a part of their research team in a welcoming environment. The lessons I learned from my supervisors during my Master's degree broadened my knowledge and are worth much more than could be said. In addition, I had the opportunity to participate in two of Dr Noel's courses, and I enjoyed the simplicity and application of these courses. I was a TA for a course offered by Dr Noel, and it was a valuable experience for me to familiarize myself with the friendly environment of his class. Moreover, I thank Dr Hajiloo for keeping reviewing my thesis and enhancing my knowledge with scientific aspects of the research.

In addition, without lab supervisors' dedication and hard work, this project could have faced more challenges. Thanks to Muslim Majeed and Gamal Elnabelsya for their countless assistance regarding the experimental work, and their pieces of training were of great significance in the progress of this thesis.

Special thanks to a number of my co-researchers in the laboratory, including Aws Hasak, Issa Fowai, Seyed Alireza Alavi, Amir Sabziparvar. These fellow students helped me overcome the challenging conditions in the lab, and their help was of great importance.

I would also like to thank Dr Zkaria Omeman for his excellent help writing and organizing my thesis. He provided many comments and my supervisors to improve the quality of this research.

I also would like to thank senior administrative officer "Luc Cloutier " for his help in my Master' program. His assistance in providing me with two teaching assistants and my Master'degree is greatly appreciated.

Last but not least, I would like to express my sincere thanks to my family and my friends, including Mohanna Babazadeh, Mohammad Shojaei, Daniel Khadivar, Mostafa Sorkhi, Mobin Babazadeh, and Nariman Abyar for supporting me unconditionally to achieve this priceless goal.

ABSTRACT

Maintenance and rehabilitation of existing masonry and reinforced concrete structures are of great importance in the field of civil engineering. Due to deterioration and severe environment, numerous structures fail to meet functional or safety requirements, and as a result, they should be strengthened. Several methods have been utilized to repair the structures, including steel plate bonding, cable post-tensioning, and section enlargement. However, these methods bring disadvantages, such as significant added dead load and high labour cost. Therefore, externally bonding with composite materials has attracted considerable attention recently.

Externally bonded fibre-reinforced polymer (FRP) sheets have been widely used to strengthen reinforced concrete and masonry structures. FRP has been a common method to provide a higher service life for structures for several decades. However, strengthening structural members with FRP introduces certain drawbacks, such as their poor performance in fire scenarios caused by the rapid softening of the polymer-based resin. An alternative strengthening system known as a fabric-reinforced cementitious matrix (FRCM) has been developed to address this issue by replacing resin-based material with an inorganic cementitious-based matrix. Nonetheless, the performance of FRCM at high temperatures has not been investigated sufficiently so far. Hence, this research focused on the mechanical behaviour of FRCM at high temperatures.

This experimental research investigates the tensile performance of carbon FRCM at high temperatures. First, the temperature distribution within the specimens during heating was studied using nine specimens with one, two, or three layers to reveal the required time for the inner fabric to reach a steady temperature. Then, the tension and stiffness degradation of FRCM coupons were studied at different temperatures. A total of 84 FRCM coupons were fabricated and tested in tension; 60 of the tests were conducted at steady-state conditions in which temperature was held constant and load increased, and 24 specimens were carried out in transient-state tests, in which load was constant, and temperature grew. In order to provide a more comprehensive knowledge concerning the FRCM composite, some key variables were included in this research. These parameters are the number of layers (1, 2, 3) leading to different thicknesses (20, 30, 40 mm), the orientation of the fabric layer (unidirectional and bidirectional), target temperature (ambient, 100, 200, 300, 400°C), and heating condition (steady-state, transient state). These tests aimed to reveal the primary mechanical characteristics such as ultimate strength and cracked elastic modulus at different temperatures and compare them with control specimens tested at room temperature.

With the increase in the number of fabric grids from one to two and three, the stress at failure decreased by about 11 and 18%, respectively. With regards to cracked elastic modulus two and three-layered specimens showed 18 and 20% reduction in value. It is also noteworthy to mention that overall load capacity of specimens rose with the increase in number of layers; however, due to the more significant increase in area, the stress was reduced. The same decreases in the cracked elastic modulus and ultimate strength were observed as the target temperature

increased. Increasing the temperature to 400°C led to a decrease in ultimate strength and cracked elastic modulus of approximately 60 to 70%. Furthermore, the bidirectional specimens showed a better behaviour than unidirectional specimens in terms of ultimate strength; however, their cracked elastic moduli were almost the same. With regards to the transient-state tests, as the material became thicker, the failure temperature increased considerably. For instance, a 20-mm specimen failed at 467°C with a 20% sustained load, while a 30-mm specimen failed at 558°C. Another vital parameter studied in transient-state tests was the decrease in temperature with the increase in sustained load. An example of this is the 20-mm specimens which failed at 352 and 258°C, while they were preloaded to 40 and 60% of their capacities. The conclusions of this study suggest that FRCM materials do retain a non-negligible strength capacity at high temperatures. However, further investigations to reveal FRCM bond behaviour and retrofitted structural members at high temperatures are still required to provide comprehensive knowledge.

Keywords: Fabric-Reinforced-Cementitious Matrix, Tensile strength, Elastic modulus, Mechanical properties, Steady-state, Transient-state, Elevated temperature.

NOTATIONS

Symbols	Definition
A_f	Fabric area (mm^2)
A_{gross}	Gross area of FRCM section (mm^2)
E_f	Cracked modulus of elasticity (MPa)
N	Number of fabric layers
T_g	Glass transition temperature (°C)
f_{fu}	Ultimate tensile stress (MPa)
ε_{fu}	Ultimate tensile strain (mm/mm)
ρ_f	Reinforcement ratio (%)

ACRONYMS

Acronym	Definition
ACI	American Concrete Institute
ACIC	Advanced Composites in Construction
ASTM	American Society for Testing and Materials
ARTBA	American Road and Transportation Builders Association
CFRP	Carbon Fibre Reinforced Polymer
DIC	Digital Image Correlation
FRCM	Fabric Reinforced Cementitious Matrix
FRP	Fibre Reinforced Polymer
HPM	High-Performance Mortar
LVDT	Linear Variable Displacement Transducer
PBO	Phenylene Benzo-Bisoxazole
RC	Reinforced Concrete
TRC	Textile Reinforced Concrete
TRM	Textile Reinforced Mortar

List of Content

List of Figures

List of Tables

1 INTRODUCTION

1.1 General

The number of structures that require strengthening is growing worldwide due to several reasons, including deterioration of materials and changes in loading. According to ARTBA (American Road and Transportation Builders Association, 2020), more than 220,000 bridges in the US are functionally deficient and are considered to be in poor condition. In order to rehabilitate these bridges or replace them, $41.8 billion is needed.

Rehabilitation is a term used to describe both strengthening and repair of structures. Strengthening can be defined as a process that increases the capacity of the existing structure. Repair is a word commonly used to describe retrofits aiming to restore the original capacity.

In the past few decades, conventional rehabilitation techniques included adding new mortar mix, replacing corroded steel reinforcement, increasing sectional area, applying steel plates, etc. However, there are several disadvantages associated with these conventional techniques, such as corrosion of steel plates, as well as cost and difficulty in handling and installation, which have resulted in the widespread use of advanced composite materials for strengthening. Recently, upgrading existing concrete and masonry structures with composite materials has gained significant popularity. Composite materials, e.g., fibre-reinforced polymers (FRPs), possess favourable properties, including high strength fibres, ease of installation, and corrosion resistance. Numerous researchers have conducted studies to reveal the FRP effect in strengthening masonry and concrete structures (Bisby et al. 2013; Cerniauskas et al. 2016; Dong et al. 2013; Donnini et al. 2019b; Raoof and Bournas 2017b; Tetta and Bournas 2016; Trapko 2013). Although FRP composites can effectively increase the structures' capacity, it bears a few disadvantages, such as poor performance at elevated temperature and incompatibility with wet surfaces, both of which are mainly due to the polymer-based adhesive (Bisby et al., 2013; Raoof and Bournas 2017a; b; Spagnuolo et al. 2018a). Hence, researchers have started conducting studies on another type of composite called fabric-reinforced cementitious matrices (FRCM) (Bisby et al. 2013; Carozzi et al. 2017a) fabricated using an inorganic matrix instead of resins such as epoxy.

Similarly to FRP, FRCM systems are externally bonded to the surface of different structural members (beams, columns, walls, slabs) for capacity enhancement, as shown in Figure 1-1. The wet matrix is typically sprayed by shotcrete; however, it can also be applied to the substrate by hand troweling. FRCM composites overcome a few drawbacks related to FRPs. They are generally thought to exhibit better resistance at elevated temperatures, be more compatible with wet surfaces than FRP, and be easier to handle. Nevertheless, there is a lack of research conducted

by previous researchers to quantify their performance at high temperatures for use in design and structural evaluation.

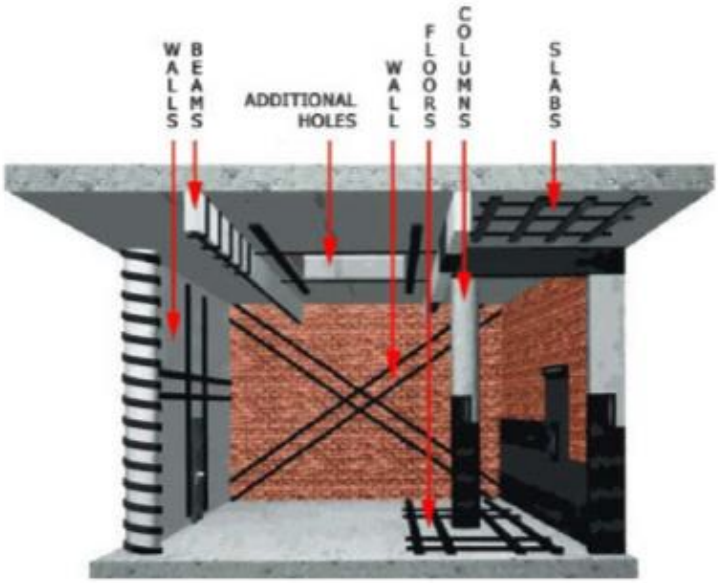

Figure 1-1: Different members strengthened by FRP or FRCM (Jung 2020a).

1.2 Objectives and Scope

The main objective of this study is to evaluate the tensile performance of carbon FRCM composites at high temperatures to contribute toward the current lack of quantitative data needed to develop practical design guidelines. In order to achieve this objective, this thesis covers the following scope:

1. Nine heating tests were conducted in order to achieve the critical findings of internal and external temperature distributions. Moreover, these tests helped identify a proper testing protocol in which the inner fabric was thoroughly exposed to the fire-simulated condition.

2. Eighty-four carbon FRCM tensile coupons were tested at elevated temperatures of up to 400°C (steady-state) and 500°C (transient state) using clevis-type grips. The effect of temperature, fabric type, number of layers, and cover thickness on ultimate tensile strength and cracked section modulus was considered.

3. Based on an analysis of the experimental results, preliminary design recommendations are provided for the carbon FRCM system considered in this study.

1.3 Thesis organization

This thesis is divided into eight chapters:

Chapter 1 - Introduction:

This section provides the overall scope of this research.

Chapter 2 - Literature review:

This chapter includes an extensive review of relevant studies related to FRCM material and its application, as well as available research on their performance at elevated temperatures.

Chapter 3 - Experimental program:

This chapter describes the entire procedure of fabricating and manufacturing the specimens and the main properties of the material tested. The various test setups and procedures used in this study are also described.

Chapter 4 - Experimental results:

The main results achieved by the investigation are presented in this chapter, including graphs and calculations. A detailed discussion is provided to interpret the findings.

Chapter 5 - Discussion:

In this chapter, an overall discussion of the main findings of this study and implications in the design and application of strengthening is discussed.

Chapter 6 - Conclusions:

This chapter includes a summary of the experimental results as the central part of the research, as well as their implications for design.

Chapter 7 – Recommendations for future work:

This chapter suggests some ideas that are worth investigating for future researchers.

Chapter 8 - References:

This chapter lists the academic and industrial references that helped acquire the information.

2 LITERATURE REVIEW

This chapter reviews studies and research that provide background information associated with FRCM, FRP, and their tensile, shear, and axial strengthening applications in various conditions. Existing studies on the performance of these strengthening systems at high temperatures are also discussed.

2.1 Constituents of the FRCM composite

The two main components of FRCM are the fabric grid and the cement-based matrix. Other names have also been used in the literature to refer to this system, including textile reinforced mortar (TRM) (Caggegi et al. 2017b; Maroudas and Papanicolaou 2017; Raoof and Bournas 2017a; Tetta and Bournas 2016) and textile reinforced concrete (TRC) (Larbi et al. 2010). The fabric mesh provides strength to the composite and additional resistance to the member. The cementitious matrix is typically applied with shotcrete or troweled by hand to fill the gaps between the fibres and achieve desirable strength, transfer loads between fibres and the concrete substrate, and provide structural integrity.

2.1.1 Fabric

FRCM and steel-reinforced grout (SRG) are textile materials used to reinforce the composite and carry the load. Due to the recent developments in textile engineering, the use of two and three-directional textiles have been achieved in various research studies. The fibres are assembled by weaving, knitting, and tufting, and each strand is made of thousands of fibres, as shown in Figure 2-1. The fabric is mainly divided into two groups: artificial and natural fabric. The synthetic fabric material is fabricated from carbon (the most common fabric), glass, Phenylene benzo-bisoxazole (PBO), basalt, aramid, or steel with nylon fibres as a supporting mesh, as shown in Figure 2-2. However, fabric yarns could also be made from natural materials such as sisal, jute, hemp, flax, as displayed in Figure 2-3. The fibres are usually dry (i.e., not impregnated by a resin-based material); however, this leads to a limited bond adhesion between the mortar and the fibres at the mortar interface (Donnini et al. 2017; Donnini and Corinaldesi 2017a). Therefore, fibres are sometimes partially coated with epoxy resin to improve the bonding strength. The fabrics can be designed to resist loads in either one or two orthogonal directions (Figure 2-4).

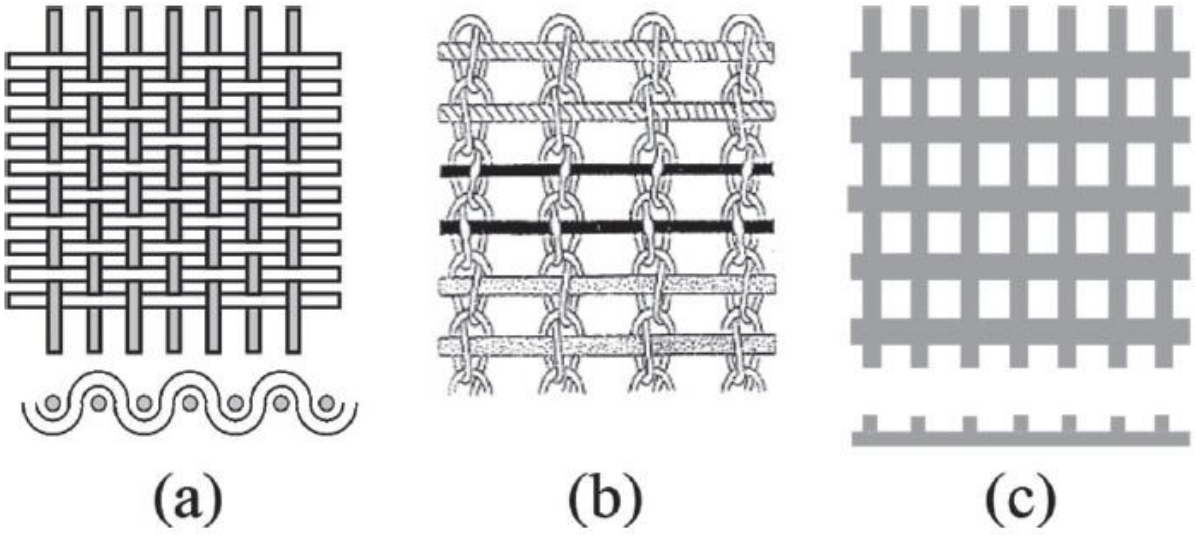

Figure 2-1: Types of fabric assembly: a) woven, b) knitted, c) bonded. (ACI 549.R-20).

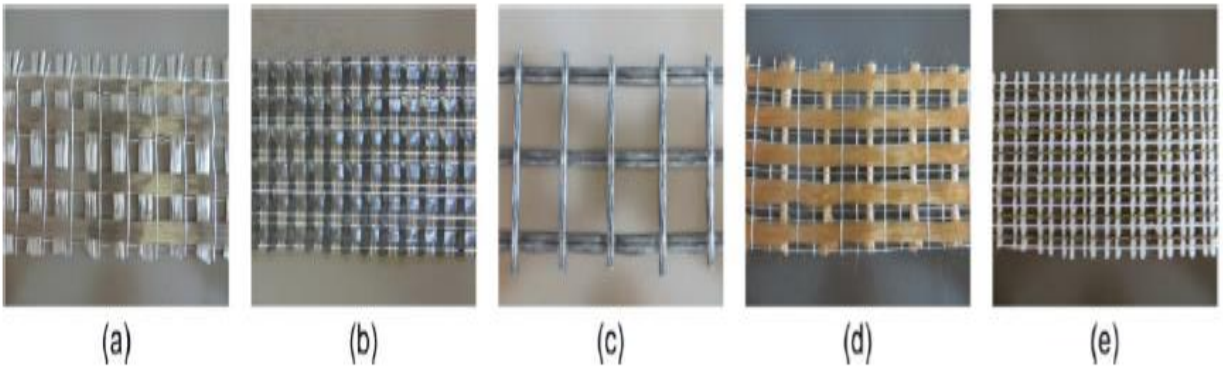

Figure 2-2: Types of fibres fabricated artificially: a) basalt, b) carbon c) glass d) PBO e) steel (Escrig et al. 2017).

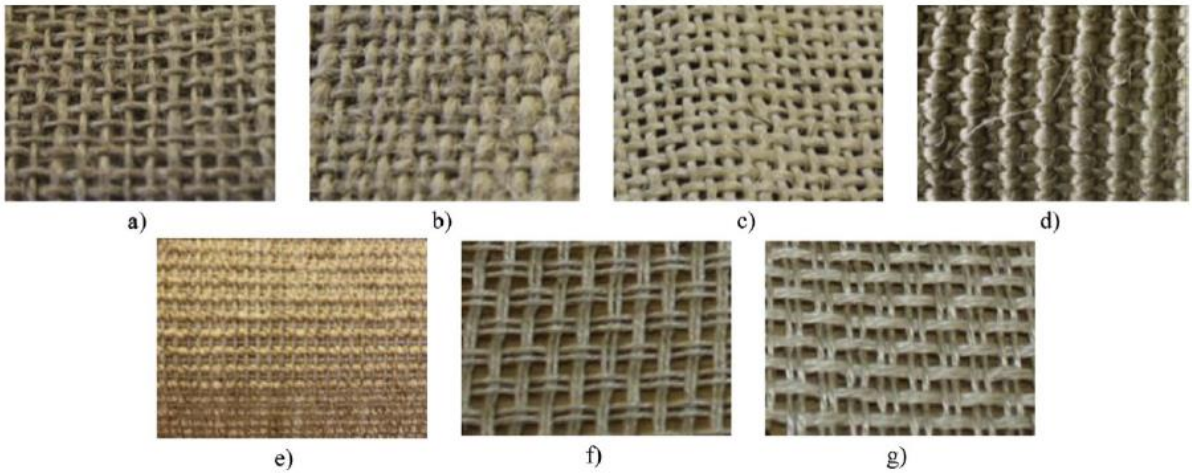

Figure 2-3: Fabrics made of natural materials: a-c) jute, d,e) sisal, f) hemp, g) flax (Codispoti et al. 2015).

Figure 2-4: Unidirectional and bidirectional carbon grid (Simpson, 2020).

Each type of material introduces various mechanical characteristics, typically evaluated in a tensile test. Table 2-1 shows the general mechanical properties of different fabric materials. PBO-FRCM is a material that primarily provides significant ultimate strength and Young's modulus, followed by carbon FRCM systems. However, glass FRCM generally has a lower resistance capacity and elastic modulus. Regardless of the material type, the mechanical properties of FRCM are heavily influenced by different fabric configurations, including geometry (Peled 2007; Peled et al. 1998; Peled and Bentur 2000).

Table 2-1: Mechanical properties for different fibre materials (Jabr et al. 2017).

Type of fabric	Young's Modulus (GPa)	Ultimate Tensile Strength (MPa)	Ultimate Tensile Strain (mm/mm)	Density ($g/cm^{3)}$)	Fibre Area, A_f (mm^2/mm)	Equivalent Thickness (mm)
Glass	80	2600	0.0345	2.6	0.0475	0.023
PBO	270	5800	0.0215	1.56	0.05	0.046
Carbon	240	4800	0.018	1.82	0.05	0.047

2.1.2 Cementitious matrix

The cementitious matrix is the second major component that provides confinement for fabric. It is commonly comprised of a cement or lime-based grout with a low dosage of dry organic polymers. Cement-based mortars are typically used to rehabilitate concrete structures, while lime-based mortars are used for masonry repair. The purpose of using a low dosage of dry polymers in cement (5% of the weight of cement) is that workability and ductility are enhanced (ACI 549.4R-20). Compared to other significant parameters determining the mechanical features of FRCM, such as the fabric type and the number of layers, the cementitious matrix has not been extensively investigated. However, in this chapter, several studies are mentioned.

Donnini and Corinaldesi (2017a) studied the mechanical characteristics (stiffness and tensile strength) of FRCM with a lime-based and cement-based matrix. Specimens fabricated with cement-based material showed a better performance than those of lime-based materials.

Cascardi et al. (2018) conducted research in which different inorganic matrices were utilized to confine masonry columns. This study aimed at three types of matrices based on their compressive strength. The fabric used in this study was manufactured from glass material, and inorganic matrices were fabricated from 4 and 7 MPa lime-based mortar and 23 MPa cement-based mortar. The conclusion proved that masonry columns could be significantly improved by FRCM-strengthening when proper mortar is employed. Based on results, 4, 7, and 23 MPa mortars increased the ultimate strength of the columns by 6, 31, and 87% compared to control un-strengthened columns. This clearly highlighted the significant effect of well-prepared mortar on strengthening a structural member.

Figure 2-5 displays the cementitious matrix mixed with water that will be shot to the substrate. After placing the fabric, this material is applied with hand troweling or shotcrete to cover the fabric and provide the last layer.

Figure 2-5: Cementitious matrix (Simpson, 2020).

2.2 Tensile behaviour

One of the essential aspects of FRCM in design and application is its mechanical performance evaluated using direct tensile tests. These tests identify the behaviour of FRCM composites and reveal how they resist the load. As a result, this information is of significant interest to designers and researchers. Therefore, this section attempts to synthesize existing knowledge on the primary mechanical characteristics of FRCM composite systems.

2.2.1 Fabric type

Caggegi et al. (2017a) conducted tensile tests on PBO, basalt, and aramid- FRCM to identify their differences. The orientation of the PBO fibre was bidirectional, while, for aramid fibres, the orientation was unidirectional and quadriaxial in which the fibres were assembled diagonally (Figure 2-6). This experimental research revealed that the tensile behaviour of the FRCM composite is substantially affected by the fabric material. During the tensile tests, one main crack was initiated in PBO-FRCM specimens, while multiple cracks were observed in the basalt-FRCM tests. With regards to the stress-strain curves, in the case of coupons reinforced with PBO fibres, specimens showed a distinct un-cracked stage prior to cracking. The basalt-FRCM coupons resulted in a three-phase diagram in the uniaxial test, while the quadriaxial reinforcement illustrated a two-staged curve in the stress-strain graph. The failure mode is another important outcome in which materials performed differently. The common mode of failure for PBO-FRCM was the slippage of fabric within the surrounding matrix; however, aramid-FRCM coupons mainly failed due to the matrix detachment from fibres.

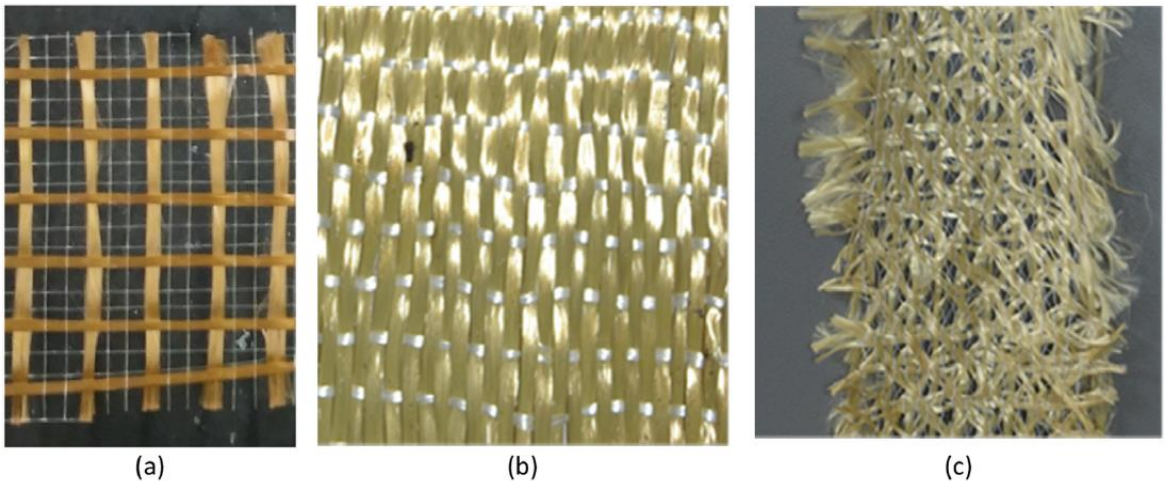

Figure 2-6: Assembly of different fibres, from left to right, PBO (bidirectional), aramid (unidirectional), aramid (quadriaxial) (Caggegi et al. 2017a).

Bellini et al. (2019b) utilized various materials for the fabric, including glass, basalt, aramid-glass, and carbon, to fabricate FRCM samples and reveal their performances in uniaxial tensile tests. In this research, six different specimen types were utilized depending on fibre impregnation level and spacing. The results demonstrate that the stress-strain curve of each type was affected by the fabric type and configuration. Carbon and basalt-FRCM coupons showed a trilinear behaviour in the stress-strain curve. On the other hand, specimens reinforced with glass fabric resulted in a bilinear stress-strain curve. The effect of fabric configuration and its orientation on mechanical performance was also identified by a similar study conducted by Bilotta et al. (2017b). This research employed coated bidirectional glass-FRCM and unidirectional SRG to evaluate their efficiency and stiffness. This study's conclusion stated that SRG resisted the load more effectively due to the lower spacing between the rows of fibres, with the efficiency of 65 and 63% with respect to nominal tensile stress for G-FRCM and SRG, respectively. Furthermore, in the second stage of the stress-strain curve after the first crack initiation, G-FRCM showed a more dramatic drop, while tension stiffening in SRG improved the behaviour.

Younis et al. (2017a) conducted research consisting of three types of fabric: PBO, carbon, and glass. Fifteen specimens of each type were fabricated to identify the performance and efficiency of FRCM based on different materials. Afterwards, the uniaxial testing machine was employed to test the coupons. According to the conclusions, the larger spacing between the fabric rows in G-FRCM led to a lower stiffness in the first stage. Regarding the failure mode, in carbon and PBO-FRCM, embedded fabric slipped within the matrix, while in G-FRCM, fabric rupture occurred, which was a brittle mode of failure. Moreover, in carbon and PBO-reinforced FRCM, more cracks initiated than with G-FRCM. The average peak tensile strengths of PBO, carbon, and glass-FRCM were 1235, 1178, and 767 MPa, respectively.

Carozzi and Poggi (2015) carried out tensile tests on FRCM fabricated from PBO, carbon, and glass fabric to characterize the mechanical behaviour of FRCM composite systems. The analyses showed that in most specimens a trilinear stress-strain curve occurred. In the first stage, both fabric and cementitious matrix resisted the load, followed by the initiation of the first crack, which led to the second stage. In the second stage, more cracks propagated, and the stiffness was reduced. Eventually, in the third stage, the load was resisted merely by fibres, and as a result, the slope of the stress-strain curve was approximately the same as the stiffness of the plain fabric. Furthermore, for all types of FRCM in this investigation, the first two stages in the stress-strain curve were similar; However, due to differences in the elastic modulus, more variabilities were observed in the third stage. The PBO-FRCM resisted the highest value of peak strength; however, considerable scatter in the data was observed. On the other hand, G-FRCM showed low mechanical properties as well as scatter in the data compared with its other counterparts.

Bilotta et al. (2017a) investigated the efficiency of various fabric materials, including steel mesh, pre-impregnated basalt, as well as pre-impregnated glass. Digital Image Correlation (DIC) was also utilized as an innovative non-contact measuring technique in this research. The analyses of the results demonstrated that in G-FRCM, few cracks developed due to the spacing between filaments. In contrast, in the case of tests conducted with B-FRCM and S-FRCM, more cracks were observed on the specimens. With regards to failure modes, B-FRCM coupons reached a higher value of ultimate strength because of the high bond between embedded fabric and cement. On the other hand, in S-FRCM, slippage of mesh within the matrix occurred and led to a misalignment of the cords in the behaviour. Last but not least, in coupons reinforced with glass fabric, a premature tensile failure happened due to the high spacing between bundles.

It is clear from previous studies that the performance of different FRCM systems can vary considerably depending on the constituent materials and manufacturing process, which makes it challenging to extract clear trends. Nevertheless, in general, FRCM composites made from either PBO or carbon fabrics have been shown to present excellent tensile properties for strengthening of structural members.

2.2.2 Number of layers

Wei et al. (2020) carried out uniaxial tensile tests to investigate the performance of FRCM as the number of fabric layers increases. In this research, coupons were fabricated with one, two, and four plied fabric layers. The results showed that as the number of layers increased, the energy absorption occurring from the formation of a crack also increased. Furthermore, two and four-layered coupons showed greater cracking strength than single-layered specimens. In one-layered specimens, drops in stiffness and strength were observed, while in multiple-layered coupons, trilinear behaviour in the stress-strain curve was illustrated. Concerning the typical failure mode experienced in this research, slippage of fibres within the matrix and premature fibre failure were noted in multiple and single-layered specimens, respectively.

D’Anna et al. (2021) conducted experimental research to identify the difference in performance and mechanical features of basalt-FRCM. In this paper, one, two, and three plies of the grid were used to compare the results and identify the effect of the number of layers. The stress-strain curves achieved from the tested specimens revealed that all specimens failed in a trilinear behaviour in the stress-strain diagram regardless of the number of layers. Moreover, the ultimate load and the number of cracks induced in specimens grew as the number of fabric layers increased. Nonetheless, the nominal stress declined due to the cement's higher cross-sectional area at multiple-layered samples. Regarding the failure mode of FRCM coupons, the rupture of fabric in the third stage was the common failure mode irrespective of the number of basalt grids.

2.2.3 Fibre orientation

Carozzi et al. (2017a) investigated carbon FRCM to evaluate differences in mechanical properties caused by various mesh configurations. In this research, six orientation systems were employed, and spacings from mid-fibre to mid-fibre were 30, 10, 17.5, 9.4, and 20 mm. The fabric with 10 mm spacing was manufactured in orthogonal and bidirectional orientation. In 10 mm spacing fabric, fibres were pre-impregnated prior to testing. The conclusions stated that coupons showed a trilinear behaviour in the stress-strain diagram for most types of configurations. However, this phenomenon was not observed in 10 mm bidirectional samples. It is noteworthy to mention that the standard failure mode was rupture of fabric within the cementitious matrix. Nonetheless, in several specimens, slippage of fibres within the matrix also occurred.

Donnini et al. (2019a) conducted an experimental study to identify G-FRCM composite systems' mechanical performance when the overlapping length was used. In this research, displacement was deeply measured with DIC technique. The coupon size in this study was 400 mm long, 70 mm wide, and 10 mm thick. The overlapping lengths in different configurations were 100, 150, and 200 mm. According to the results, in order to fully achieve the stress transfer between two layers of the grid, a minimum value of 150 mm overlapping length should be provided. Specimens reinforced with two layers with 150 and 200 mm overlapping length showed the same ultimate strength as the continuous fabric specimen; however, the material's stiffness was greatly improved. By contrast, 100 mm overlapped specimens showed a lower value of ultimate stress than one-layered specimens and most of the cracks developed at the overlapped region. With regards to the modes of failure, a few cracks were initiated in the continuous fabric specimens, and finally, specimens failed due to rupture of fabric. Conversely, fabric slippage within the matrix was the typical failure mode in overlapped specimens.

2.2.4 Stress-strain curve of FRCM

The typical tensile stress-strain curve of FRCM under the uniaxial tensile test is idealized in different distinct phases (Arboleda et al. 2016; Ascione et al. 2015; Jabr et al. 2017a; Wang et al. 2020; Younis et al. 2017). In Figure 2-7, a three-stage stress-strain curve is demonstrated as an idealized performance of the FRCM composite. The first phase indicates the pre-cracked state of

the composite with a resistance of both fibres and matrix. In this stage, the modulus of elasticity comprises the stiffness of fibres and matrix. The second phase forms when the first crack initiates, and the stiffness decreases significantly. Therefore, this will lead to more cracks developing, and the fabric carries the load at the crack location. The last phase of the curve is called the post-cracked region, where the existing cracks become more comprehensive up to the point where the final failure occurs. The final failures are caused either by slippage of fibres from the matrix or rupture of fibres. In this phase, only the fibres resist the load. Hence, the stiffness is equal to the stiffness of fibres. In other words, the slope of the curve is the same as the slope of fibres in uniaxial tension and E_3 of this phase is nearly equal to the modulus of elasticity of the bare fibres. Table 2-2 shows several mechanical characteristics of FRCM composite systems based on textile material. As exhibited, carbon provides a high value of stiffness as well as ultimate strength between different types of FRCM followed by basalt and glass.

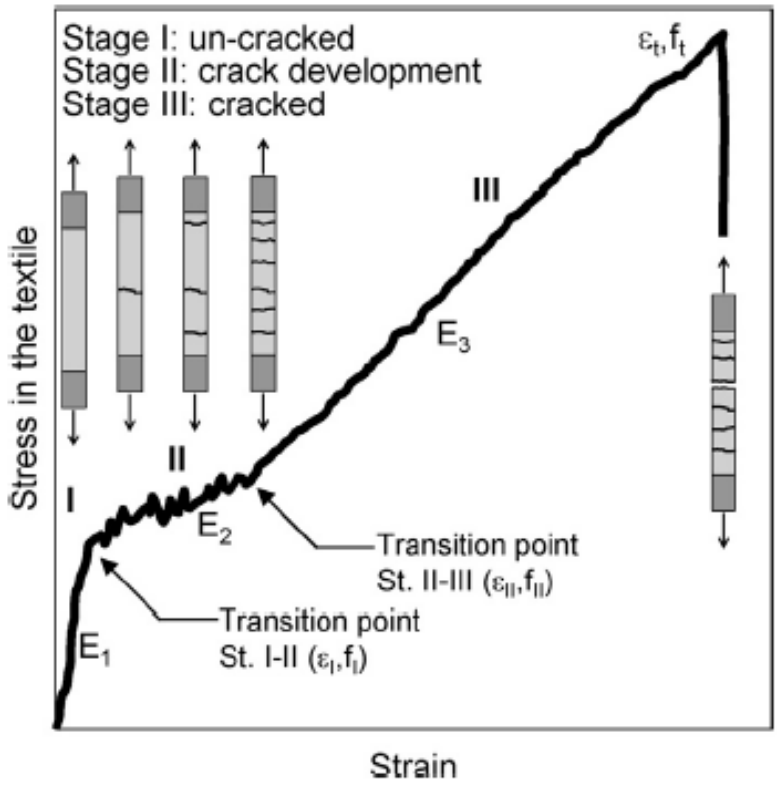

Figure 2-7: Tensile stress-strain curve of FRCM coupons (Ascione et al. 2015).

Table 2-2: Mechanical characteristics of different FRCM (Ismail et al. 2018b)

Fabric type	ρ_f[1] (g/m^2)	ρ_m[2] (g/cm^3)	A_f mm^2/m	f_u (MPa)	ε_u (%)	E_f (GPa)
Glass	435	2.5	174	603	2.7	67.8
Carbon	196	1.8	107	2241	2.0	211
Basalt	250	2.7	90.9	660	1.8	89.0

[1)]density of fabric in area.
[(2)]density of cementitious matrix in area.

2.2.5 ACI guidelines

There are currently no Canadian guidelines addressing the design of structures strengthened with FRCM. ACI 549.4R-20 contains information related to major mechanical properties of FRCM composites, including tensile strength, modulus of elasticity, and ultimate strain. These values are acquired according to the manufacturer's datasheet. ACI549.4R-20 simplifies FRCM tensile stress-strain graph as a two-phase curve (Figure 2-8). Some values to identify tensile properties are as follows:

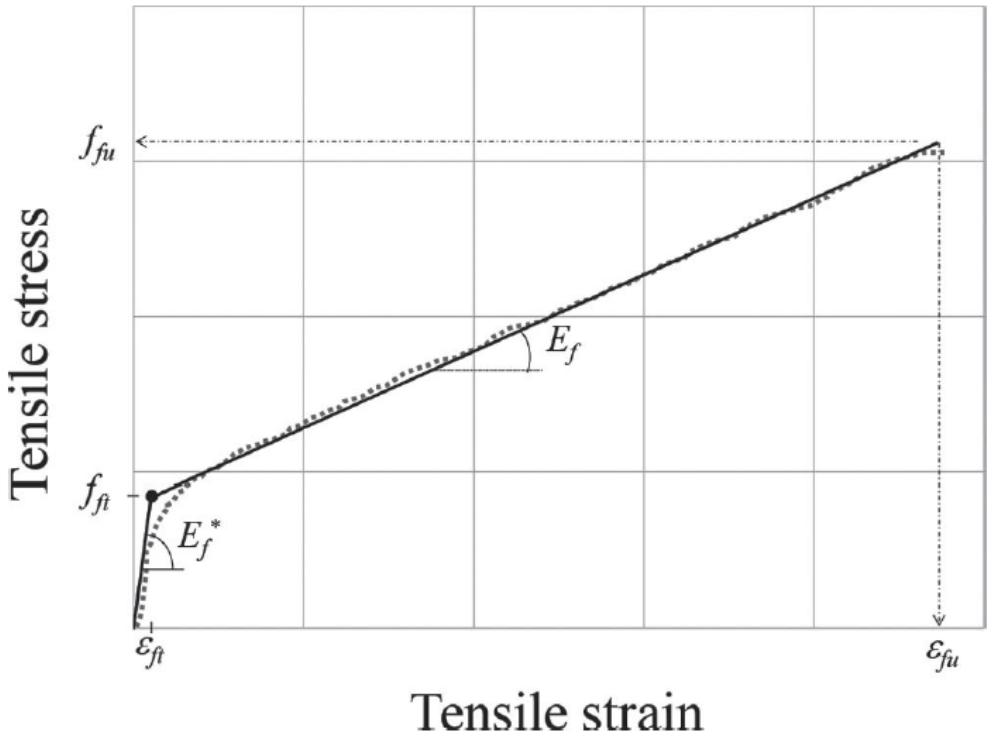

Figure 2-8: Idealized bilinear curve for FRCM for tensile test (Annex A of AC434).

- Tensile strain at transition point (ε_{ft})
- Ultimate tensile strain (ε_{fu})
- Tensile stress at transition point (f_{ft})
- Ultimate tensile stress (f_{fu})
- Modulus of elasticity at post-cracking stage (E_f)

In this curve, FRCM coupons start carrying the load, and both matrix and fabric resist the load. At the transition point, the first crack initiates, corresponding to tensile stress and strain at the transition point. In this stage, the fabric carries most of the load with a cracked modulus of elasticity. Figure 2-7 shows the graph obtained by conducting a tensile test on five FRCM coupons based on Annex A of AC434 guidelines. Two points are collected at 60 and 90% of the ultimate stress to calculate the modulus of elasticity. The equation to determine the cracked modulus of elasticity is as follows:

$$E_f = \Delta f/\Delta\varepsilon = (0.90f_{fu} - 0.60f_{fu})/ (0.90\varepsilon_{f@0.90f(fu)} - 0.60\ \varepsilon_{f@0.90f(fu)}) \qquad \textit{Equation 1}$$

In this chapter, guidelines and several studies are presented that prove the ability of FRCM to increase the flexural, shear, and axial capacities of structures. Moreover, mechanical properties of various materials such as carbon, aramid etc., durability, manufacturing are covered in this chapter. Table 2-3 demonstrates some design limitations for FRCM-retrofitted structural members.

Table 2-3: Design restriction (ACI 549.4R-20).

Parameters	Concrete		
	Flexure	Shear	Axial
ε_{fe} or ε_{fu}	Less than 0.012	Less than 0.004	Less than 0.012 and ε_{ccu} less than 0.01
Φ	0.9 to 0.65 based on ε_t	0.75	0.9 to 0.65 based on ε_t
f_{fs}/f_{fu}	0.2 ro 0.55 based on fibre	NA	NA
Allowable maximum enhancement	Per ACI 562	Per ACI 562	Per ACI 562

Table 2-4 shows some common mechanical characteristics of 150-mm long coupons under the tensile test. Two high-strength fabric type is mentioned in this table that contained high degree of stiffness as well as ultimate strength.

Table 2-4: Mechanical properties of PBO and Carbon-reinforced FRCM (ACI 549.4R-20).

FRCM property	Symbol	PBO-FRCM		Carbon-FRCM	
		Mean	STD	Mean	STD
Modulus of elasticity of the uncracked specimen, msi (GPa)	E_f^*	261 (1805)	65 (452)	74 (512)	19 (130)
Modulus of elasticity of the cracked specimen, msi (GPa)	E_f	18 (128)	2 (15)	12 (80)	3 (18)
Tensile stress corresponding to the transition point, ksi (MPa)	f_{ft}	54 (375)	12 (82)	66 (458)	7 (48)
Tensile strain corresponding to the transition point, %	ε_{ft}	0.0172	0.0044	0.1020	0.0449
Ultimate tensile strength, ksi (MPa)	f_{fu}	241 (1664)	11 (77)	150 (1031)	8 (54)
Ultimate tensile strain, %	ε_{fu}	1.7565	0.1338	1.0000	0.1405

2.2.6 Modes of failure

The types of failure modes in a direct tensile test depend on the level of impregnation of fabric and the type of gripping system. In Figure 2-9, four different failure modes that the FRCM composite may experience during the uniaxial tensile test are shown (Donnini and Corinaldesi 2017a; Truong et al. 2019; Younis et al. 2020). In failure mode A, the fabric near the gripping area ruptures, resulting in a significant drop in the resistance of the composite system. According to Truong et al. (2019), failure mode A results from transverse compression at the gripping area

combined with applied tension. Failure mode B is caused by fabric rupturing after the mortar cracks. Failure mode C indicates cementitious matrix cracking accompanied by fibre slippage within the surrounding fabric. This failure mode usually occurs when the bonding between the inner fabric and cement cannot hold the fabric. Failure mode D shows debonding failure between fibre and matrix. Ascione et al. (2015) conducted tensile and shear bond tests to identify mechanical features of externally bonded FRCM. In shear tests investigated by the researchers, different failure modes were discussed as shown in Figure 2-10.

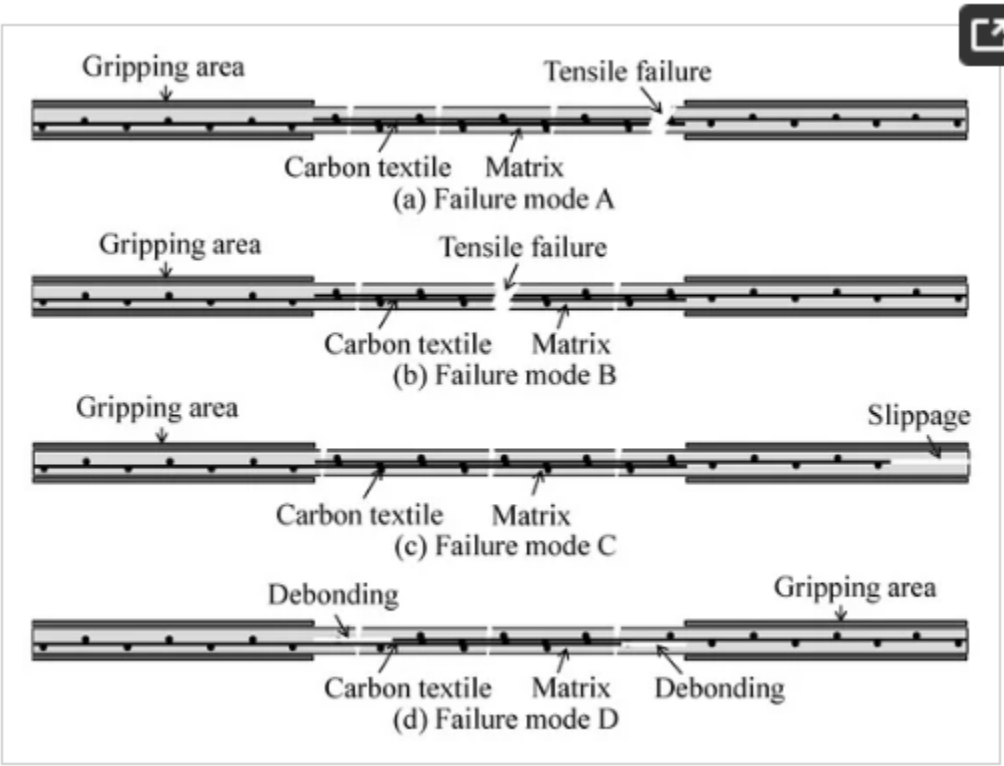

Figure 2-9: Failure modes of tensile test of FRCM coupons

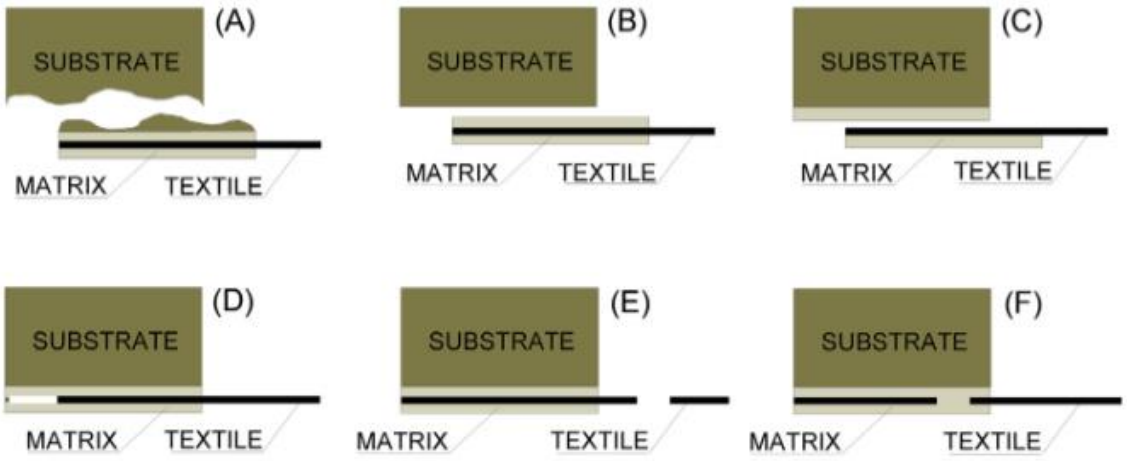

Figure 2-10: Probable failure modes in shear bond tests (A) debonding within substrate (B) debonding at interface of matrix and substrate (C) debonding at matrix and textile interface (D) slippage of matrix within surrounding matrix (E) rupture of textile in the bare fabric area (F) rupture of textile grid within matrix (Ascione et al. 2015).

2.2.7 Experimental test set-ups

Various test setups have been used for the uniaxial tensile test of FRCM composites. Rectangular FRCM specimens are generally tested using two methods (Arboleda et al. 2016) (Figure 2-10). The most common test in North America is the clevis grip method mentioned by ACI 549.4R-20. In the clevis grip method, the load is transferred to the coupon by adhesive tension and shear through FRP or steel tabs at the end of coupons. On the other hand, another type of test using clamping grips has also been used widely. In the clamping-grip method, the specimen is directly gripped by the tensile machine at the ends of the specimen with tabs to distribute the load and apply uniform normal stress. As a result, the chance of failure due to the cracking of the matrix is reduced. In Figure 2-11, FRCM coupons tested with clevis-method and clamping-method are displayed.

There are different types of instruments mentioned in the literature for measuring tensile strain, such as strain gauges, Linear Variable Differential Transformer (LVDT), extensometers and DIC (Bilotta et al. 2017a). Strain gauges come with a major drawback: providing strain measurement at one specific location (Pohoryles et al. 2017). On the other hand, LVDTs measure the average elongation of the specimen over a greater length. DIC is another measurement technique that provides a non-contact measurement to identify the strain and local cracks that are invisible to the naked eye.

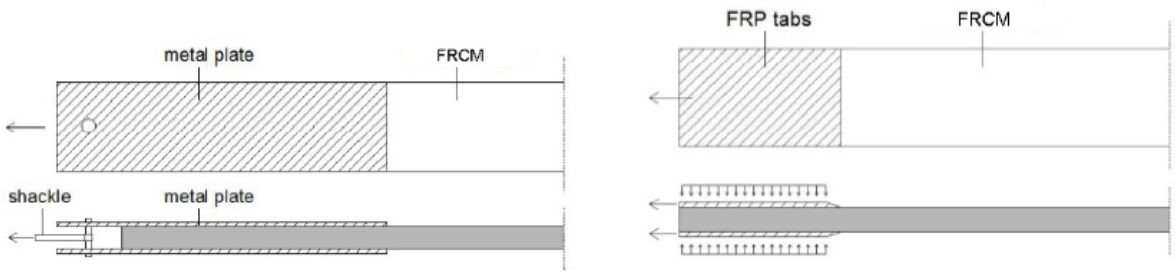

Figure 2-11: Clevis method (left) and clamping method (right) (Arboleda et al. 2016).

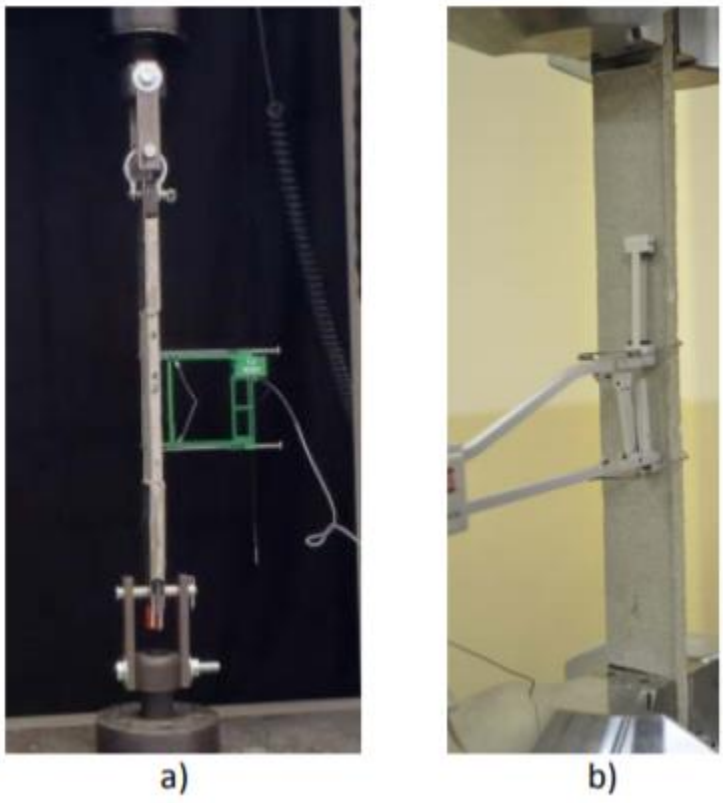

Figure 2-12: Different tensile test set-up: a) clevis grip method; b) clamping grip method (Arboleda et al. 2016).

2.3 Strengthening applications

This section briefly outlines a few of the many studies conducted by previous researchers on the application of FRCM composites for strengthening. FRCM composites could be used in various applications, including bending, shear, and axial capacity enhancement of various structural members. The studies presented below have been selected primarily to demonstrate the types of applications for which FRCM strengthening systems are typically used.

2.3.1 Flexural strengthening

Aljazaeri et al. (2019) used different anchorage systems to clarify their effectiveness with respect to the flexural capacity increase of RC beams. In this experimental research, PBO-FRCM was used in two and four layers to characterize their behaviour. The anchorage systems in this study consisted of glass spikes and U-wrapped anchors, and the conclusions stated that anchorage systems prevented debonding failure. Regarding the ultimate load of strengthened beams, the highest value belonged to the RC beam strengthened with four layers of PBO-FRCM and U-novel anchorage system. In some cases, anchorage systems did not affect the flexural capacity, however, they changed the mode of failure from debonding to slippage. Both glass spike and U-wrapped PBO strips were investigated, and the latter showed a better performance due to its tensile characteristics.

Feng et al. (2020a) carried out a bending test on carbon-FRCM reinforced corroded and uncorroded beams to demonstrate their flexural enhancement degree. They strengthened the beams in a U-shaped wrapping configuration and studied modes of failure, ultimate load capacities, and deflections. According to the results, the failure modes of strengthened beams combined different failure modes, including debonding of composite from the substrate, fibre slippage within the matrix, and fracture of the U-shaped wrapping system. The more layers of FRCM were employed, the higher level of the ultimate load and brittle behaviour was shown. Moreover, strengthened uncorroded beams resulted in a higher ductility than corroded beams.

Bisby et al. (2009) fabricated reinforced concrete beams to identify the flexural performance of beams strengthened with FRP and FRCM. In this study, beams were externally bonded with single layer unidirectional carbon FRP fabric and PBO-FRCM. The results indicated that beams retrofitted with PBO-FRCM showed a lower flexural stiffness than FRP-strengthened beams, however, both were effective. This investigation also concluded that FRCM is a viable option for structural members exposed to high temperatures up to 120°C.

2.3.2 Shear strengthening

Gonzalez-Libreros et al. (2017) carried out a study to identify shear enhancement of concrete beams strengthened with FRCM and FRP. Steel and carbon fibres were used in this investigation. The results show that the increase in shear capacity depends on axial stiffness in the composite system. With the same stiffness, both retrofitting systems showed the same improvement in strength, indicating that type of matrix did not affect the strength enhancement significantly.

Trapko et al. (2015) fabricated PBO-FRCM strengthened RC beams in order to identify the impact of different alignment (90°, 45°, 30°, 60°) of PBO-FRCM composite systems, which are shown in Figure 2-12. According to the conclusions, FRCM strips aligned at 90° concerning the longitudinal axis of the beam showed the highest value of resistance. Some anchorage systems were utilized in order to identify the mode of failure, and externally bonded FRCM mainly was extracted in the anchorage region.

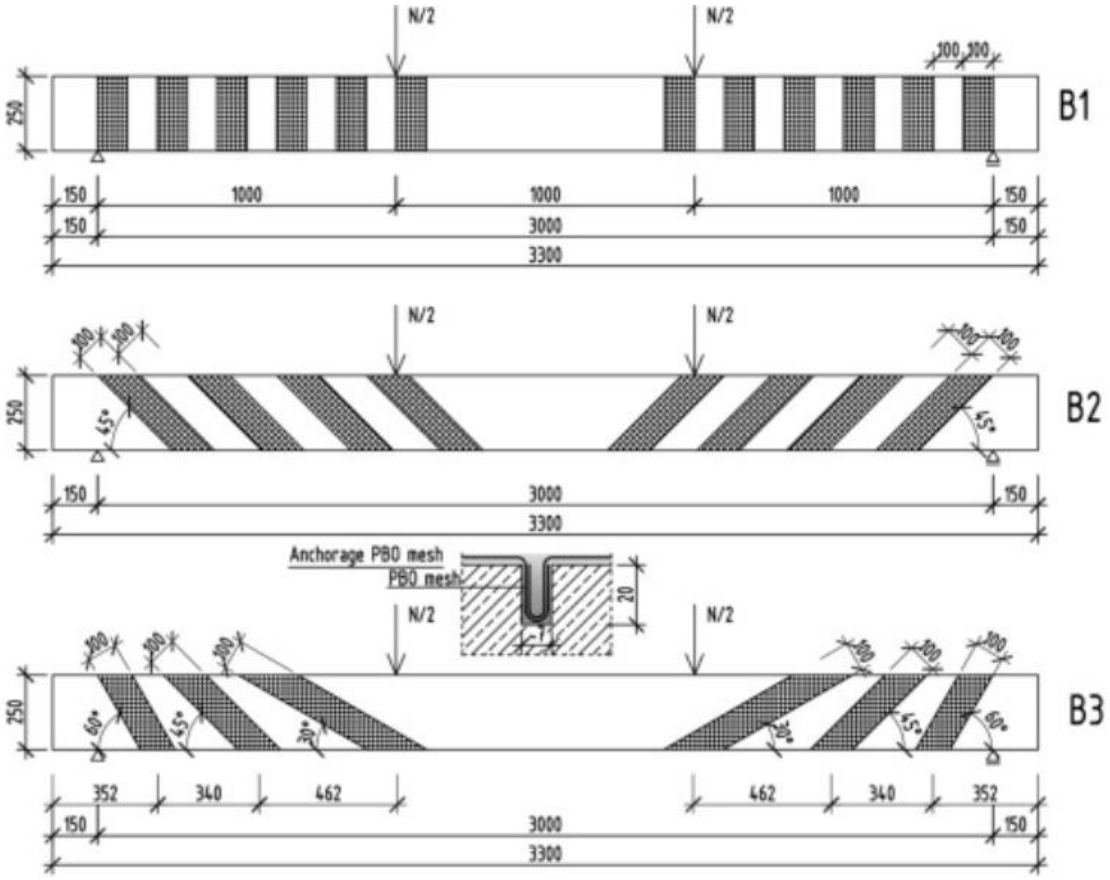

Figure 2-13: Different alignments for strengthened beams (Trapko et al. 2015).

Younis et al. (2017a) conducted tests to evaluate the FRCM effect on shear strengthening of RC beams. The results showed that the average enhancement in shear capacity was 51% compared to the non-strengthened control beam. G-FRCM, C-FRCM, and PBO-FRCM were used in this study, and the crack width measured in this study was the smallest in C-FRCM strengthened beams.

2.3.3 Axial confinement

Donnini et al. (2019b) investigated characteristics of FRCM and FRP in confining concrete columns. The results indicated that carbon-FRCM was less effective in strengthening axial capacity than PBO-FRCM and FRP. The failure mechanism for FRCM composites was due to slippage of the fibres within the matrix. However, in the case of concrete columns confined with FRP, fibre rupture was the main failure mode shown in Figure 2-13. Regardless of the type of composite system for strengthening, increased ductility and compressive strength of the columns were achieved.

Figure 2-14: Failure mechanisms in confined concrete columns (Donnini et al. 2019b).

Toska et al. (2021) carried out axial tests on reinforced concrete columns confined with carbon FRCM in order to identify the effectiveness of the composite system in increasing capacity. In this study, both circular and square-shaped columns were tested. In the case of circular specimens, the repaired samples increased the ultimate strength by 2.18 times that of control unconfined columns. However, this value was around 1.75 times the control samples for the square-shaped cross-section.

2.3.4 Torsional strengthening

Alabdulhady et al. (2017a) conducted an experimental investigation to identify the performance of externally bonded reinforced beams with PBO-FRCM. Different wrapping configurations were built to study types of failures, torsional strengths, and performances. The 4-sided wrapped beams showed a better performance compared to the 3-sided wrapping system. Also, a 4-sided wrapping configuration provided confinement which delayed concrete cracking. Figure 2-14 illustrates the types of configurations used in this investigation.

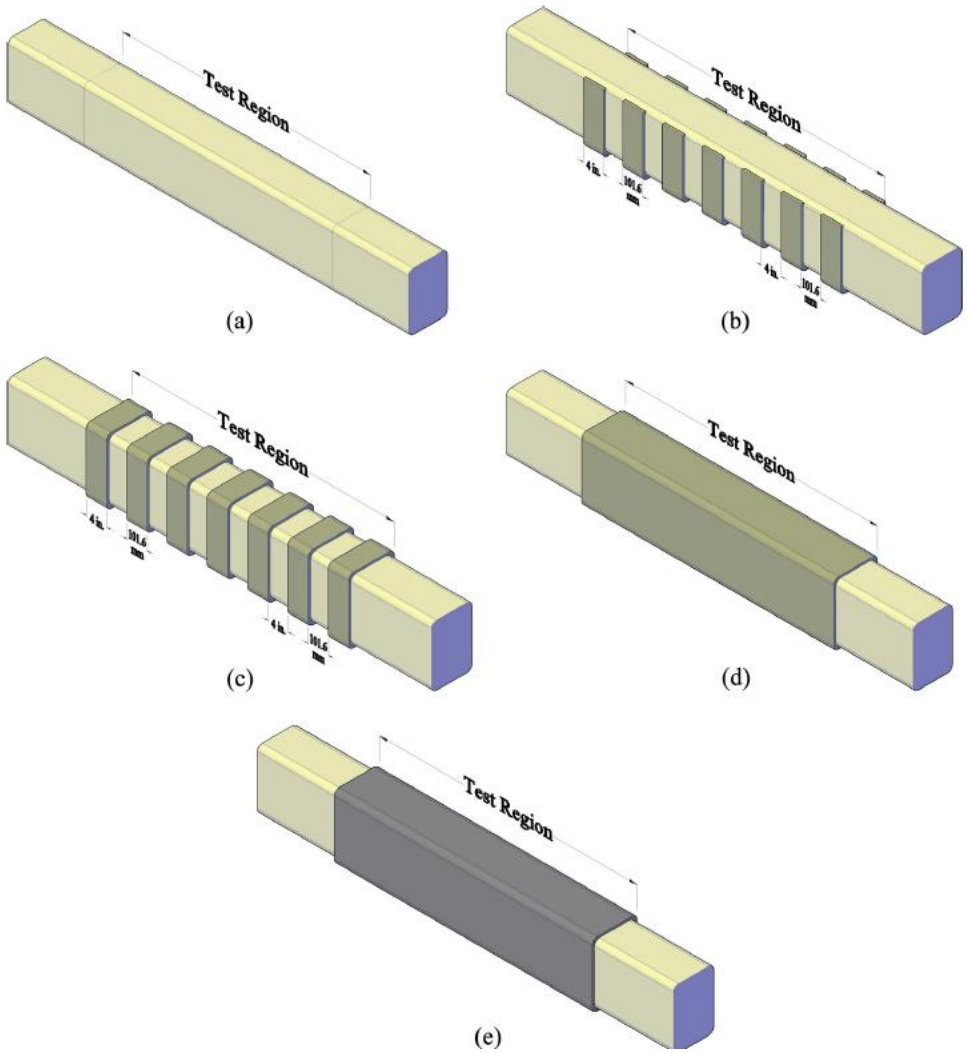

Figure 2-15: Configurations of strengthened beams (a) control beam, (b) 3-sided strips wrapped, (c) 4-sided strips wrapped, (d) one-layered continuous wrapped, (e) two-layered continuous wrapped.

2.3.5 Example projects

2.3.5.1 Rehabilitation of unreinforced concrete bridge

FRCM composites have been used to rehabilitate an unreinforced concrete bridge in the Rome-Formia-Naples railway in Italy (ACI 549.4R-20). Prior to strengthening, field investigators characterized bridge geometry and material properties. The goal of this strengthening was to change the failure mechanism and increase safety. The design calculations showed that two layers of PBO-FRCM were needed for strengthening. The bridge prior to rehabilitation is shown in Figure 2-15.

Figure 2-16: Strengthening an unreinforced concrete bridge in Italy with PBO-FRCM composite (ACI 549.4R-20).

2.3.5.2 Repair of trestle pedestal

In this rehabilitation project, FRCM composite was used to strengthen and confine concrete pedestals in northern New York, US (ACI549.4R-20). Significant cracking was observed, and weathering caused significant cracking and spalling of concrete (Figure 2-16). Even though the pedestals were adequate to carry the loads, they were strengthened in order to increase strength and, more importantly, ensure a better long-term performance. The deteriorated concrete was removed, the substrate surface was prepared, and one layer of the matrix was added to the surface (Figure 2-17). Then, a PBO-FRCM grid was pressed into the matrix (Figure 2-18), and eventually, another layer of the matrix was added to complete the repair.

Figure 2-17: The deteriorated surface of a pedestal (ACI 549.4R-20).

Figure 2-18: Preparing the substrate of pedestal ACI 549.4R-20).

Figure 2-19: One sheet of PBO-FRCM composite is being applied to the surface (ACI 549.4R-20).

2.3.5.3 Roof strengthening at elevated temperature

Strengthening with PBO-FRCM was used for an opening in a roof. The designers needed to add an opening for a duct to be operated at elevated temperatures. Since FRP composite systems do not show a promising performance at high temperatures, FRCM was selected. The designers selected the area prior to cutting the slab. First, the roof was cut, followed by the preparation of the concrete surface. Afterwards, one layer of mortar was mixed and added to the roof and fabric (Figure 2-19) and immediately, the last layer of wet mortar was immediately added on top.

Figure 2-20: PBO-FRCM placement on the roof around the duct for strengthening (ACI 549.4R-20).

2.4 Fire behaviour

2.4.1 Fire performance of FRP

Al-Salloum et al. (2011a) investigated the thermal behaviour of FRP-confined concrete prisms at 100 and 200°C. Uniaxial compression tests were conducted on unwrapped reinforced concrete columns and carbon- and glass-wrapped columns. Specimens were tested after 1, 2, and 3h of heat exposure and in some cases at ambient temperature. Three concrete prisms were strengthened with CFRP and GFRP sheets be utilized in pull-off tests at high temperatures. According to the results, with the increase in temperature, epoxy deteriorated significantly. The authors suggested that structural members reinforced with externally bonded FRP should not be exposed to temperatures higher than 2.5 times the glass transition temperature. Moreover, it is stated that higher duration of exposure to elevated temperature led to higher loss of strength. With regards to pull-off tests, the data demonstrated a considerable deterioration of epoxy between FRP and substrate at 200°C. However, the decrease in bond strength was more considerable in CFRP-strengthened prisms compared to GFRP-strengthened.

Chowdhury et al. (2007) conducted compression tests on FRP-strengthened columns to identify their mechanical behaviour. In this research two systems of FRP were employed: columns strengthened with FRP and fire insulation, and columns strengthened with FRP. The derived results showed that by utilizing an additional fire insulation, strengthened concrete columns are able to withstand more than 300 min in fire condition. It was also claimed that the insulating system used in this study could efficiently maintain a low temperature for concrete and internal reinforcement and as a result specimens retained their original load-bearing capacity. However, the insulation could only delay the degradation of FRP.

Kashwani and Al-Tamimi (2014) conducted tensile tests to characterize the thermal behaviour of GFRP with three loading rates: 0.2, 0.5, 2 mm/min. The GFRP bars were 150 mm in length and 8 mm in diameter. A temperature of 350°C appeared to be the transition temperature at which GFRP bars began to degrade severely. The increase in ductility can be considered as a warning of FRP degradation. Moreover, the loading rate and degree of temperature affected the behaviour of material significantly. The strength reduction for different material was nearly linear and 32% decrease in tensile strength was observed.

2.4.2 Fire Performance of FRCM

One of the widely accepted advantages of FRCM systems over FRP is an improved behaviour at elevated temperatures due to the greater thermal stability of the matrix. Researchers have reported that FRCM systems are able to resist loads at higher temperatures compared to conventional FRP (Raoof and Bournas 2017a; b; Trapko 2013). Therefore, FRCM is expected to show a more promising behaviour in fire scenarios (Donnini et al. 2017; Maroudas and Papanicolaou 2017). Figure 2-20 shows an example of an FRCM coupon exposed to high

temperature during a uniaxial tensile test. The contribution of FRP composites in fires are typically assumed to be negligible since their integrity is comprised with even slight temperature increases; it is not clear whether a similar approach is appropriate for FRCM systems (mainly if a thicker mortar layer is used).

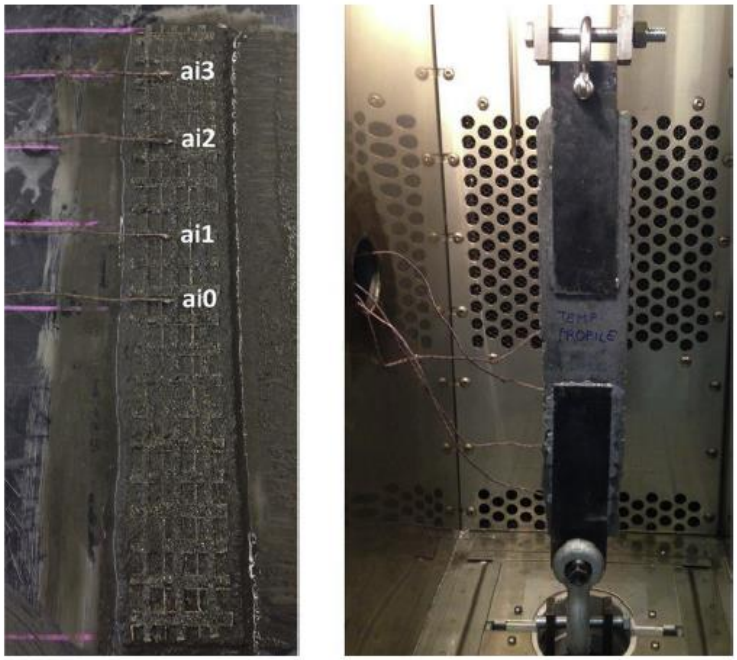

Figure 2-21: Thermocouple locations within the fabric-matrix interface (Donnini et al. 2017).

With the rise of temperature, there will be a decrease in strength and stiffness of structural members, increasing their likelihood of experiencing damage (Al-Salloum et al. 2011a; Chowdhury et al. 2007; D'Ambrisi et al. 2013; Green et al. 2006; Yaqub and Bailey 2011). The degradation of fabric as the main constituent in FRCM composite for resisting the load is exhibited in Figure 2-21. As a result, the interest in improving structures performance during a fire increases. However, structures exposed to fire show complicated behaviours, and researchers have been using simplified methods to design structures in different fire scenarios.

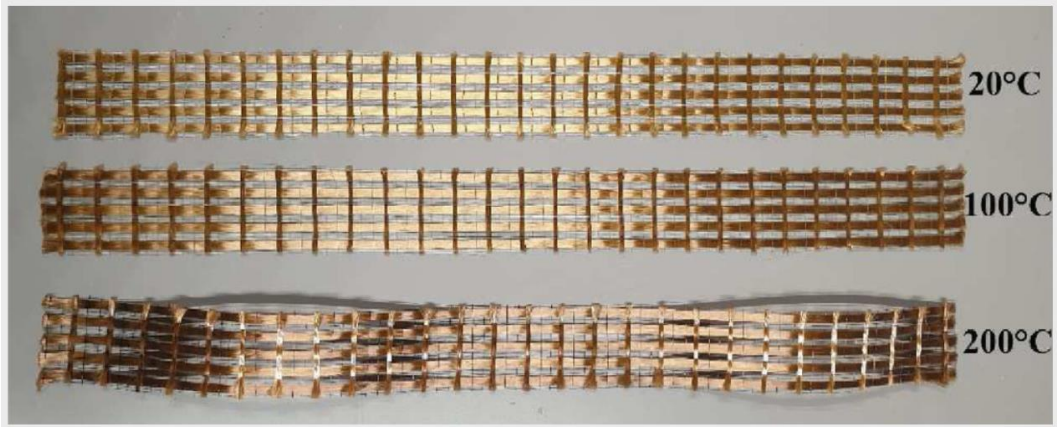

Figure 2-22: PBO-fabric after exposure to ambient and high temperature (Ombres et al. 2022).

The performance of structures in fire has attracted recent attention following the widely publicized destruction of the Notre Dame Cathedral in Paris. Even though concrete and masonry structures have low conductivity and perform relatively well in fire, collapse may occur due to reduced strength when internal reinforcement reaches critical temperatures. Externally bonded strengthening systems are even more sensitive to fires because of the lack of protection provided by the concrete cover. Consequently, researchers put effort into understanding the performance of FRCM composites at elevated temperatures.

2.4.2.1 Tensile performance

Truong et al. (2019) conducted a study to evaluate the tensile behaviour of carbon TRM at high temperatures. In this study, different overlap splice lengths (180, 200, 220 mm), fabric surface treatments (epoxy impregnation, aluminium oxide powder impregnation, coated with carbon fibre fabric), and temperatures (250, 350°C) were the investigated parameters. The results proved that a slight increase in ultimate strength took place due to different overlapping lengths. For instance, coupons with 200 and 220 mm overlapping length resulted in 2.5 and 12.9% growth in ultimate strength compared to that of the specimen with 180 mm lap splice length. In terms of the high-temperature effect, ultimate strength as a critical parameter representing the mechanical characteristic of FRCM showed a significant reduction as temperature grew. For example, specimens with 200 mm lap splice length exhibited 43 and 68% lower peak stress values than the ambient temperature test. The failure mode was fabric rupture in specimens. Utilizing lap splice length in this study did not influence the cracking stiffness and strength; however, the peak strength increased. Another main conclusion showed that employing surface treatment for fabric allowed the specimen to experience the peak load followed by a gradual drop in strength. On the other hand, specimens with no treatment showed a steep descending branch after the peak load.

Colombo et al. (2011) conducted an investigation to identify the residual tensile characteristics of coated TRM after exposure to 20, 200, 400, and 600°C. In this research, TRM coupons were reinforced with two layers of AR glass and exposed to thermal cycles in an oven with 30°C/h and 15°C/h when the temperature increased and decreased. The test results showed degradation in the ultimate strength with the temperature growth. TRM coupons tested at ambient temperature failed at 19.76 MPa, while the average ultimate strength of specimens exposed to 200, 400, and 600°C resulted in 20.64, 6.90, and 4.00 MPa, respectively. Specimens showed a high level of degradation, and after cooling, the material behaved in a more brittle manner. However, the specimens' coating resisted exposure to 200°C even though it started degrading.

Kapsalis et al. (2021) focused on the post-fire residual performance of TRC by conducting tensile tests. The parameters included fabric coating (coated and uncoated), fibre material (carbon, glass, carbon-glass), and temperature (200, 300°C). The results showed that axial stiffness and cracking strength are heavily dependent on the matrix properties. The combination of the fabric in this research was fabricated of two plies, including uncoated carbon, coated glass-uncoated carbon, and coated glass-coated carbon. In hybrid carbon-glass specimens, the material strength relied on carbon fabric that was more resistant at higher temperatures. Furthermore, the post-crack stiffness mainly was controlled by the stiffer material (carbon), indicating that cracking strength experienced more degradation than ultimate strength. The cracking patterns also did not change up to 300°C. Results showed that the effect of exposure to high temperature was more significant for the pre-cracking stage than the post-cracking stage. For example, in the tests, the cracking strength of the material experienced drops of around 10 to 50%, 30 to 40%, and 10 to 20% for uncoated carbon, uncoated glass-uncoated carbon, and coated carbon glass-coated carbon at approximately 200 and 300°C. Conversely, between different materials, uncoated carbon experienced the highest reduction of 10% in ultimate strength. Furthermore, in terms of post-cracking stage modulus of elasticity of uncoated carbon and coated glass-uncoated carbon did not behave differently, indicating that the stiffer material mainly influences the stiffness of the hybrid material. Nonetheless, an increase in the stiffness of coated glass-coated carbon was observed, which could correspond to the impregnation of inner fibres after epoxy deterioration.

Tran et al. (2020) experimentally and numerically analyzed the tensile performance of carbon TRC at elevated temperatures. In this investigation, the variables include types of carbon textile (epoxy-impregnated and amorphous silica pre-impregnated known as GC_1 and GC_2, respectively) and different temperatures (from 25 to 600°C). With regards to the experimental analysis, high temperature affected the material capacity and behaviour drastically. For instance, in case of specimens of GC_1, with the increase of temperature from ambient to 600°C, the ultimate strength was reduced from 12.76 to 1.83 MPa, an estimated 86% drop observed. In the numerical approach, ANSYS software was used to assume specimen damage and nonlinear behaviour of concrete and perfect bonding between textile and cementitious matrix. In the experimental tests, both types of textile showed a strain-hardening stage. The distance between the mesh could lead to different crack patterns. Numerical modelling predicted a three-phase material

behaviour at temperatures lower than 400°C and splitting behaviour at higher elevated temperatures. The numerical specimens showed transversal cracks failure mode in the cases of specimens exposed to high-temperature lower than 400°C. With regards to a higher temperature, only one crack was initiated in the coupon. In the experiments, some unexpected events such as fabric slippage occurred, which were not considered in numerical analysis. Overall, a good agreement in the behaviour of TRC coupons in the experimental program and numerical modelling was observed.

2.4.2.2 Flexural strengthening

Bisby et al. (2013) conducted a study to characterize the performance of FRP, TRM, and FRCM composite for flexural strengthening at ambient and high temperature in which beams were subjected to a sustained load of around 19 KN and exposed to fire afterwards. If beams did not fail under high temperatures, they were tested at a residual state. This study used unidirectional carbon/epoxy FRP, open-weave bidirectional basalt textile reinforced mortar, and open-weave bidirectional PBO-FRCM systems. According to the study, in the ambient tests, FRCM increased the flexural capacity by the highest value of 60%, followed by FRP and TRM-strengthened beams. Six beams were tested at elevated temperatures, and 5 of them survived the condition and, therefore, were tested at residual state. The TRM-strengthened beam failed at an elevated temperature of 96°C, while other beams maintained their sustained load up to around 500°C. In the residual state tests, the resistance of the strengthened beams were comparable; however, beams strengthened with the FRCM system failed at the highest value of the load, 25.6 KN.

Raoof and Bournas (2017c) increased the flexural capacity of reinforced concrete beams to investigate the performance of FRP and TRM at elevated temperatures. In this study, the main parameters included strengthening composite system (TRM and FRP), the material of fibres (carbon, basalt, and glass), fibre surface treatment (coated and uncoated), number of layers (one, three, and seven), the anchorage system (end-anchored, unanchored), as well as temperature (20 and 150°C). According to this study, FRP-strengthened beams showed a better behaviour than TRM-strengthened beams at ambient temperature. Regarding elevated temperature tests, TRM outperformed FRP with 55% sustained load at 150°C. On the other hand, FRP could only maintain 10% of the initial load at 150°C, corresponding to the higher degradation of epoxy resin than mortar.

Sui et al. (2020) utilized CFRP and TRM to strengthen reinforced concrete hollow slabs and identify their post-fire flexural performance. In this study, retrofitting material (CFRP and TRM), the number of FRP layers (one, two), as well as exposure to fire (exposed, unexposed) were the main variables. The slabs were exposed to fire in a simulated environment for one hour and tested under four-point bending. The results showed that both composite systems effectively increased the cracking and ultimate loads. Slabs retrofitted with TRM failed under a higher cracking load, lower cracking deflection, and ultimate load and larger deflection. This phenomenon was attributed to the greater flexural stiffness of TRM-strengthened slabs than

CFRP-strengthened slabs in the prior crack stage. By comparing the ultimate load of the fire-damaged unstrengthened slab with the fire-damaged TRM-strengthened slab, it was identified that the peak load was almost restored. Therefore, this indicated the significant performance of TRM-strengthened slabs after being exposed to fire.

2.4.2.3 Shear strengthening

Iorfida et al. (2019) conducted a single lap shear test to identify the behaviour of carbon and basalt FRCM after exposure to 20, 300, 500°C. The researchers concluded that a high portion of shear peak load was reduced with the increase in temperature. At 300°C and 500°C, 36% and 61% of the C-FRCM peak load was decreased. With regards to the tests conducted for low-density basalt-FRCM, peak load experienced a 74% reduction, and in bundles of fibres, a rupture occurred in the bonded region and outside of the bonded region for tests conducted at 300 and 500°C, respectively. For high-density basalt-FRCM, a 65% decline was observed for specimens tested at 500°C.

Tetta and Bournas (2016) conducted an experimental program to identify the effectiveness of TRM and FRP jackets in shear strengthening at elevated temperatures. The variables included temperature (20, 100, 150, 250°C), shear strengthening schemes (fully wrapping, U-wrapping, side-wrapping), composite type (FRP, TRM) and the number of fabric layers (2, 3). The results showed that TRM maintained shear capacity more than FRP at elevated temperatures. In the tests conducted at high temperatures, the contribution of the FRP system in load resistance declined by 60 and 88% at 100 and 150°C, respectively. On the other hand, in TRM-strengthened beams, the effectiveness of strengthening materials decreased by 31, 44, and 36% for tests conducted at 100, 150, 250°C. In addition, fully-wrapping was the most effective configuration, followed by U-wrapping and side-bonding. Moreover, failures were dependent on the number of layers.

Maroudas and Papanicolaou (2017) carried out shear bond tests at elevated temperatures using glass FRCM bonded to clay brick masonry. At 100°C, 200°C, and 300°C, the residual shear load sustained 65%, 60%, and 50% of its capacity at ambient temperature.

2.4.2.4 Axial strengthening

Cerniauskas et al. (2016) carried out 24 concentric compression tests on reinforced concrete columns in order to compare the effectiveness of FRP jackets versus TRM at high temperatures (from 20 to 400°C). The concrete columns in this study were confined in single and three layers of TRM and FRP composites. The conclusions stated that FRP-strengthened specimens experienced a higher reduction in strength due to resin degradation. As an example, TRM-confined concrete columns failed at 23% lower strength than that of ambient temperature. On the other hand, columns confined with TRM composite showed a higher level of strength at 400°C. The reduction in compressive strength with the increase in temperature is shown in Figure 2-22.

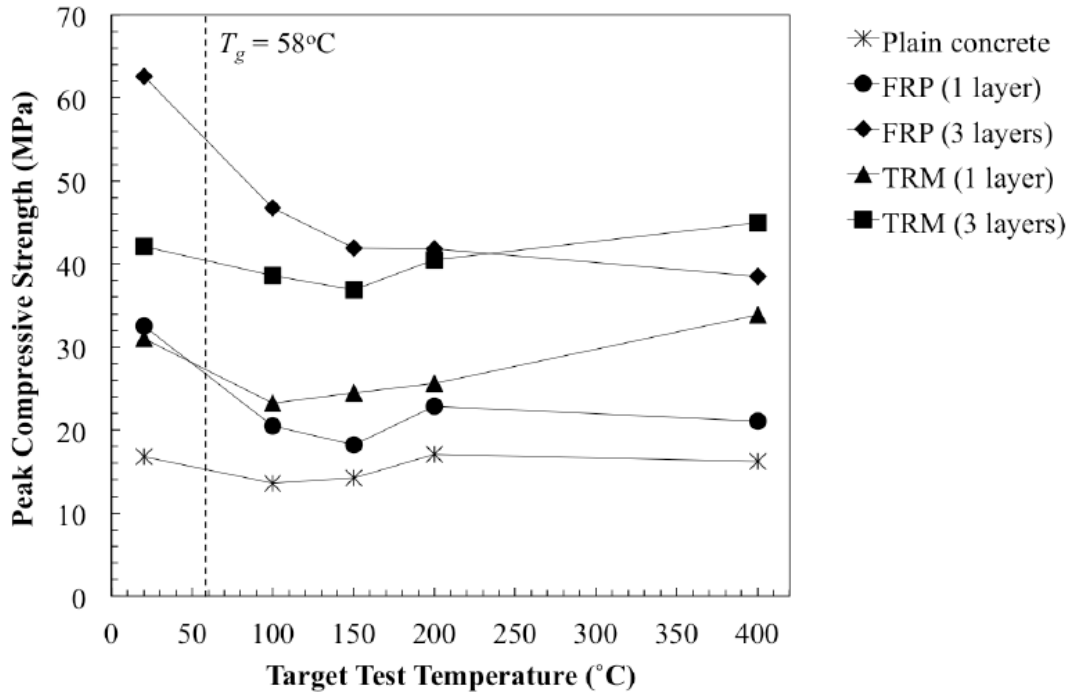

Figure 2-23: Ultimate compressive strength decrease with the growth of temperature (Cerniauskas et al. 2016).

Trapko (2013) strengthened a concrete cylinder with PBO-FRCM and CFRP to show the composites' resistance at the residual state. In this experiment, concrete columns were exposed to high temperatures (40, 60, 80°C) for 24 h and tested under a uniaxial compression machine. Based on the results, the drop in compressive strength due to the temperature growth for CFRP-confined columns was more significant than FRCM-confined columns. For instance, the reduction in confined compressive strength of CFRP-confined columns per 20°C was 10%, while in the case of FRCM-confined columns, 5 to 10% was observed.

2.4.2.5 Cyclic performance

Park et al. (2021) fabricated reinforced concrete columns and strengthened them with lap-spliced TRM composite to perform cyclic tests at high temperatures. This study aimed to assess the seismic performance of TRM-strengthened columns. The main variables in this study were the number of carbon fabric layers and surface treatment in the lap-spliced area. The results exhibited that at 250°C, some microcracks were initiated in the unstrengthened specimen while macrocrack patterns were observed for TRM-retrofitted columns. In cyclic tests after exposure to high temperature, TRM-retrofitted columns ended in a ductile mode of failure and effectively maintained their strength and deformation compared to the control specimen. In addition, at 250°C, retrofitted specimens showed a higher energy dissipation and lower decrease in secant stiffness compared to the control column.

2.5 Research gap

Although a small number of studies have investigated various performances of FRCM composites at high temperatures in recent years, most of these studies focused on FRCM-strengthened members (Ehlig and Hothan 2011; Maroudas and Papanicolaou 2017; Michels et al. 2014; Xu et al. 2014) without an in-depth investigation of material behaviour. One critical aspect of FRCM composites is their tensile performance. Various strengthening applications remain dependent on the mechanical properties of FRCM. Therefore, it is imperative to quantify the load-bearing capacity and axial stiffness of various types of FRCM composites at high temperatures. This is a prerequisite to developing practical design guidelines for FRCM that consider fire safety.

In every design, individual structural components play a crucial role in maintaining overall structural integrity. One of the severe incidents that could notably reduce the strength of members is fire. As a result, identifying the performance of FRCM in different fire scenarios can help designers to utilize this composite system more efficiently. However, there have not been any studies to clarify the tensile behaviour of FRCM with different thicknesses at high temperatures to provide a comprehensive scope. In a real fire scenario, dead load and a portion of live load are sustained while the environment's temperature increases; this is referred to as a transient-state condition. On the other hand, the vast majority of reported tests have been conducted under steady-state conditions (increasing loads at a constant temperature). In this study, tests were conducted in both steady-state and transient-state in order to provide meaningful comparisons with other studies while also considering more realistic conditions.

2.6 Summary of literature review

FRCM composites are well-suited for strengthening and rehabilitation of damaged structures worldwide. Due to their advantages, such as high compatibility, vapour permeability, and better performance at elevated temperatures, this innovative system is a viable alternative to externally bonded FRP sheets. The tensile stress-strain behaviour is a trilinear curve that is affected by the coating of fibres, number of layers, type of fibres, and mortars. Depending on the structure and gripping method, various types of failure, including fibre fracture, slippage, and debonding, could happen.

Two common types of test setups are used to reveal the tensile performance of specimens. In the clamping grip method, the coupon is directly connected to the tensile machine; however, in the clevis grip method the coupon is connected with a clevis joint for testing, which applies compressive force.

Previous investigations prove that the FRCM strengthening systems can enhance reinforced concrete and masonry members' flexural, shear, and axial capacity when applied to the main transferring stress direction. Depending on the number of layers, coating fibres, type of fibres and mortar, application method, the method's effectiveness varies.

There are a limited number of studies conducted by other researchers on the behaviour of FRCM at high temperatures to simulate fire scenarios. In general, the performance of FRCM is superior to that of FRP as temperature increases. Nevertheless, the tensile behaviour of FRCM coupons at high temperatures has not been quantified systematically, and as a result, rational design guides for fire safety are not available. This study presents an important first step towards this end.

3 EXPERIMENTAL PROGRAM

In this research, an experimental investigation was conducted at the University of Ottawa Structural Laboratory. A commercially available FRCM system comprised of a carbon mesh and a polymer-modified cementitious matrix were used to fabricate 84 tension coupons. Uniaxial tensile tests were conducted in which the variables include the number of fabric layers (1, 2, 3) leading to different thicknesses (20, 30, 40 mm), temperature (ambient, 100, 200, 300, 400°C), sustained load (20, 40, 60, and 80% of the room temperature strength), loading conditions (steady-state, transient state), and orientation of fabric (unidirectional, bidirectional). In this test, a clevis-grip method was chosen to apply the load. The significant parameters gathered from the tests are ultimate tensile strength, ultimate tensile strain, cracked section modulus of elasticity, and type of failure mode.

3.1 Specimen fabrication

The carbon fibre mesh used in this research is supplied in a 1.95 $\times$ 50 m roll and is available in two forms: unidirectional and bidirectional, shown in Figures 3-1 and 3-2. The carbon grids utilized in this study were pre-impregnated with epoxy to increase the bonding between fibres and the surrounding matrix. The mesh was first to cut into 550 x 1000 mm sections to prepare the test samples. (The samples were initially intended to have a length of 1000 mm for furnace testing at the National Research Council of Canada; following the lab closures caused by the COVID-19 pandemic, the coupon length was reduced to fit within the test fixtures at the UOttawa lab.) The cementitious matrix was delivered in 24.9 kg bags, and 3.2 L of water was used per bag of cement according to the instructions on the manufacturer's datasheet. Wooden formwork with dimensions of 550 mm by 1000 mm was prepared with adjustable walls to prepare slabs with different thicknesses to accommodate different numbers of layers. The formwork was coated with oil prior to casting to demold the samples from the formwork more efficiently, as shown in Figure 3-3. Afterwards, the wet mortar was placed in the formwork, and one layer of carbon fibre was placed on the mortar and pressed gently. Finally, another layer of cement was added to cover the carbon fibre as shown in Figure 3-4. Depending on the thickness of the specimen, the number of cement bags used for casting varied. Tables 3-1 to 3-3 display the main characteristics of cementitious matrix and different fabric types.

Table 3-1: Characteristics of unidirectional carbon fabric (Simpson, 2020).

Grid properties	
Weight (g/m^2)	440
Weight of fibres (g/m^2)	280
Dry Fabric Thickness (mm)	0.157
Ultimate Tensile Strength (kN/m)	450
Ultimate Tensile Strain (%)	1.5
Area per unit width (mm^2/m)	157
Axial stiffness by width unit (kN/m)	30,000
Area by width unit (mm^2/m)	157
Cured composite properties[(1)]	
Cracked Elastic Modulus (MPa)	49,000
Ultimate Tensile Strength (MPa)	885
Ultimate Tensile Strain (%)	1.1
Thickness per layer (mm)	13

[(1)]properties when mixed with the cementitious matrix.

Table 3-2: Characteristics of bidirectional carbon fabric (Simpson, 2020).

Grid properties	
Weight (g/m^2)	130
Weight of fibres (g/m^2)	80
Dry Fabric Thickness (mm)	0.044
Ultimate Tensile Strength (kN/m)	138
Ultimate Tensile Strain (%)	1.5
Area per unit width (mm^2/m)	44
Axial stiffness by width unit (kN/m)	9,200
Area by width unit (mm^2/m)	44
Cured composite properties[(1)]	
Cracked Elastic Modulus (MPa)	48,300
Ultimate Tensile Strength (MPa)	986
Ultimate Tensile Strain (%)	1.1
Thickness per layer (mm)	13

[(1)] properties when mixed with the cementitious matrix.

Table 3-3: Characteristics of cementitious matrix (Simpson, 2020).

Mixed properties	
Tensile Modulus at 28 days (GPa)	26.8
Direct Tensile Bond Strength at 28 days (MPa)	2.7
Direct Shear Bond Strength at 28 days (MPa)	2.1
Flexural Strength at 28 days (MPa)	6.9
Compressive Strength at 28 days (MPa)	52

Figure 3-1: Unidirectional fibre.

Figure 3-2: Bidirectional fibre.

Figure 3-3: Wooden formwork.

Figure 3-4: Cast FRCM panel.

Figure 3-5: Rectangular panel of FRCM before cutting into coupons (left) and after cutting (right).

For each mortar batch, a minimum of three cube samples were prepared to measure their compressive strength.

The rectangular FRCM samples were cut into coupons with a wet saw in the lab to prevent any dust caused by cutting. The size of the FRCM coupons was 500 mm in length, 62.5 mm in width, and thickness varied from 20 to 40 mm. Figure 3-5 displays the size of the FRCM prior to cutting in panel form and after cutting in coupon form. Afterwards, steel plates with holes were bonded with high-strength epoxy at each end of the coupons (Figure 3-6). High strength pins were fabricated to go inside these holes and apply the load.

Figure 3-6: FRCM coupon with bonded steel tabs.

3.2 Test set-up

Two main types of tensile tests have been conducted in order to evaluate FRCM tensile characteristics: clamping-grip and clevis-grip method. In the clamping-grip setup, the load is transferred from the machine to the specimen by applying compressive stress perpendicular to the ends of coupons. On the other hand, in the clevis-grip method, as recommended by ACI 549.4R-20, two metallic plates with holes are bonded to each end of the coupons and tension is transferred to the plates using a pin to minimize the potential for end moments in the specimen. In this research, the clevis-grip method is used (Figure 3-7 and 3-8).

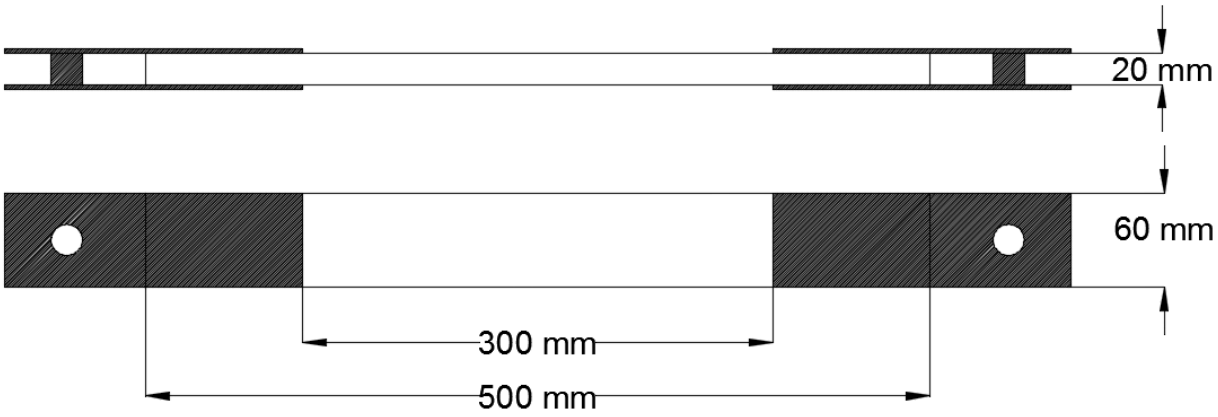

Figure 3-7: Geometric properties of one-layered FRCM coupon.

Figure 3-8: Test sample in the test frame.

3.2.1 Heating test set-up

Nine heating tests were conducted to evaluate the temperature distribution in unloaded FRCM samples subjected to high temperatures. In these tests, 20-, 30-, and 40-mm thick specimens were heated up to 200, 300, and 400 degrees Celsius.

Two holes were drilled in the 20-mm specimen to measure the temperature at specific locations. These holes were 10 mm deep and located in the middle of the thickness and 25 mm away from the edge of the coupon. Three holes were inserted for 30 and 40-mm specimens to measure temperatures at various locations along the thickness profile. In these holes, thermocouples were inserted to read and record the temperature during the test. A cement slurry was used to patch the holes after inserting the thermocouples. Figure 3-9 illustrates the location of the holes for 30 and 20-mm specimens prior to and after grouting, respectively. Schematic Figures of unidirectional 20, 30, and 40-mm thick specimens as well bidirectional 20-mm thick specimen are shown in Figures 3-10 to 3-14, respectively. Finally, the specimens were wrapped with heating tape and insulation to maintain the heat inside and help the external thermocouple be as close as possible to the heating tape to monitor the external temperature more precisely. Using a heating tape and a controller, the heat was introduced to each specimen. The temperature was reached with a controller set to 5°C/min up to the target temperature. These tests aimed to identify the time needed for the inner fabric to reach a constant temperature. Fig 3-14 represents the setup of the heating test prior to and after placement of fibreglass insulation.

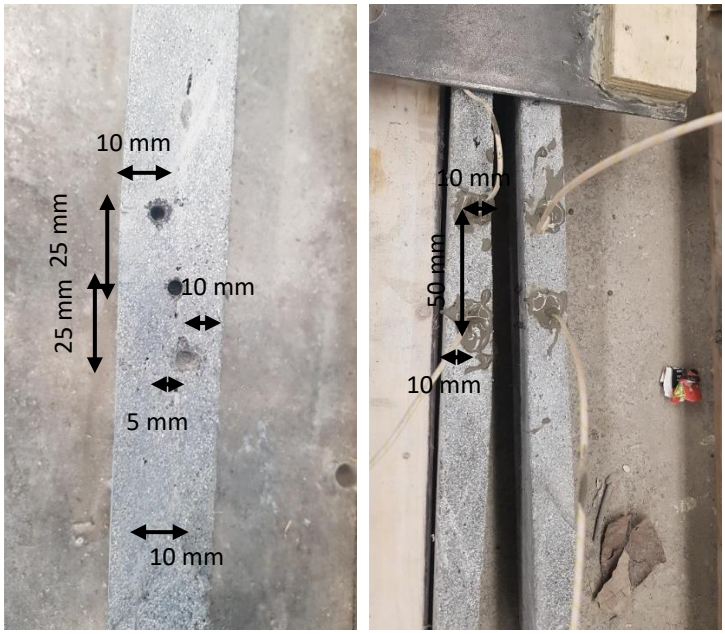

Figure 3-9: Holes drilled in FRCM coupons prior to grout injection (left) and after injection (right).

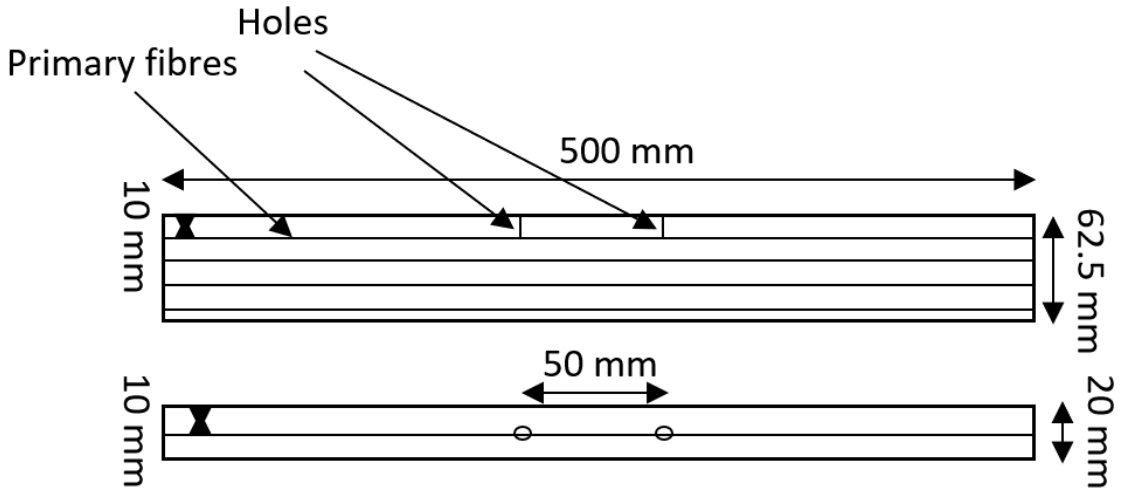

Figure 3-10: Locations of two drilled holes in unidirectional 20-mm specimen.

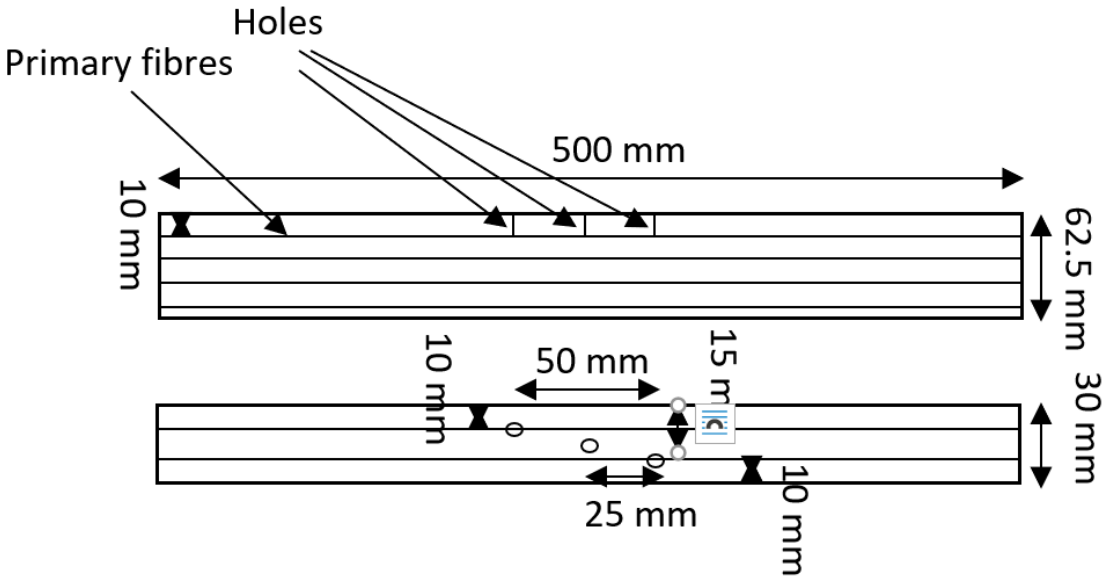

Figure 3-11: Locations of three drilled holes in unidirectional 30-mm specimen.

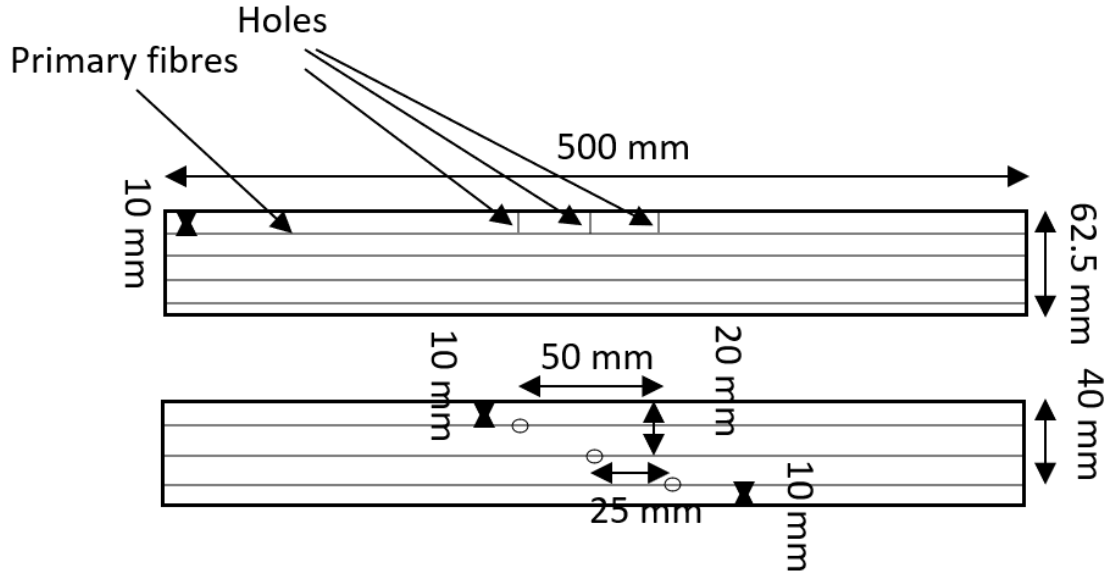

Figure 3-12: Locations of three drilled holes in unidirectional 40-mm specimen.

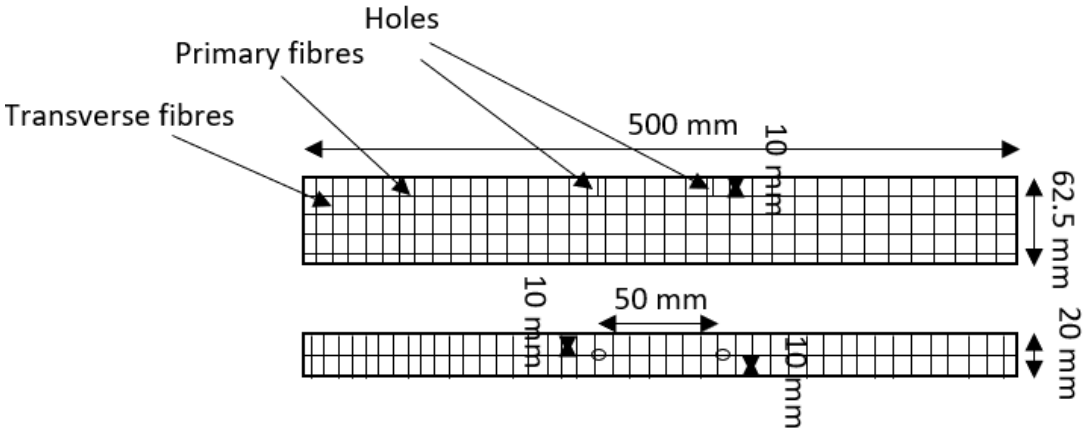

Figure 3-13: Locations of two drilled holes in bidirectional 20-mm specimen.

Figure 3-14: Heating test setup prior to insulating and after insulating.

3.2.2 Loading test set-up

Eighty-four uniaxial tension tests were conducted in order to obtain the ultimate strength of the material as well as the cracking strength and post-cracking elastic modulus. Table 3-4 shows that the specimens were tested in two primary conditions, and each test was repeated three times. In the steady-state condition, which consisted of 60 specimens, the specimen was first heated up to the target temperature at the same rate as the heating test (5°C/min). In this stage, the specimen was first covered with heating tape, and one thermocouple was placed between the specimen and the heating tape to measure the surface temperature. Afterwards, the specimen was wrapped with fibreglass insulation to maintain the heat. After reaching the target temperature, the controller held the temperature constant for 45 minutes in order to account for the soak time. Finally, the specimen was loaded using displacement control at a rate of 0.25 mm/min to identify its tensile performance at elevated temperature. On the other hand, 24 specimens were set aside for the transient state test in which a portion of the ultimate load recorded in the ambient temperature test was applied to the specimen and then was held constant. The controller was set to increase the temperature with a 5°C/min heating rate until the material could not resist the load for any longer and failure occurred. The latter condition is a better representative of a real fire scenario in which there are some pre-existing dead and live loads, and suddenly due to exposure to fire, the material begins to lose strength. The transient state tests were conducted on one-layer FRCM specimens with either 20- or 30-mm total thickness to evaluate to what degree a thicker cover might improve fire resistance. Two cable transducers with 300 mm gauge length were used to capture the displacement; one load cell was employed as well to record the force for stress calculation. Figure 3-15 shows the loading test setup.

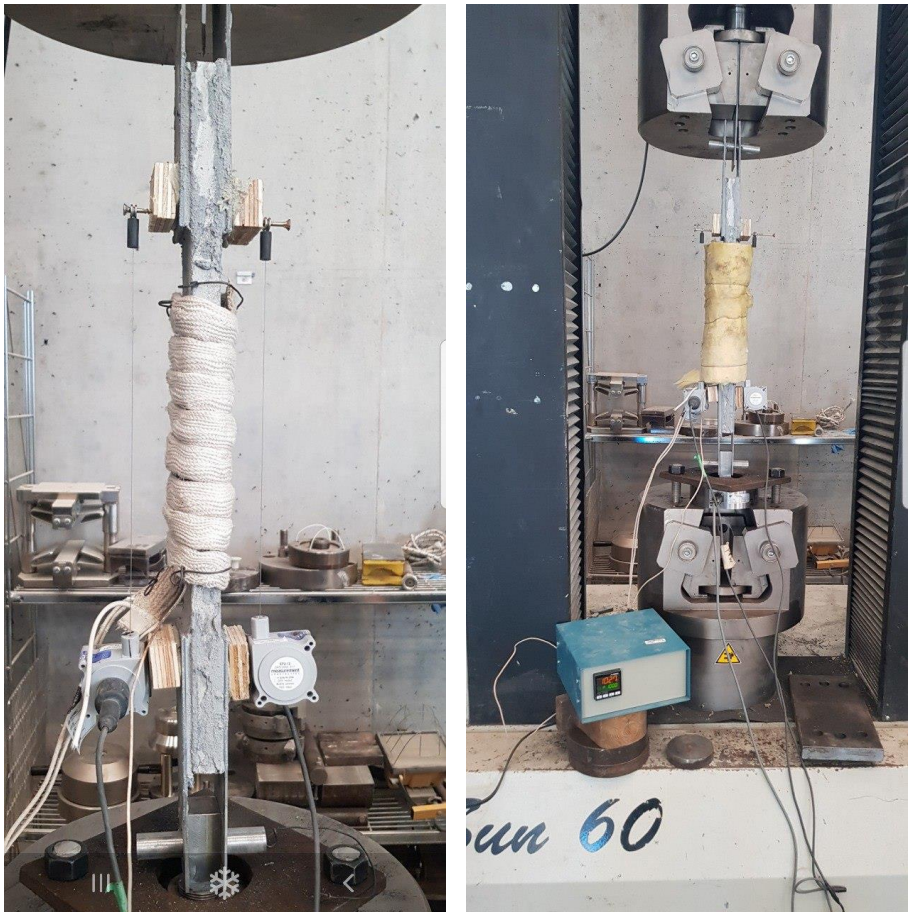

Figure 3-15: Loading test setup (left) before fibreglass wrapping and (right) after fibreglass wrapping.

The goal of the loading test was to reveal the tensile performance of FRCM material at high temperatures. Moreover, the impact of fire on the mechanical properties, including cracking strength, cracked elastic modulus, ultimate strength, the failure mode, is assessed.

Table 3-4: Experimental program variables

Steady-state tests				
Grid type	Number of layers	Temperature (C°)	Thickness (mm)	Number of samples
Unidirectional carbon grid	1	20	20	3
		100	20	3
		200	20	3
		300	20	3
		400	20	3
	2	20	30	3
		100	30	3
		200	30	3
		300	30	3
		400	30	3
	3	20	40	3
		100	40	3
		200	40	3
		300	40	3
		400	40	3
Bidirectional carbon grid	1	20	20	3
		100	20	3
		200	20	3
		300	20	3
		400	20	3
Transient state tests				
Grid type	Number of layers	Sustained load level (%f_{fu})*	Thickness (mm)	Number of samples
Unidirectional carbon grid	1	20	20	3
		40	20	3
		60	20	3
		80	20	3
		20	30	3
		40	30	3
		60	30	3
		80	30	3

*Sustained load level = the load level the specimen can resist at ambient temperature.

4 EXPERIMENTAL RESULTS

4.1 Compression test results

A number of cubic samples were fabricated from the cementitious matrix for compression testing while casting the FRCM samples. Based on the technical datasheet, the expected compressive strength of the cement mortar at 28 days of age is 52 MPa. In this research, six samples were tested at 28 days, and the remaining thirty samples were tested at the time of the coupon tests after several months of curing in ambient lab conditions. In Table 4-3, the compressive test results are shown regarding the particular test date. The mean value for the tests conducted at 28 days and testing date are 48.4 and 54.7 MPa, respectively. In Figure 4-28, a cubic sample before and after the test is displayed. The cubic sample was subjected to the uniaxial loading at a rate of 1350 N/mm in accordance with ASTM standard C 109/C 109M - 02 allowable loading rate range, which is 900 to 1800 N/mm. Based on the ASTM instruction the load was applied at the centre of the specimen.

Table 4-1: The compressive strength of cementitious matrix at 28 days and testing date.

Compressive strength			
28 days		Testing day	
Mean value (MPa)	COV (%)	Mean value (MPa)	COV (%)
48.4	8.6	54.7	12.1

Figure 4-1: cubic cementitious matrix prior (left) and after the test (right).

4.2 Heating test results

These tests were conducted to monitor the temperature distribution at different depths along with the thickness of single and multilayer specimens. After the temperature reached approximately 100°C, specimens started to smoke due to the adhesive used to bond the fabric together and some moisture inside the specimen evaporated by the heat. The main goal of conducting heating tests was to allow the inner fabric grids to reach a constant value and this was achieved after holding external temperature for 45 minutes for all specimens. By exposing the inner fabric at the same level of temperature for sufficient amount of time, the specimen showed a higher extent of degradation compared to real fire scenario.

4.2.1 Temperature comparison

4.2.1.1 20-mm thickness

The graphs obtained from the heating tests were plotted in order to compare temperature patterns for specimens with the same thickness. In Figure 4-2 three temperature distributions with different target temperatures (200, 300, 400°C) for 20-mm specimens are portrayed. The 10-mm lines represent the temperature at the fabric layer in the middle of the thickness of FRCM coupons. For 200°C as the highest temperature, the internal temperature reached follows a milder slope up to 200°C than the external temperature. However, for the peak temperature of 300° after 45 minutes of soak time, a round-shaped curve was formed for the internal temperature. Even though internal thermocouples did reach a thorough constant value, sufficient amount of time was spent to ensure the constant value of internal temperature. The slope of internal temperature was less than that of the surface temperature. Regarding the specimen heated up to 400°C, the fabric temperature formed a plateau and dropped at the same rate as the surface temperature. However, while increasing temperature, the fabric layer experienced a milder slope increase. In general, 45 minutes of soak time was sufficient for all target temperatures to allow the internal fabrics to reach a relatively stable temperature. The temperature difference between the internal and external thermocouples during the soak time was the greatest at 300°C, followed by 200 and 400°C. Moreover, the external and internal thermocouples in the test aimed at 400°C showed nearly identical behaviour.

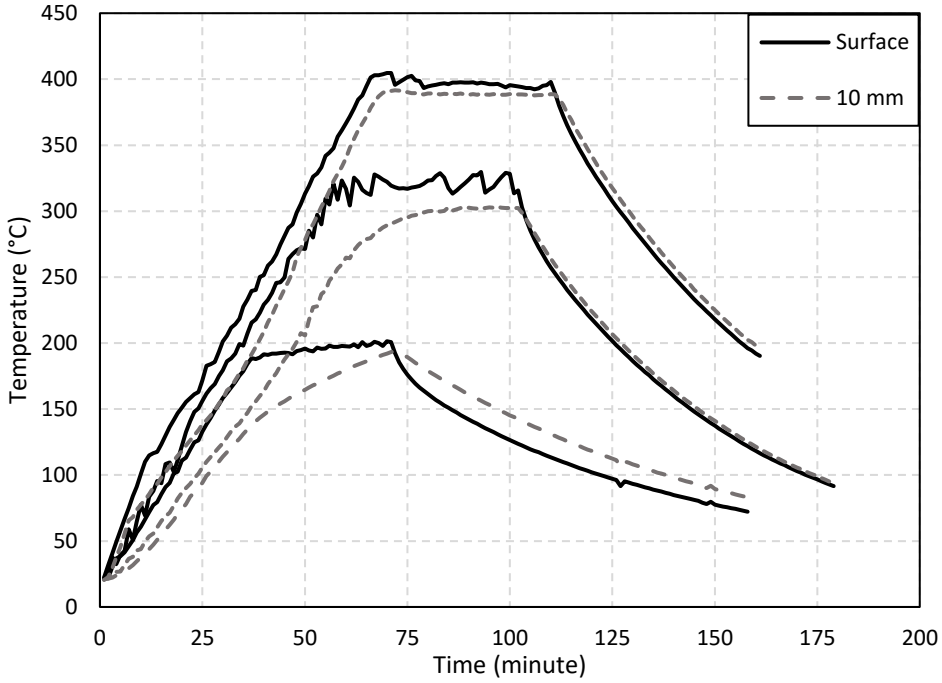

Figure 4-2: Different temperature distributions for 20-mm thick specimens

4.2.1.2 30-mm thickness

For three 30-mm specimens, heating tests were conducted to show the insulation effect and temperature gradient. In Figure 4-3, the numbers in the legend indicate the distance between the location of the thermocouple and the surface of the specimen. For all specimens, the dashed line representing the internal thermocouples placed in the middle (15 mm from surface) followed at a slower rate than their counterparts. In the 200°C test, the difference in the internal temperatures was consistent until they reached the peak temperature. Finally, the internal temperature started to decrease as the external temperature dropped simultaneously. Concerning the specimen heated to 300°C, the internal temperature had sufficient time to form a plateau after 45 minutes and gradually dropped. The internal temperatures were almost identical until 250°C. Afterwards, the thermocouple placed in the middle of the thickness sensed a slightly lower temperature. Eventually, all internal and external temperatures decreased during the cooling period after exposure to soak time. The slope in the temperature decreasing stage was nearly the same for all temperatures. In the test performed at 400°C, internal temperatures were identical up to 320°C and started to show a more significant difference toward the end of the soak time. All of the tests proved that 45 minutes of soak time spent on the tests was sufficient to allow the internal temperature to reach a relatively steady temperature.

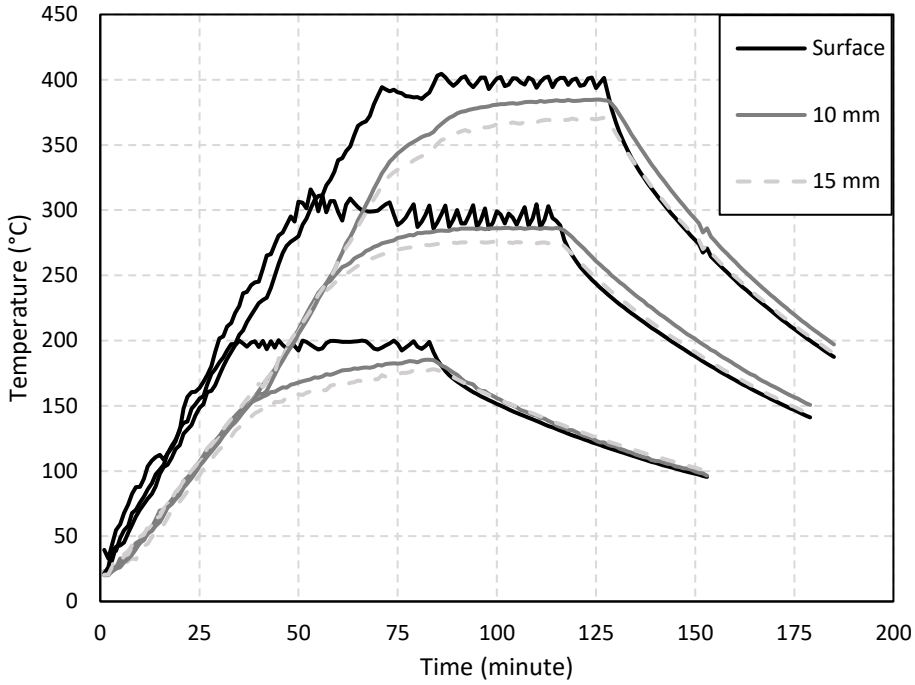

Figure 4-3: Different temperature distributions for 30-mm thick specimens

4.2.1.3 40-mm thickness

The difference between internal and external temperatures was notable in the heating tests conducted for the thickest coupons. According to Figure 4-4, in the heating test performed at 200°C, the internal thermocouple located 20 mm from the surface was approximately 75°C lower than the surface temperature after 45 minutes of soak time, and increasing at a very slow rate. During the cooling period, the internal temperatures declined more slowly than the external temperature. Regarding the test conducted at 300°C as the highest surface temperature, the internal temperatures gradually increased at a slower rate than the external temperature. With 45 minutes of soak time, the inner fabric layers reached temperatures that were within 50°C of the target temperature. All three thermocouples followed the same decreasing rate with almost constant temperature differences during the cooling period. Regarding the test conducted at 400°C, all the thermocouples representing external and internal temperatures showed a constant value after 45 minutes of soak time. The difference between the external and internal temperature at a depth of 20 mm was approximately 50°C. The behaviour of external and internal thermocouples during the cooling period was similar with a slightly steeper slope for the surface temperature. Based on the results of these tests, it was determined that 45 minutes of soak time was sufficient for the inner fabric to reach a relatively stable temperature, even though a complete plateau was not formed in some cases.

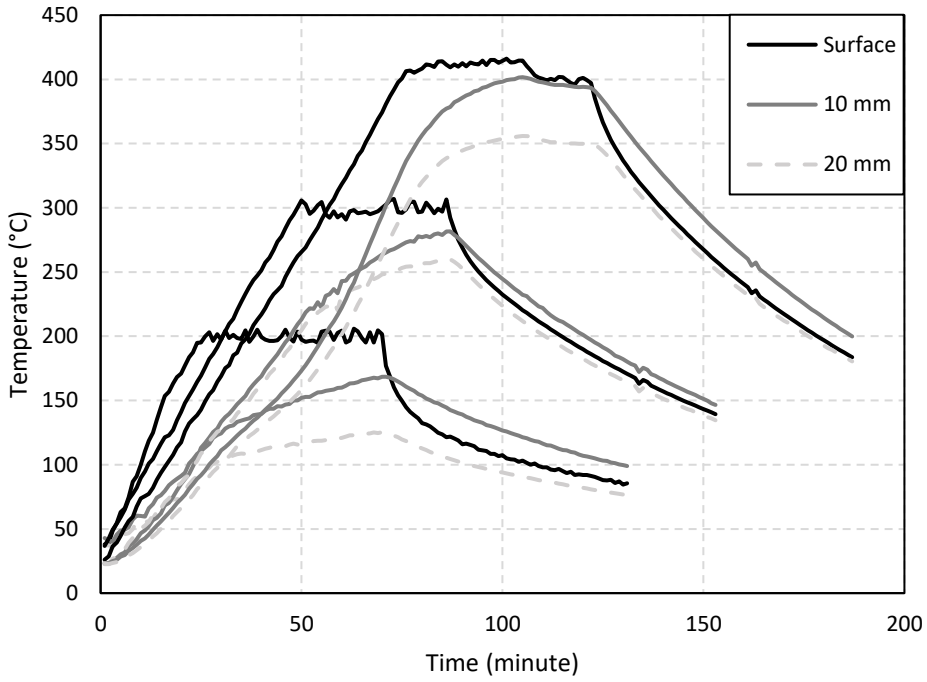

Figure 4-4: Different temperature distributions for the 40-mm thick specimens

4.2.2 Thickness comparison

4.2.2.1 Target temperature at 200°C

The results presented in Figure 4-5 show the effect of insulation (i.e., the thickness of the FRCM) on the performance of FRCM coupons. In this figure, solid, dashed, and dotted lines represent 20, 30, and 40-mm thick specimens, respectively. The curves were plotted to compare different temperature values in each layer of FRCM. It is assumed that the other surface of the specimen sensed the same temperature. This phenomenon was repeated in Figures 4-5 and 4-6 as well. According to the curves shown in Figure 4-4, the initial temperature for all specimens was approximately 25°C. However, with the increase in time, the temperature difference for surface temperature and fabric layers became more considerable. This phenomenon was noted by observing the U-shaped temperature profile obtained at higher temperatures. Furthermore, in the dotted lines (40 mm thick), the temperature difference was more notable than dashed (30 mm) and solid (20 mm) lines, indicating that the inner fabrics in the thickest specimens were less affected by elevated temperature. However, there was a temperature difference in some cases due to thermocouples' errors in recording temperature as they are extremely sensitive to the surrounding environment. For instance, after 20 minutes, the surface temperature of a one-layered specimen was 111°C, while a three-layered specimen showed 170.9°C. This difference

could be attributed to the sensitivity of the thermocouples and the fluctuation of surface temperature set by the controller.

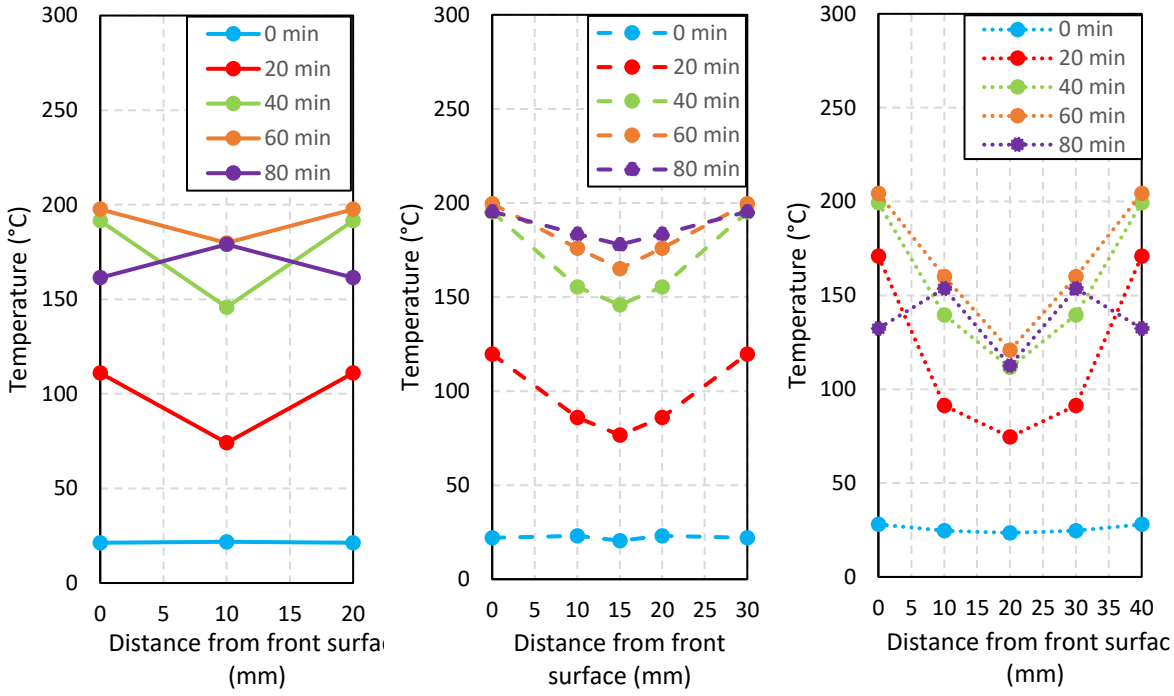

Figure 4-5: Different temperature distributions for 200°C target temperature (solid, dashed, and dotted lines correspond to 20, 30, and 40-mm specimens, respectively.

4.2.2.2 Target temperature at 300°C

In Figure 4-6, the temperature curve with respect to distance from the surface is shown for each type of coupon. In this figure, solid, dashed, and dotted lines correspond to the 20, 30, and 40-mm thick specimens. In the case of the initial temperature, all of the specimens were exposed to the room temperature around 25°C, and as a result, the internal and external thermocouples showed a similar temperature. However, as the test started and the controller increased the temperature, the difference between the inner fabric and the surface temperature became more substantial. The U-shaped temperature profiles induced by the effect of cementitious matrix placed between the fabric is visible in this figure. With the increase in thickness, the difference between internal and external thermocouples was more significant. For the 20-mm thick specimen, the internal temperature could almost reach the external temperature. In contrast, the curves still maintained their U-shape for thicker samples even after the 45 minutes of soak time. This phenomenon highlighted the excellent performance of the matrix in retaining the inner fabric properties. In this test, approximately 55 minutes was spent in the heating process and 45 minutes for soak time; therefore, the temperature until the soak time was almost the same as

the temperature recorded in the middle of the soak time represented by the purple line, the lines after 100 minutes were drawn.

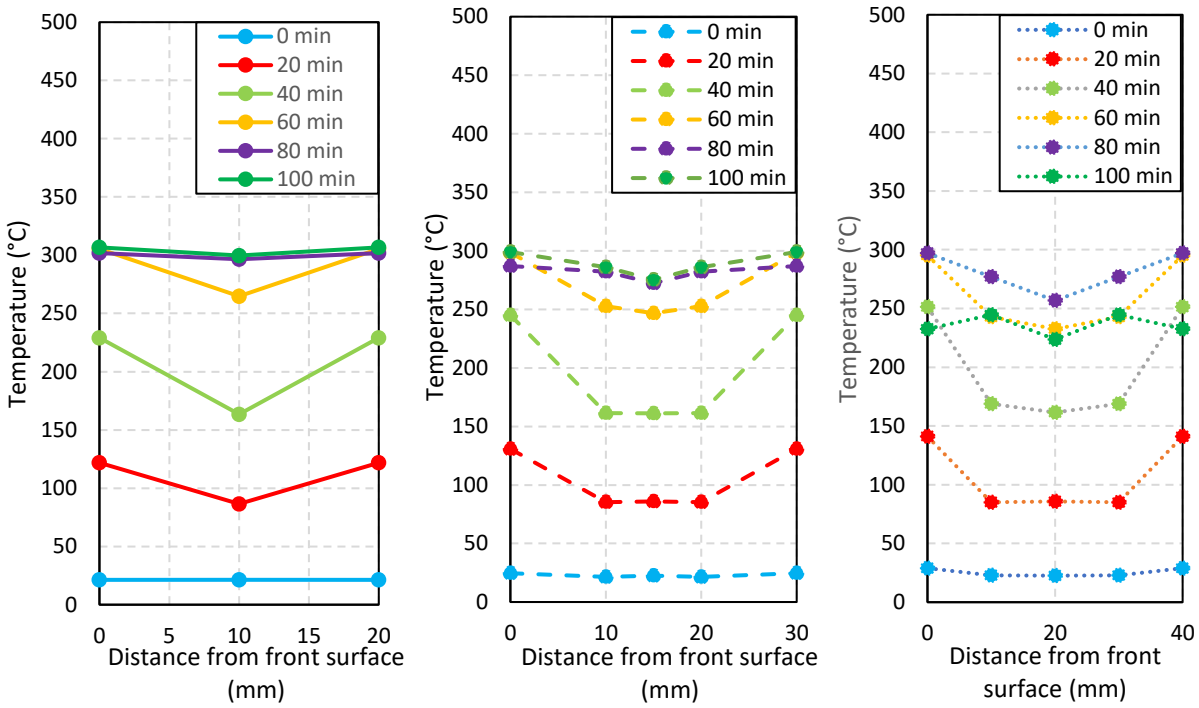

Figure 4-6: Different temperature distributions for 300°C target temperature (solid, dashed, and dotted lines correspond to 20, 30, and 40-mm specimens, respectively.

4.2.2.3 Target temperature at 400°C

The curves of different specimens are presented in Figure 4-7 in order to identify the effect of thickness on the temperature sensed by fabric plies. In this figure, one, two, and three-layered specimens were represented by solid, dashed, and dotted lines, respectively. The initial temperatures sensed by all thermocouples were estimated at 25°C regardless of the specimen type. As the temperature grew, more distinction between internal and external temperature was observed. In the yellow lines representing the testing condition after 100 minutes, it is observable that multiple-layered specimens had not reached their constant temperature. For the 20-mm specimen, the fabric layer reached the highest value. This event demonstrated that thicker specimens provided a higher level of heat protection. Moreover, the internal and surface temperature difference was greater in thicker specimens, leading the curve to become U-shaped. This temperature difference is due to the lowest temperature sensed in the mid-thickness of the specimen.

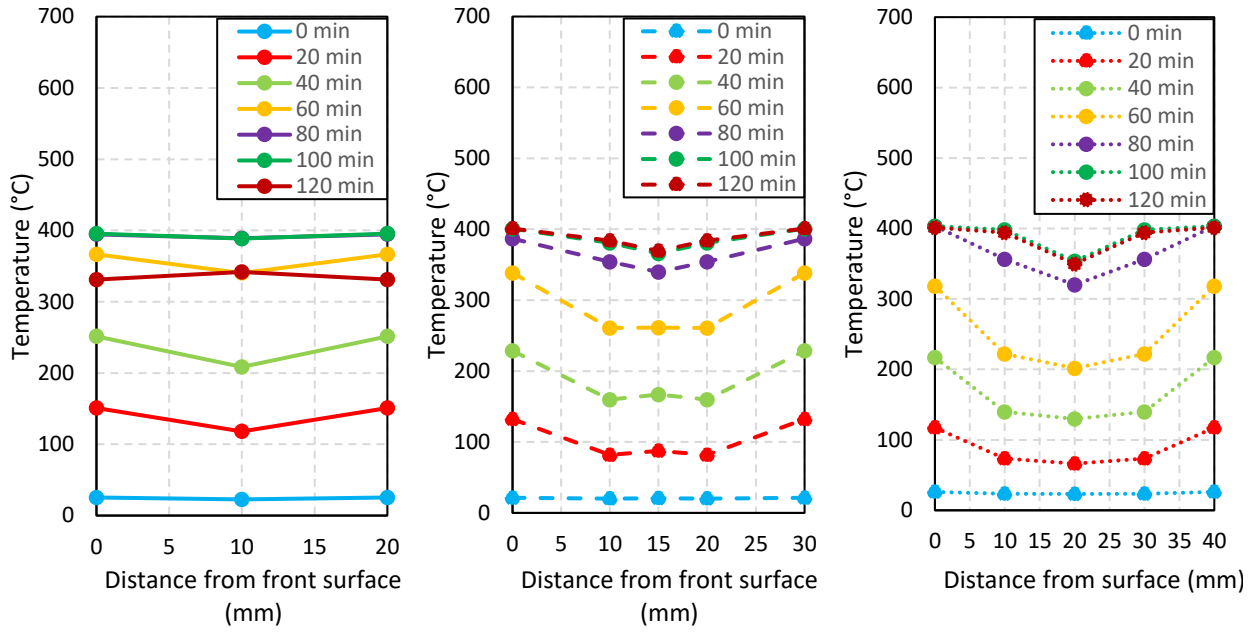

Figure 4-7: Different temperature distributions for 400°C target temperature (solid, dashed, and dotted lines correspond to 20, 30, and 40-mm specimens, respectively.

4.2.3 Summary of heating tests

According to the results of the heating tests, the temperature gradients in the various samples following the soak time varied. In most cases, the temperatures were relatively stable at the end of 45 minutes and the maximum temperature difference was usually less than 50°C between the innermost thermocouple and the surface of the sample. Thicker test specimens generally showed a higher difference in temperature than thinner specimens. Moreover, by comparing temperature variation with respect to thickness, it is assumed that the inner fabric of thicker samples would perform better as they would be less affected.

These tests suggest that the selected heating rate of 5°C/min and 45 minutes soak time are appropriate for the loading tests. The results also suggest that different fabric layers within multi-layer specimens may experience different temperatures even under steady state test conditions. As a result, inner fabric layers may exhibit a greater contribution to mechanical properties at high temperatures. Moreover, the probability of slippage of fabric within the surrounding cement would increase as high-level degradation occurred at elevated temperatures.

4.3 Tensile test results

4.3.1 Expected load in the direct tensile test

This section will calculate the expected failure load of the FRCM coupons subjected to direct tension at ambient temperatures. The method conducted in this section to calculate the expected load was discussed in ACI 549.4R-20.

The expected failure load in the direct tensile test of FRCM coupons will be calculated as follows:

Load amount = number fabric of layers * fabric area * ultimate tensile strength of composite

$$P = n * A_f * f_u \qquad \text{Equation 2}$$

Where n is the number of FRCM layers, A_f is the area of carbon grid by unit width, and f_u is the ultimate strength of the cured composite reported by the manufacturer (Simpson, 2020). Hence:

Area of each bundle in unidirectional specimen:

$A_f = 157\ mm^2/m$

Approximately 59 bundles were fit in one meter, therefore:

$A_{bundle} = 157\ mm^2 / 59 = 2.65\ mm^2$

Since we have a 62.5 mm wide sample with four fibre rows in each sample, therefore the area of fibres in one specimen is as follows:

$A_f = 4 * 2.65 = 10.6\ mm^2$

Area of each bundle in bidirectional specimen:

$A_f = 44\ mm^2/m$

Approximately 46 bundles were fit in one meter, therefore:

$A_{bundle} = 44\ mm^2 / 46 = 0.96\ mm^2$

Since we have a 62.5 mm wide sample, therefore area of fibres in one specimen is as follows:

$A_f = 4 * 0.96 = 3.84\ mm^2$

The specimens are 62.5 mm wide, and the clear distance between the carbon grid is 10 mm in the main direction; however, the diameter of each bundle contribute to the number of rows that each specimen contains.

Another significant characteristic of the FRCM composite system is its reinforcing ratio. This value is obtainable simply by dividing the reinforcing fabric area by the whole cross-section of the specimen.

A_f = (number of bundles) * (bundle area) Equation 3

A_{gross} = (Width of specimen) * (thickness of specimens) Equation 4

$\rho_f = A_f/A_{gross}$ Equation 5

The cross section of each row of fabric is 2.66 and 0.96 mm^2 for unidirectional and bidirectional specimens respectively, and in each specimen, there are 4 rows of fabric. Hence, for single-layered and multiple-layered specimens the reinforcing ratio are summarized in Table 4-2:

Table 4-2: Prediction value of area and ultimate load for various specimens.

	Unidirectional one-layered	Unidirectional two-layered	Unidirectional three-layered	Bidirectional one-layered
Fabric area, A_f (mm^2)	10.6	21.2	31.8	3.84
Section area, A_{gross} (mm^2)	1250	1875	2500	1250
Reinforcement, ρ_f ratio (%)	0.85	1.1	1.3	0.31
Ultimate load, P (KN)	9.38	18.76	28.14	3.79

4.3.2 Steady-state results

Sixty-four FRCM coupons were fabricated and tested with different parameters in the steady-state condition. Table 4-2 summarizes the mechanical properties obtained by these tests. The results employed various combinations of each parameter to provide a comprehensive behaviour of FRCM at elevated temperatures. Significant outcomes are presented in this chapter based on the parameters of this study. The steady-state tests parameters included fabric orientation, number of layers (thickness), and temperature.

The target temperature shown in Table 4-3 was measured by a thermocouple placed on the surface of the specimens. The ratio of the ultimate stress at each particular temperature to the average maximum strength at ambient (room) temperature is normalized and shown as a stress ratio. In order to compare the stress-strain values for different specimens, the applied load was divided by the area of fabric embedded in coupons. Furthermore, for calculation of cracked elastic modulus, ACI instructions were adopted in which 60 and 90% of ultimate strength were found as well as their corresponding strain to use the slope as an indication of cracked elastic modulus. With regards to crack development, all cracks initiated within the gauge length, even though in some cases cracks propagated close to the anchorage zone. For example, Figure 4-8 shows a specimen in which two cracks occurred, one close to the bonding plate and one in the middle.

The primary failure mode in all the specimens was the slippage of fibres inside the cementitious matrix (Figure 4-9). This type of failure mode is mainly attributed to the loading mechanism in which coupons were subjected to load with tabs that caused some shear stress. This phenomenon was recognizable with a gradual behaviour at the end of the tests. However, in thicker specimens due to a higher level of force at failure, some premature debonding of the plate at the epoxy interface and plate also occurred; these tests were repeated and are not included in the results presented in this chapter. Only failures which occurred within the gauge length of the tension coupons are considered in this work.

Figure 4-8: Crack development within the gauge length.

Figure 4-9: Fabric slippage within the surrounding matrix.

Table 4-3: Summary of direct tensile tests on FRCM coupons in the steady-state condition.

Target temperature (C°)	Thickness (mm)	Number of layers	Orientation	Reinforcing ratio ρ_f (%)	Peak stress (MPa)		Stress ratio (%)	Peak Load (KN)	Cracked Elastic modulus (MPa)		Failure mode
					Mean value	CoV (%)		Mean value	Mean value	CoV (%)	
Ambient	20	1	Bidirectional	0.31	882	2.0	100.0	3.4	59500	4.8	S[(1)]
100	20	1	Bidirectional	0.31	718	4.7	81.4	2.8	49000	5.6	S
200	20	1	Bidirectional	0.31	602	0.6	68.3	2.3	43400	4.8	S
300	20	1	Bidirectional	0.31	481	1.8	54.5	1.8	39200	8.0	S
400	20	1	Bidirectional	0.31	295	7.0	33.4	1.1	24800	18.8	S
Ambient	20	1	Unidirectional	0.85	791	3.6	100.0	8.4	60200	3.6	S
100	20	1	Unidirectional	0.85	632	1.2	79.9	6.7	53800	6.4	S
200	20	1	Unidirectional	0.85	555	4.4	70.2	5.9	47700	2.7	S
300	20	1	Unidirectional	0.85	424	4.4	53.6	4.5	36900	9.8	S
400	20	1	Unidirectional	0.85	276	11	34.9	2.9	24700	18.8	S
Ambient	30	2	Unidirectional	1.10	703	3.1	100.0	14.9	49300	3.6	S
100	30	2	Unidirectional	1.10	581	2.2	82.6	12.3	43600	1.1	S
200	30	2	Unidirectional	1.10	509	1.6	72.4	10.8	41300	10.0	S
300	30	2	Unidirectional	1.10	385	10.1	54.8	8.2	38400	3.8	S
400	30	2	Unidirectional	1.10	241	8.7	34.3	5.1	32700	6.7	S
Ambient	40	3	Unidirectional	1.30	650	1.4	100.0	20.7	48200	4.7	S
100	40	3	Unidirectional	1.30	557	1.8	85.7	17.7	43200	4.0	S
200	40	3	Unidirectional	1.30	446	7.0	68.6	14.2	36600	5.8	S
300	40	3	Unidirectional	1.30	326	16.0	50.2	10.4	34200	1.1	S
400	40	3	Unidirectional	1.30	199	9.4	30.6	6.3	28900	7.7	S

[(1)]Slippage of fabric within the surrounding cementitious matrix.

In Figure 4-10, the average peak stress corresponding to different temperature conditions for various types of specimens is presented. The nomenclature used in the legend indicates the number of layers in each specimen (1, 2, or 3) and the orientation of the layers (B-Bidirectional or U-Unidirectional). The strength reduction was approximately linear with respect to the increase in temperature, with a loss of roughly 17% for every 100°C. At 400°C, the average strength reduction was approximately 65%, whereas approximately 50% of the tensile strength was retained at 300°C. This observation was surprisingly consistent for all number of layers and both unidirectional and bidirectional fabrics. Even though the inner layers of the thicker samples may have been slightly more protected from the heat, as noted during the heating tests, the weaker fibres' failure near the surface was sufficient to cause the entire coupon's failure.

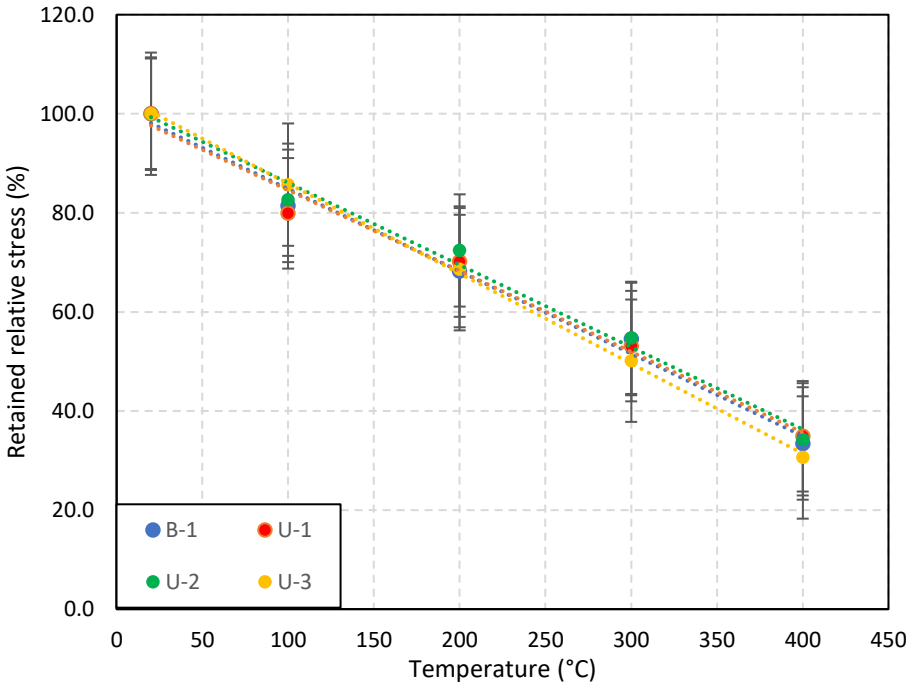

Figure 4-10: Retained ultimate stress for 20, 30, and 40-mm specimens at high temperatures.

Even though the ultimate strength reduction was relatively consistent among various specimens exposed to elevated temperatures, the cracked elastic modulus showed a higher variation depending on the specimen type. Figure 4-11 reveals the relative cracked elastic modulus versus temperature for each specimen. The abbreviation in the legend represents the type of specimen. The legends are written in X-Y format, where X denotes specimen orientation and Y denotes the number of fabric layers. It can be observed that single-layered specimens exhibited a more pronounced reduction in stiffness at higher temperatures than the thicker multilayer specimens. One-layered bidirectional and unidirectional specimens followed similar trends with a reduction of almost 60% at 400°C, while in multiple-layered specimens, the decline was less than 40% at

the same temperature. This phenomenon may be attributed to the contribution of the inner layers of fabric that experienced slightly lower temperatures than the outer surface even after extended exposure times. Although the fabric grids in the 2-layer specimens were the same distance to the surface as the 1-layer specimens, the slight temperature gradient between the surface and the core seems to have had a beneficial effect on the stiffness.

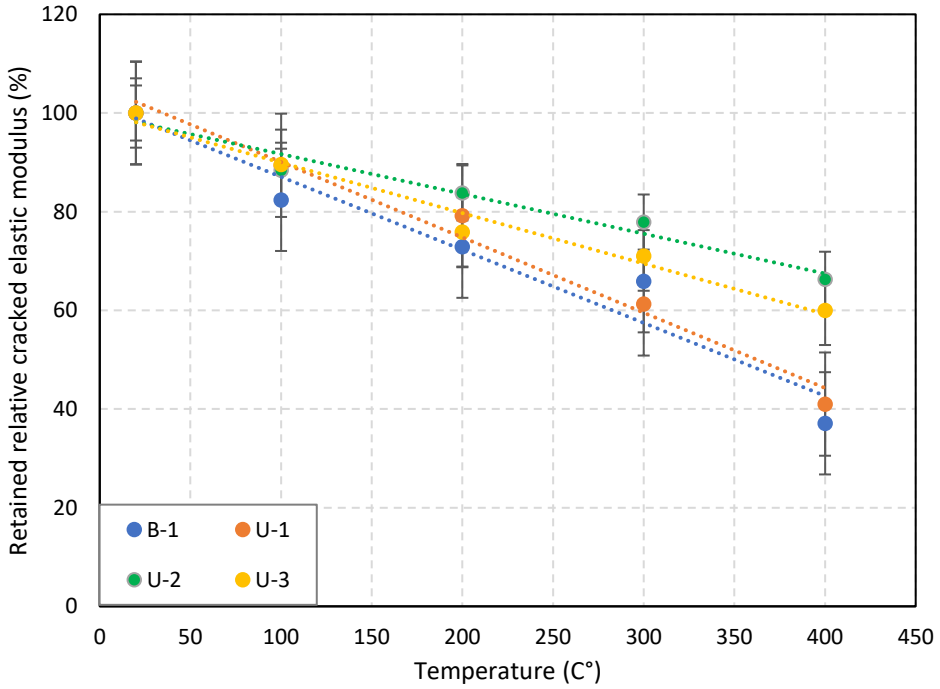

Figure 4-11: Retained cracked elastic modulus for 20, 30, and 40-mm specimens at high temperatures.

4.3.2.1 Number of layers (thickness effect)

This section views the effect of thickness on the mechanical characteristics of the specimens. As the number of fabric layers increases, the mechanical properties such as ultimate strength and cracked elastic modulus decrease due to a lower load efficiency. However, the material's ultimate force capacity and stiffness increased by increasing the number of fabric plies. Therefore, single-layer specimens showed better behaviour at ambient temperature compared to multiple-layered specimens.

4.3.2.1.1 Ambient target temperature

The curves shown in Fig 4-12 demonstrate the stress versus strain response of single and multiple-layered coupons at room temperature from selected representative samples. The gradual increase in the curve qualitatively shows the mechanical behaviour of FRCM at room temperature. The material's overall performance is identified with three main stages: pre-crack, crack propagation and post-crack. With regards to the pre-cracking stage, which is from the

beginning until 0.0004 strain, the specimen contributed to the load resistance with no drop in load, and the slope was steep; therefore, a higher stiffness was calculated. The graphs also clarify that the ultimate strength of a single-layered specimen was higher due to better efficiency and distribution of load in the fabric. Even though careful attention was taken at placing fabric in multiple layered specimens, some misalignments of fabric plies could cause varying stress distribution along the surface. All the curves show a gradual increase in strain at approximately constant load at the end of the test due to fabric slippage. For some specimens a drastic drop was observed due to the wide crack initiated by the load. The cracks observed in the tested coupons were within the gauge length and corresponded to the jagged drops in Figure 4-12. Cracked elastic modulus decreased with the increase in the number of layers.

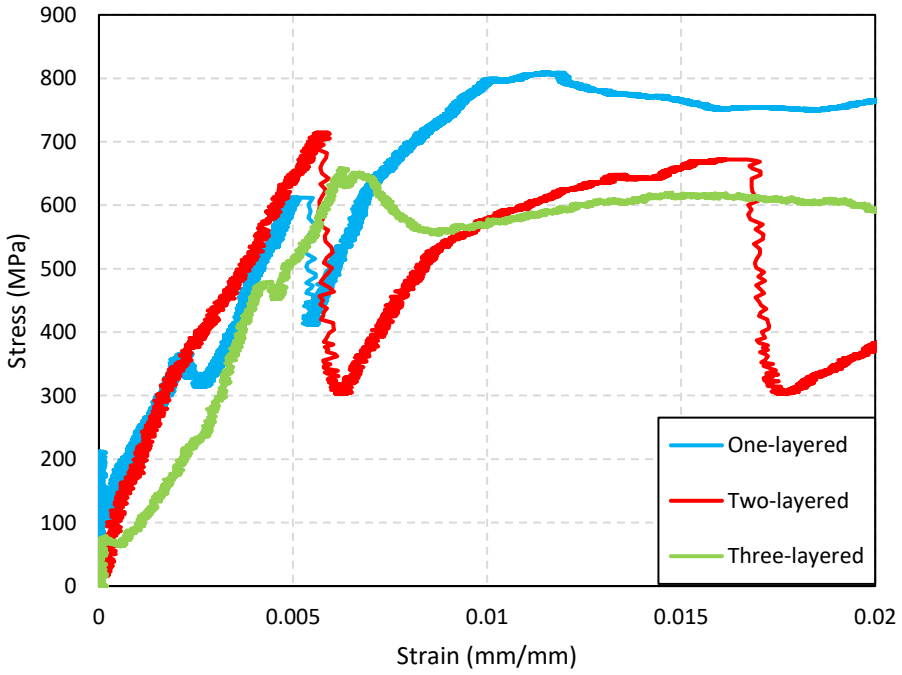

Figure 4-12: Stress-strain diagram for different number of layers at ambient temperature.

4.3.2.1.2 Target temperature at 100°C

The stress-strain curves of specimens heated to 100°C with regards to the number of layers are shown in Fig 4-13. The results show a consistent mechanical behaviour among single and multiple-layered specimens at different stages of loading. At 100°C, the specimens showed a slight reduction in ultimate load and post-crack stiffness with respect to tests conducted at room temperature. The curves shown in Fig 4-8 demonstrate a steep slope in the first stage, indicating a high-stiffness material resisting the applied load. When the first crack was initiated in the specimens, a drop in load was recorded, which is observable in the stress-strain diagram of the curves. Eventually, at 0.01 strain value, the fibres began to slip out of the surrounding matrix at

a constant load. This behaviour could be attributed to the clevis-grip loading mechanism used in this research and was concluded with the decrease in the stress value and increase in the crack width. The reduction in ultimate stress in the single-layered specimen was more significant than multiple-layered ones, demonstrating that temperature affected the ability of the fabric to carry high stresses. However, the different layers showed similar cracked elastic modulus at 100°C, resulting from a higher effect of high temperature on the thinner specimen. The crack development occurred at the last stage, resulting in a softening performance.

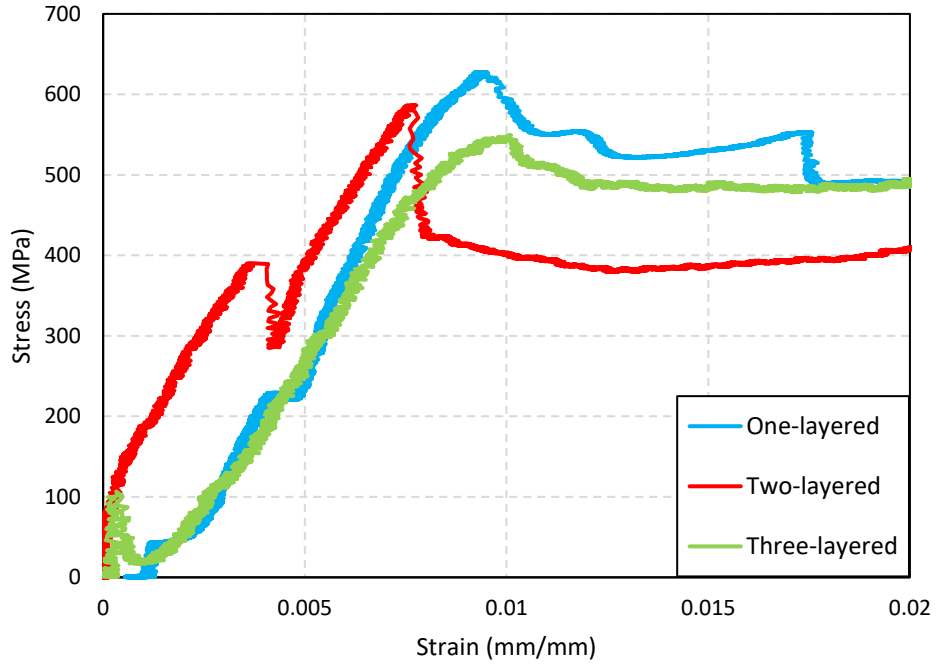

Figure 4-13: Stress-strain diagram for different number of layers at 100°C.

4.3.2.1.3 Target temperature at 200°C

Direct tensile tests were conducted at 200°C to identify the material capacity and compare the behaviour of different layers. Based on the graphs shown in Fig 4-14, all the specimens showed a high stiffness in the first stage with a drastic drop in the load contribution following the formation of the first crack. Regarding one and two-layered specimens, this first stage was followed by a less stiff behaviour until the peak load. In contrast, for the three-layered specimen, another drop in load occurred due to the formation of another crack. All the specimens showed a gradual fabric slippage and a decrease in the efficiency of the material in the last stage. In the tests conducted at 200°C, specimens with one and two layers of fabric could maintain a higher value of their strength. On the other hand, the reduction in ultimate strength for three-layered specimens was more severe. The cracked elastic modulus of one-layered specimens maintained the highest average value followed by two and three-layered samples.

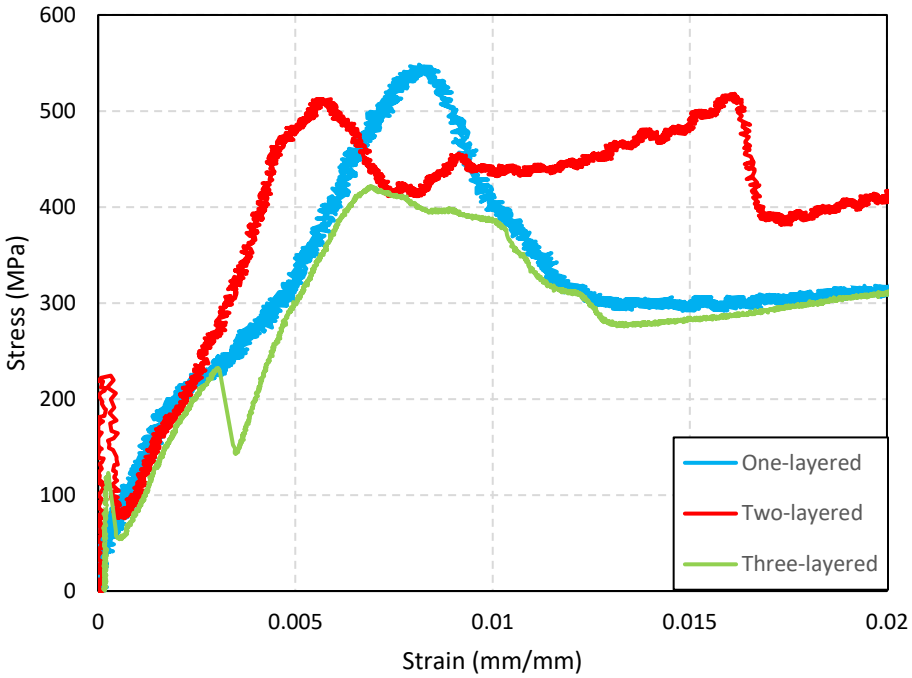

Figure 4-14: Stress-strain diagram for different number of layers at 200°C.

4.3.2.1.4 Target temperature at 300°C

Three different curves representing the different number of layers are depicted in the stress-strain curves corresponding to 300°C shown in Fig 4-15. All the specimens showed stiff behaviour at the beginning of the test. However, the load dropped following the initiation of a single crack. This drop was more significant in the case of the one-layered specimen. In the tests conducted at 300°C, the ultimate strength was reduced due to the influence of high temperature. In the post-cracked stage, the one layered specimens experienced a slight reduction in the bearing capacity. On the contrary, the specimen with two layers of fabric showed more fluctuation in stress towards the end of the test. Nonetheless, the three-plied specimen showed a gradual increase in strength. Moreover, three-layered specimens showed a higher reduction in the ultimate strength compared to one and two-layered specimens.

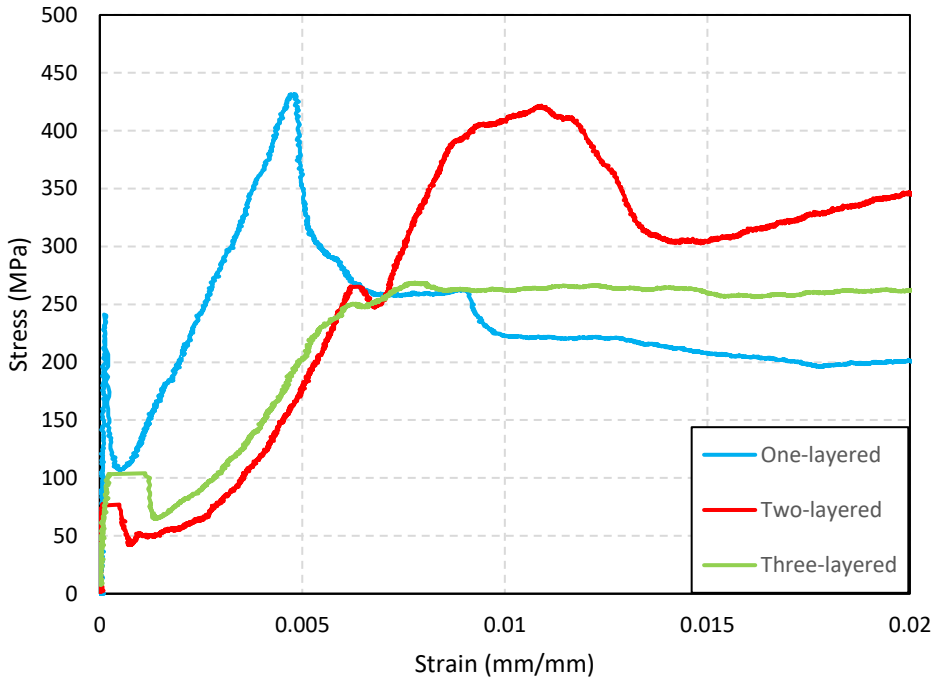

Figure 4-15: Stress-strain diagram for different number of layers at 300°C.

4.3.2.1.5 Target temperature at 400°C

FRCM coupons tested at 400°C showed a more gradual mechanical behaviour in the stress-strain curve due to the softening of the material at elevated temperatures as shown in Figure 4-16. In all the specimens, a more gradual drop in the stress was observed compared to room temperature and cracked elastic modulus decreased as well. Regarding the ultimate strength, single-layered specimens maintained their strength more than multiple-layered material. Even though the heating tests proved that fabric in thinner coupons was degraded more than thicker samples, the misalignment of embedded fabric layers could induce varying stress distribution. The samples experienced a gradual increase due to fabric slippage in the post-cracked stage, regardless of their thickness. The slippage was recognized due to a low stiff material and wide crack propagation within the gauge length.

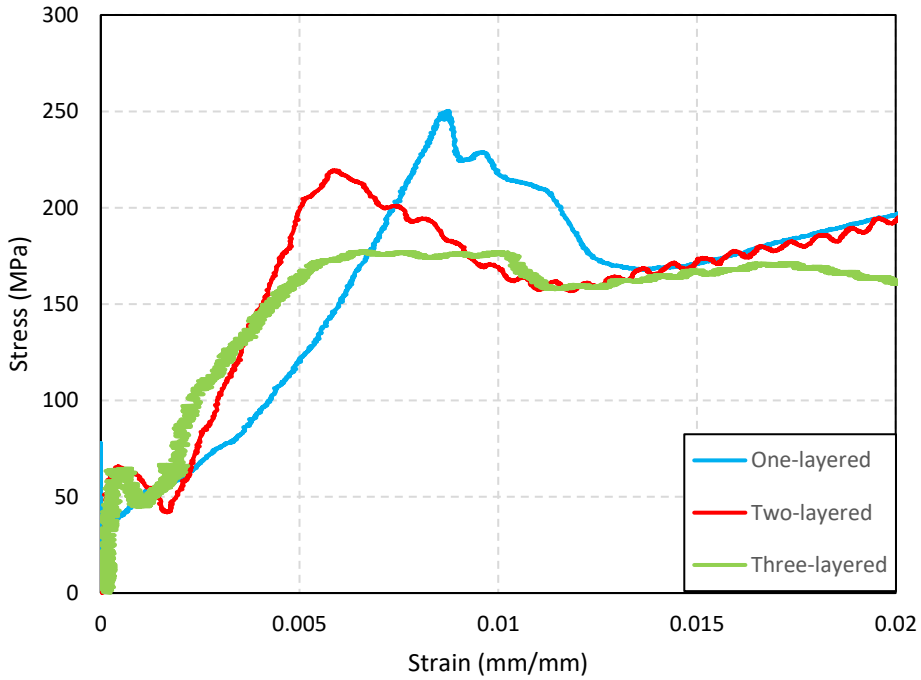

Figure 4-16: Stress-strain diagram for different number of layers at 400°C.

4.3.2.1.6 Crack development

Two main differences in the crack patterns were observed in the tests conducted for different specimen types at high temperatures. First, with the increase in the number of layers and thickness, the number of cracks inside the gauge length area decreased. The second important aspect is the location of the crack. The cracks induced by the applied load were nearer to the gripping area with thicker specimens. This location of the cracks could also result from a higher load causing a greater value of stress concentration in the thicker specimens.

In Fig 4-17, three specimens are illustrated; from right to left, one-layered, two-layered and three-layered specimens are shown. One layered specimens experienced three cracks in the gauge length; however, the main crack was close to the gripping length. With regards to the two-layered specimen, two cracks occurred. In the case of three-layered specimen, only one major crack close to the lower plate developed. Several cracks were typically observed in specimens reinforced with one layer fabric, while multiple-layered specimens failed due to one or two cracks.

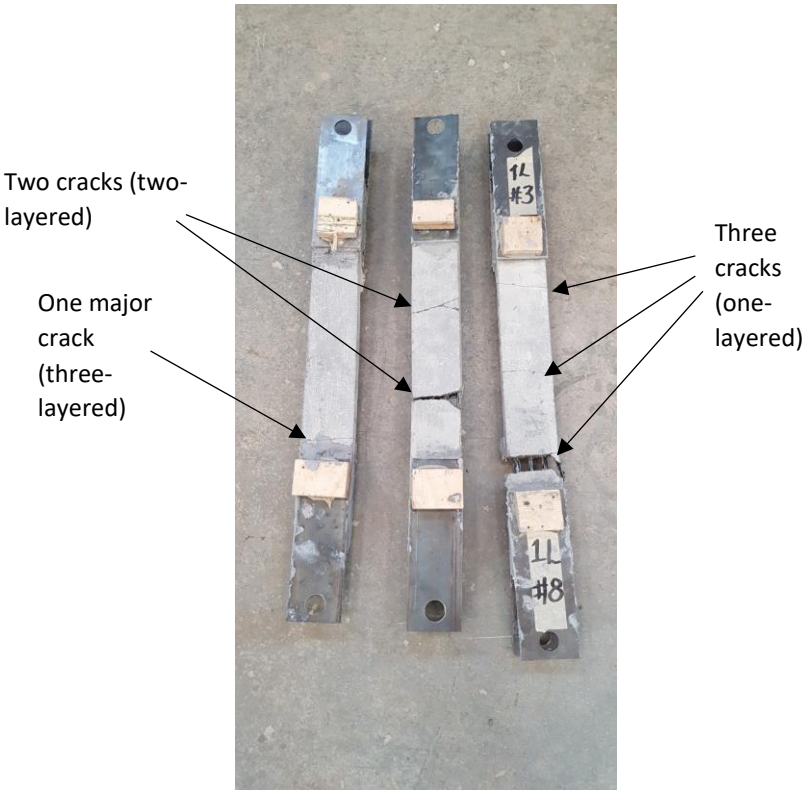

Figure 4-17: Crack patterns in tested specimens with different number of layers.

4.3.2.2 Orientation effect

Direct tensile tests were conducted to identify the differences in the mechanical performance of unidirectional and bidirectional specimens at elevated temperatures. The tests proved that bidirectional coupons showed a slightly higher level of ultimate stress value, which could be due to the stronger transverse fibre rows providing a better anchoring resistance for the fibres in the longitudinal direction. Moreover, the fibre area was lower than the unidirectional fabric which may improve bond with the cementitious matrix. However, the cracked elastic modulus of both materials was very similar. The results are discussed in more detail for each case of temperature exposure.

4.3.2.2.1 Ambient temperature

The tested specimens at ambient temperature demonstrated that both unidirectional and bidirectional specimens exhibited similar behaviour. In Figure 4-18, in the unidirectional coupon, three drops occurred, and eventually, a gradual decrease in the stress of the material was observed. This fall in the resistance was due to the slippage of fibres embedded in the specimen. Regarding the ultimate strength, the bidirectional specimen showed a higher average peak stress value. Both types of samples resulted in a three-phased stress-strain curve diagram. In the pre-cracked stage, both matrix and fabric were resisting the load. Following crack propagation, the fabric began to slip and reduce the load-bearing capacity of the material.

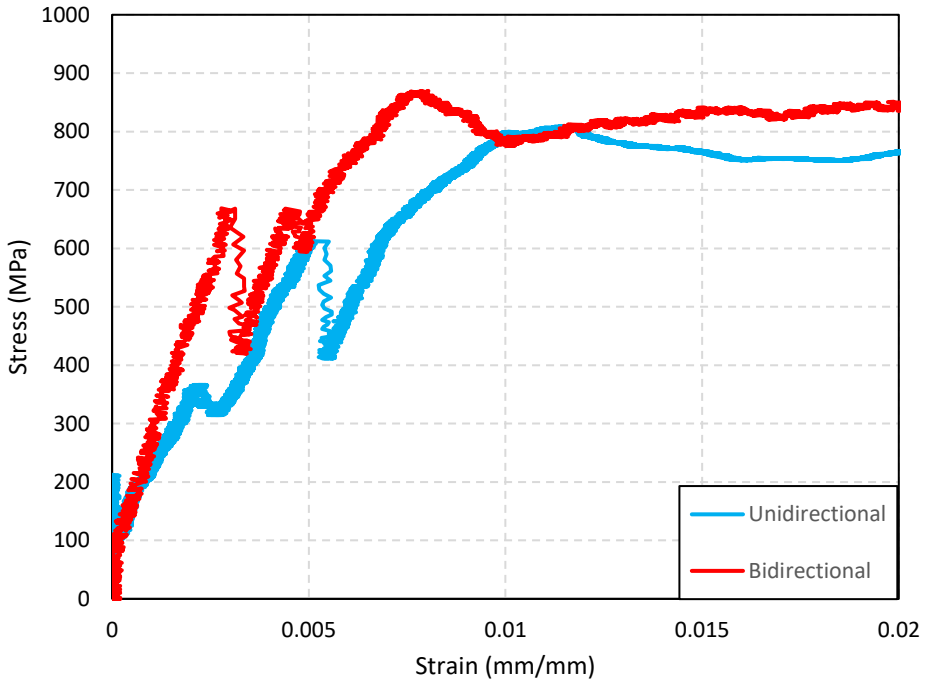

Figure 4-18: Stress-strain diagram for different orientations at ambient temperature.

4.3.2.2.2 Target temperature at 100°C

At 100°C, both unidirectional and bidirectional specimens maintained a relatively high proportion of their strength, as shown in Figure 4-19. Both types of specimens showed a similar behaviour compared to the tests conducted at room temperature. The drops caused by the crack initiation were less significant, and this behaviour could be an effect of the high temperature on the interface between the fabric and the matrix. Unidirectional specimens experienced a few slight drops and reached the ultimate load, then gradually decreased due to fabric slipping inside the specimen. However, in the case of bidirectional specimens, one reduction in stress was recorded,

and a more gradual behaviour was observed in all three stages. Finally, the nearly constant load resistance is demonstrated in the curve.

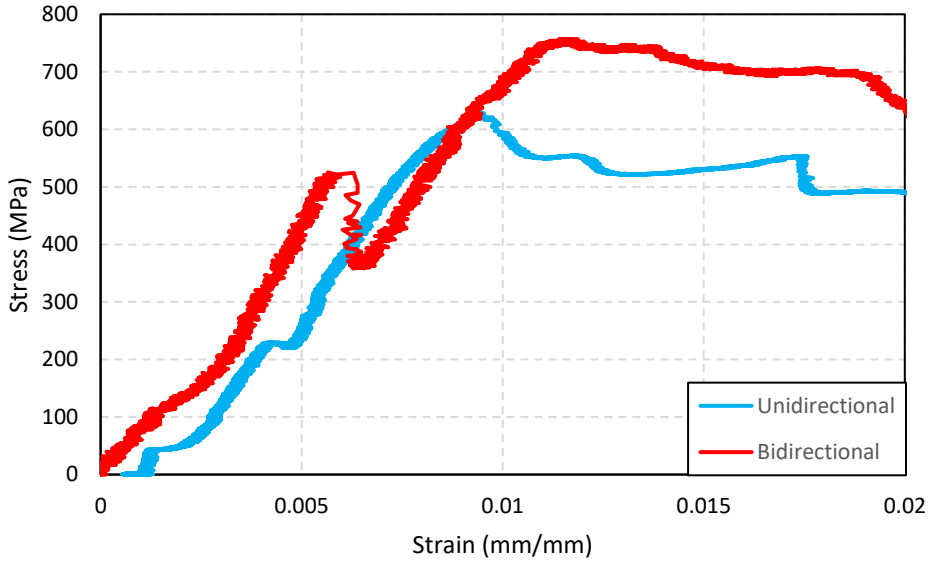

Figure 4-19: Stress-strain diagram for different orientations at 100°C.

4.3.2.2.3 Target temperature at 200°C

Direct tensile tests conducted at 200°C proved that with the increase in the temperature, less significant drop due to cracking occurred. This phenomenon is illustrated in Figure 4-20. Unidirectional specimens tested showed a gradual increase up to the peak stress followed by a decrease in the tensile stress. On the other hand, one crack occurred at a low strain in the bidirectional coupons, followed by a less stiff behaviour to the ultimate strength. Afterwards, following a reduction in load capacity to about 300 MPa, the specimens finally reached a gradual performance due to fibre slippage.

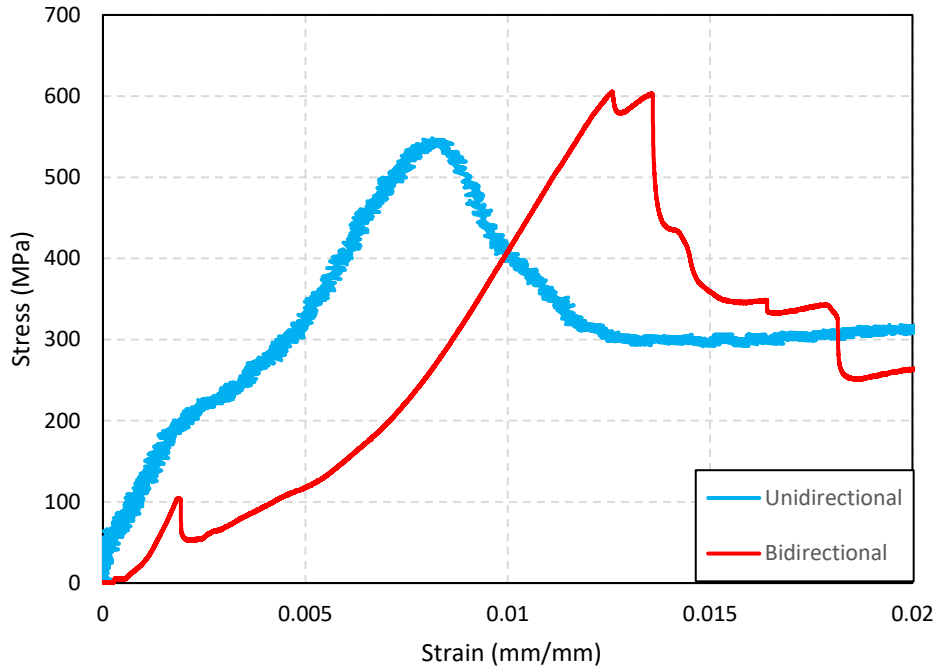

Figure 4-20: Stress-strain diagram for different orientations at 200°C.

4.3.2.2.4 Target temperature at 300°C

With regards to the tests carried out at 300°C, the performance of both unidirectional and bidirectional samples was degraded. This phenomenon is displayed in graphs shown in Figure 4-21. One crack occurred in both specimens at low strain; the mentioned drop was more significant in the case of unidirectional coupons. The bidirectional specimen showed a more gradual behaviour until peak strength, indicating that a less stiff material resisted the load. Therefore, a higher strain was measured at the peak stress of bidirectional coupons. On the other hand, unidirectional specimens reached their highest stress sooner with a greater slope and followed by a significant drop.

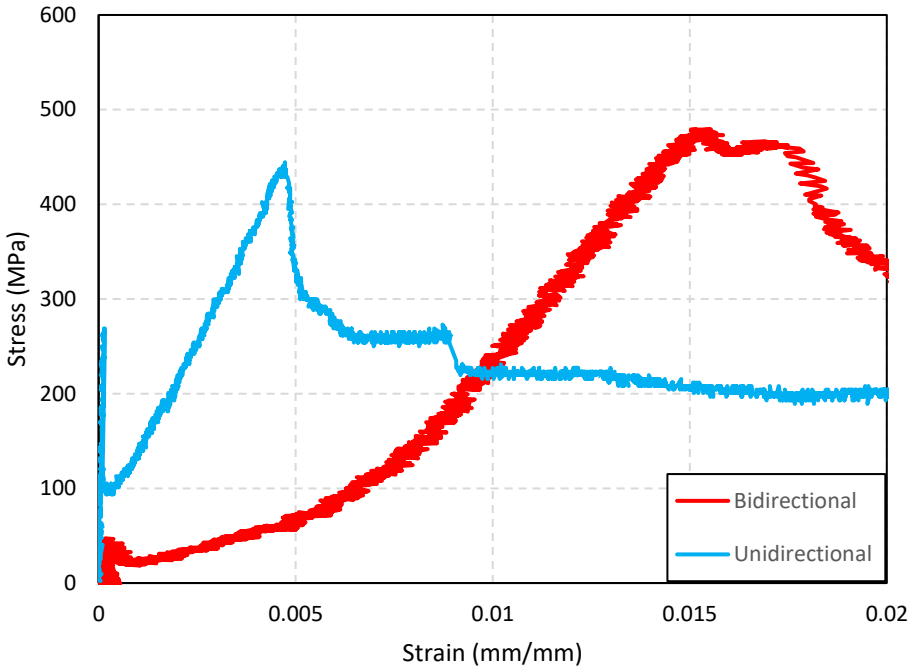

Figure 4-21: Stress-strain diagram for different orientations at 300°C.

4.3.2.2.5 Target temperature at 400°C

Based on the graphs shown in Figure 4-22, in the first stage the unidirectional specimens showed a drop at low displacement. In the second stage, the specimens continued to bear the load gradually until reaching the peak load and gradually lost strength. Finally, slippage occurred in the specimens with a gradual but slightly increasing slope. On the other hand, a crack initiated and propagated at a higher strain than that of unidirectional coupons regarding bidirectional specimens. With a decrease in the slope, the specimen kept resisting the load until the peak load, then the load gradually decreased and was followed by slippage of fabric.

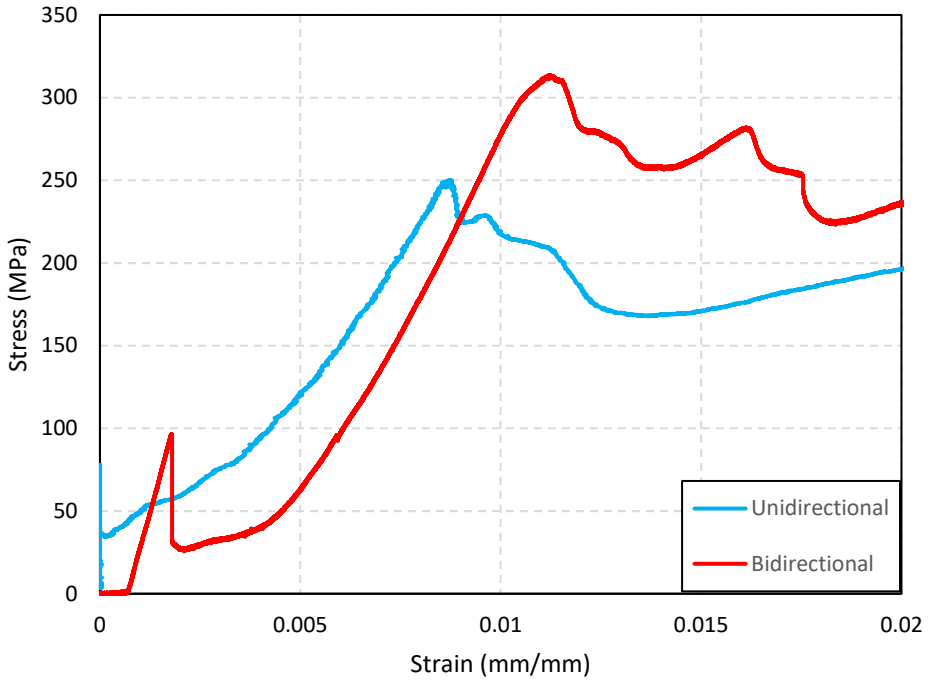

Figure 4-22: Stress-strain diagram for different orientations at 400°C.

4.3.2.3 Temperature effect

The number of tests conducted also allowed to compare the mechanical performance of each FRCM type with increasing temperature. This study simply showed the degrading effect of high temperature on the load-bearing capacity and overall behaviour of the samples. Based on the results, with the increase in the temperature, the ultimate strength, as well as cracked elastic modulus, were reduced; however, this decrease was more drastic in terms of ultimate strength. This section provides an understanding of the stress-strain curves of samples concerning elevated temperatures.

4.3.2.3.1 One-layered unidirectional

The data recorded from direct tensile tests of one-layered unidirectional specimens at the room to 400°C target temperature is shown in Figure 4-23. The ultimate strength was found to decrease significantly between tests conducted at ambient temperature compared to that of 100°C. The strain corresponding to ultimate stress was approximately 0.008 in most cases. However, in most cases of the 300°C samples, it is at 0.005. With the increase in the temperature, cracked elastic modulus decreased notably due to the low value of thickness. Samples tested at 400°C experienced a gradual increase of strength in the third stage, while, in other specimens, a decrease was observed.

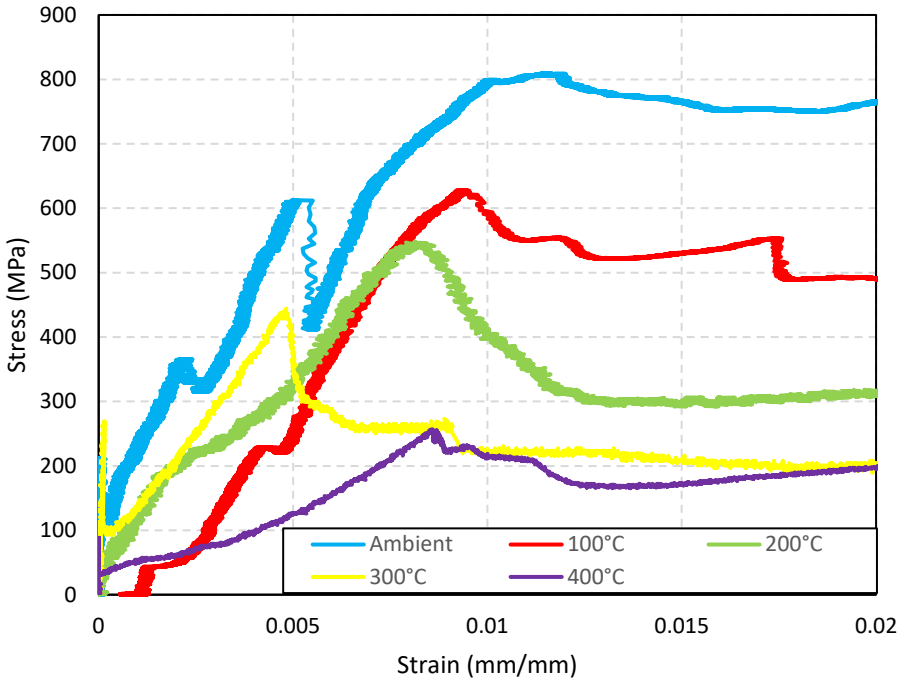

Figure 4-23: Stress-strain diagram of one-plied unidirectional specimens in different temperatures.

4.3.2.3.2 Two-layered unidirectional

With regards to the two-layered specimens tested at various temperatures, degrading occurred for both cracked elastic modulus and ultimate strength. The stress-strain curves of the conducted direct tensile tests are shown in Figure 4-24. With the increase in temperature, a drop in maximum strength is displayed due to the degrading of mechanical fabric properties at high temperatures. Another significant mechanical factor is cracked elastic modulus as a representative of serviceability. This value also decreased with temperature growth, indicating a more moderate slope until ultimate stress. The specimens showed a gradual decrease in the capacity due to fibre slippage that reduced the load; however, in tests conducted at ambient and 100°C, this phenomenon did not occur. This behaviour could result from low temperature and represent that fabric layers maintained their performance to some extent.

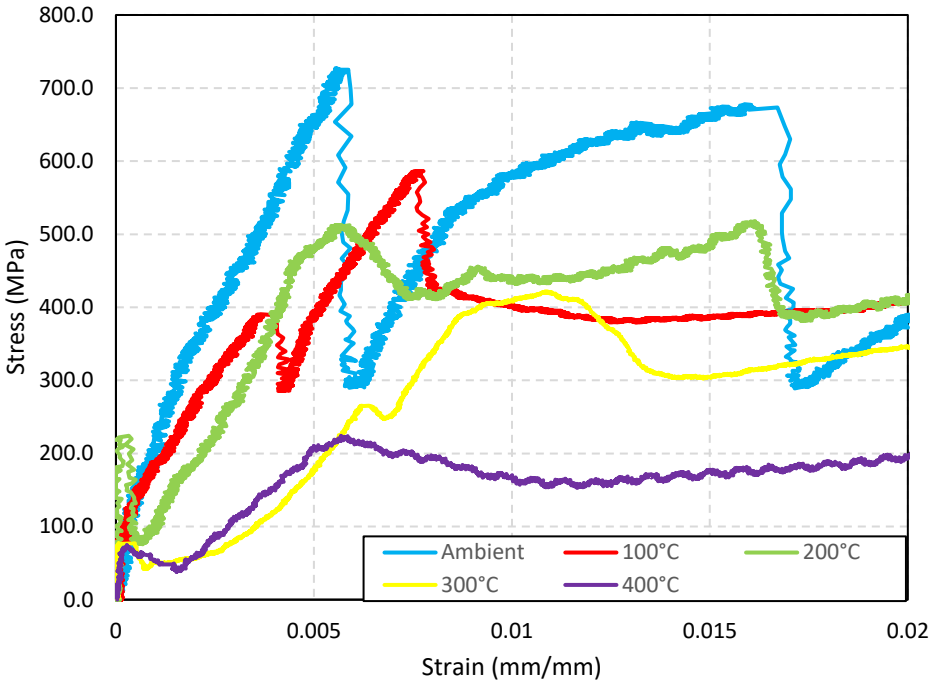

Figure 4-24: Stress-strain diagram of two-plied unidirectional specimens in different temperatures.

4.3.2.3.3 Three-layered unidirectional

The mechanical behaviour of three-layered FRCM coupons at ambient temperature and high temperature followed a similar behaviour as in one and two-layered coupons. Figure 4-25 illustrates the stress-strain performance of FRCM coupons at each temperature. The peak stress decreased with increasing temperature. Unlike the curves shown in Fig 4-19, the ultimate stress of three-layered samples did not experience a sharp drop at a particular temperature. With the increase in the temperature, the cracked elastic modulus decreased as well due to the effect of temperature. One crack initiated at low strain for all the specimens except for specimens conducted at 200°C. With regards to the slipping strength, different temperatures influenced the behaviour individually. Most specimens showed a nearly constant value of strength in the post-peak stage; nonetheless, specimens tested at 100, 200 and 400°C showed a decreasing, increasing and increasing value, in the same order.

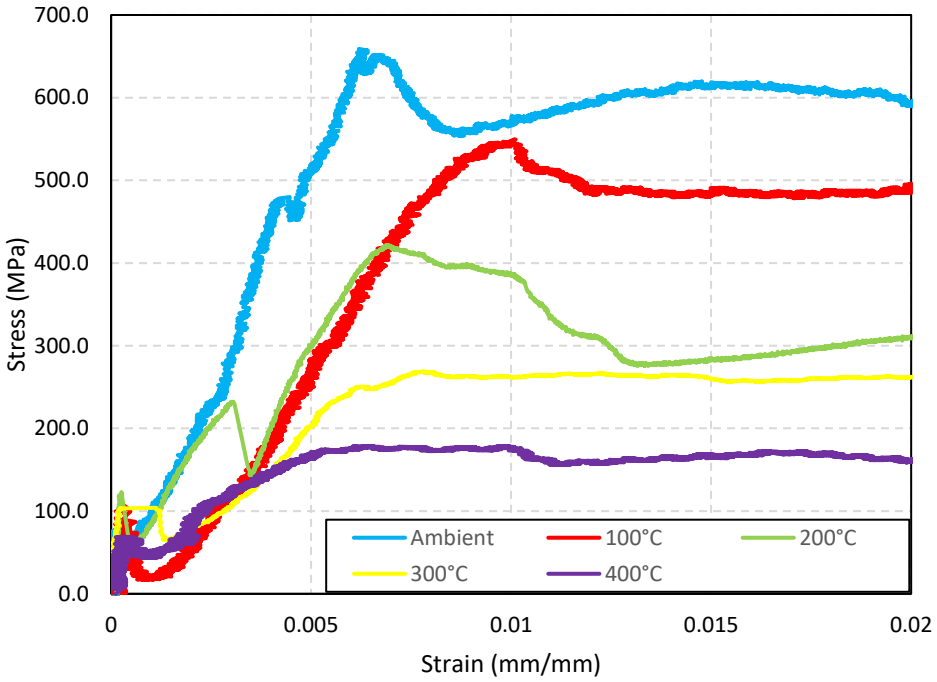

Figure 4-25: Stress-strain diagram of three-plied unidirectional specimens in different temperatures.

4.3.2.3.4 One-layered bidirectional

Figure 4-26 displays the stress-strain curves for bidirectional specimens at each particular temperature in order to compare them. With increasing temperature, the strain corresponding to ultimate stress was increased. Moreover, the specimens deformed more gradually until peak stress occurred, indicating a lower value of cracked elastic modulus induced by the high-temperature effect. The ultimate stress also decreased as a function of applied temperature. Regarding the post-cracked phase, most specimens except the tests conducted at ambient temperature exhibited a moderate increase due to slippage.

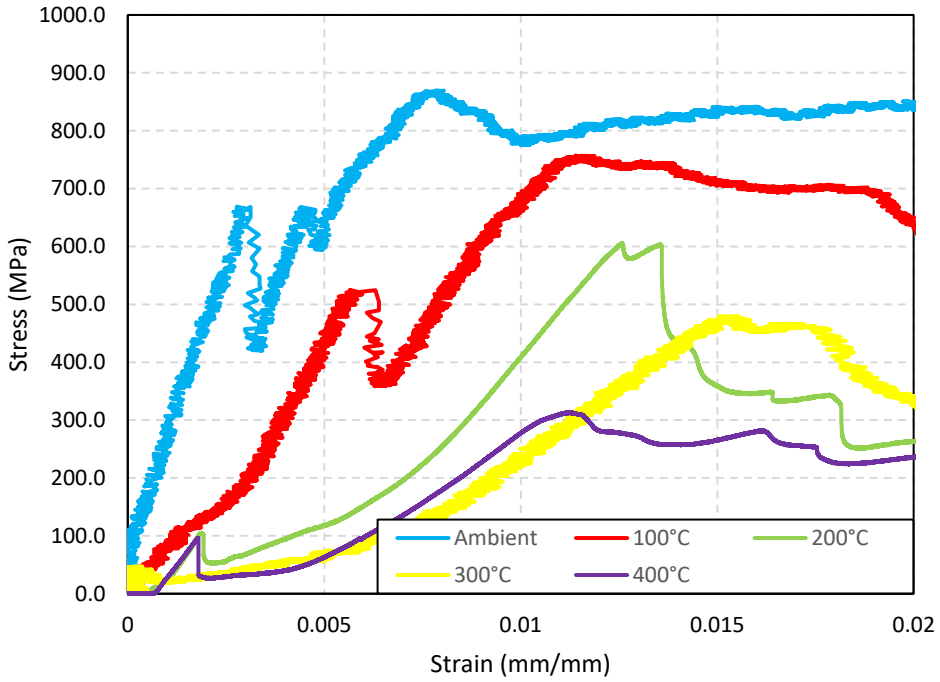

Figure 4-26: Stress-strain diagram of one-plied bidirectional specimen in different temperatures.

4.3.2.3.5 High-temperature effect on fibres

Following the tests, the mortar layers from selected specimens were crushed within the gauge length area to expose the fabric affected by temperature (Figure 4-27). At 100°C, the fabric kept its form and did not show visible signs of degradation. At 200°C, some of the fibres started to separate as the polymer resin began to disintegrate. In the case of coupon tested at 300°C, the fabric showed a high degree of degradation. This degradation significantly affected the mechanical behaviour of the material as it reduced the critical design parameters (peak strength, cracked elastic modulus). Nonetheless, the transverse plastic fibres were less affected and connected to the primary longitudinal fibre bundles. The highest temperature steady-state test at 400°C displayed a high value of degradation of the fibres in both directions. The epoxy resin was entirely destroyed, leaving the fibres to resist the load individually rather than as a composite material.

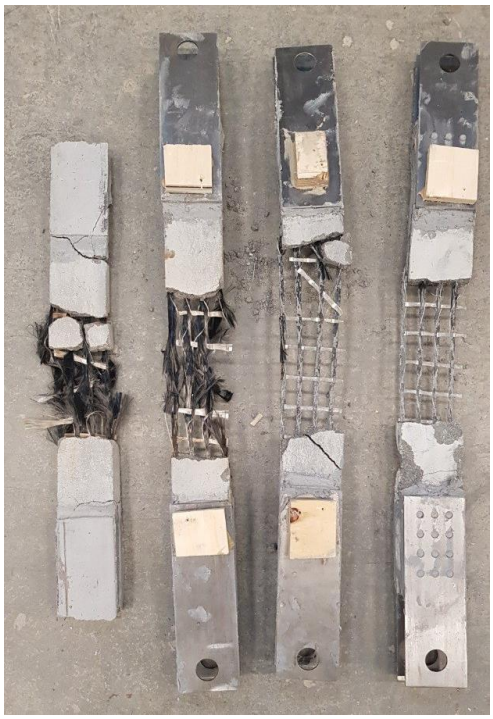

Figure 4-27: Fibre degradation due to high-temperature effect (left to right: 400, 300, 200, 100°C).

4.3.3 Transient-state condition

A total of 24 tests were conducted in the transient-state test to understand the real fire scenario in which the load is constant while temperature increases. In this section, two types of specimens were fabricated to be tested: one-layered 20-mm samples and one-layered 30-mm samples. In both of these types of specimens, one ply of fabric was placed in the mid-thickness of each specimen. This chapter aims to reveal the temperature at which failure occurred, and specimens could not carry the load.

The summary of transient test results is shown in Table 4-4, indicating primary outcomes such as failure mode and failure temperature. The sustained load was calculated first by conducting some ambient-temperature tests to reveal the ultimate strength of the specimens. Based on the results, all the specimens failed by fabric slippage within the surrounding cementitious matrix.

Generally, the critical temperature causing failure decreased with the increase in sustained load. With regards to the thicker samples, an improved insulation effect was observed, leading to the fabric grid requiring more time to reach critical temperature leading to failure. Therefore, the failure temperature was a higher value with regards to 30-mm samples compared to 20-mm samples.

Table 4-4: Summary of direct tensile tests on FRCM coupons in transient-state condition.

Sustain load (%)	Thickness (mm)	Number of layers	Orientation	Reinforcing ratio ρ_f (%)	Failure temperature (°C)		Failure mode
					Mean value	CoV (%)	
20	20	1	Unidirectional	0.85	467	0.1	S[(1)]
40	20	1	Unidirectional	0.85	352	0.1	S
60	20	1	Unidirectional	0.85	258	0.1	S
80	20	1	Unidirectional	0.85	112	0.2	S
20	30	1	Unidirectional	0.56	558	0.1	S
40	30	1	Unidirectional	0.56	447	0.1	S
60	30	1	Unidirectional	0.56	328	0.1	S
80	30	1	Unidirectional	0.56	162	0.1	S

(1) Slippage of fabric within the surrounding cementitious matrix.

4.3.3.1 *Thickness effect*

This section reviews the insulation effect provided by using a thicker layer of the cementitious matrix for FRCM strengthening. Figure 4-28 presents the failure temperature at which FRCM coupons could not continue resisting the load versus sustained load level. Trendlines were drawn in order to observe the linear decrease in the failure temperature as a function of the sustained load level. The black dotted and grey dotted trendlines represent 30 and 20 mm specimens, respectively. Based on the slope of the line, it is observable that with the increase in sustained load, the critical temperature of the various specimens converged. This behaviour indicates that insulation provided by thicker mortar layers was less efficient at high sustained load levels, which is expected since the failure load at ambient temperature is expected to be the same for both sets of one-layer specimens. Higher loads also correspond to wider cracks which increases heat penetration to the fabric layer. In other words, fibres are more susceptible to being degraded by the elevated temperature at a high value of the load, even with a thick layer confining them. Nevertheless, casting thicker samples appeared to improve their fire resistance at all load levels.

In order to compare the results of the tests achieved in both steady-state and transient-state conditions, the data obtained from unidirectional one-layered specimens in steady-state was added as well. In Figure 4-28, the green data points represent the tests conducted in the steady-state condition. Based on the results, the trendline that approximately showed the slope of the data points from steady-state was almost identical to the tests conducted at transient-state conditions. This indicated that the results obtained were consistent.

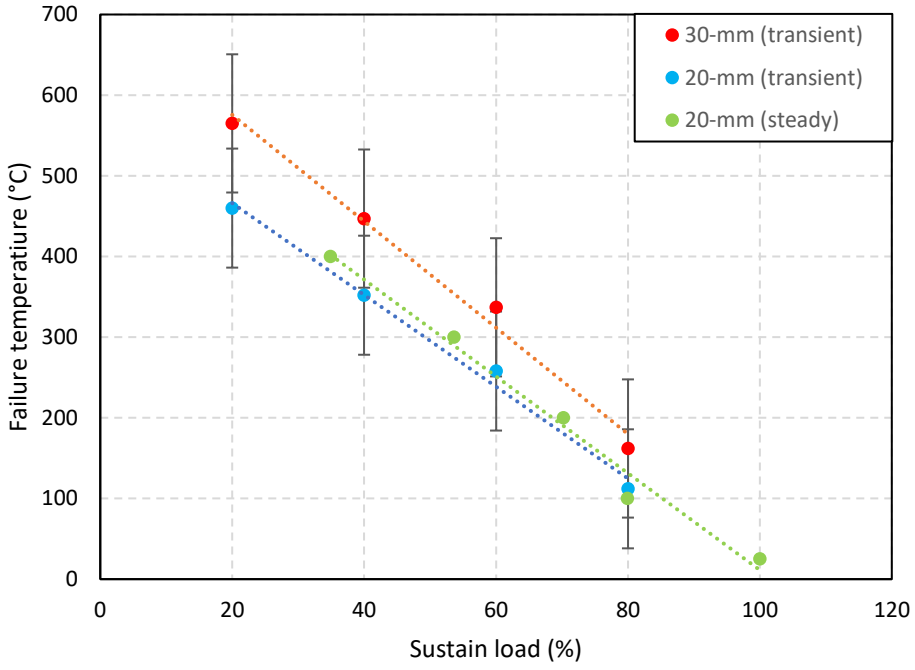

Figure 4-28: Temperature versus sustained load level for specimens with different thicknesses.

DISCUSSION

4.4 Restating the aim of the study

The purpose that this study tried to address is how FRCM composite materials behave when exposed to elevated temperatures and subjected to tensile stresses. Even though many studies have revealed the tensile behaviour of FRCM as well as its strengthening applications, few investigations focused on the thermal behaviour of FRCM. Therefore, this study investigated this performance by conducting tensile tests and utilizing heating tape to provide a fire-simulated condition. The entire research was divided into two main types of tests: steady-state and transient-state conditions. In steady-state conditions, the temperature was held constant, and load increased, which is similar to most other research studies examining the behaviour of construction materials at elevated temperatures. On the other hand, in the transient-state study, the tests attempted to bridge a closer gap from the research to a real fire scenario by keeping the load constant and increasing temperature.

The parameters in this study were selected based on a review of the literature to determine which aspects of a design are most likely to influence high temperature behaviour. One of the parameters was the number of fabric layers, which led to different thicknesses of the specimens. This parameter was chosen to reveal whether increasing the number of layers will correspondingly increase the capacity. Moreover, this parameter also helped identify the effects of temperature on inner fabric layers. Another primary variable was orientation, in which unidirectional and bidirectional specimens were manufactured. The reason to use various fabric configurations was to identify the effect of transverse fabric on the performance of the FRCM. Lastly, one parameter was chosen in transient-state in which the number of fabric layers stayed the same while thickness increased. This parameter shows the effect of insulation on the fire performance of the FRCM.

4.5 Summarizing the key findings

The results obtained from analyzing the data identified a better concept of FRCM performance at elevated temperatures. Although a more detailed summary is provided in the conclusion section, the critical qualitative findings that this experimental research achieved throughout the tests are briefly reviewed to facilitate a discussion of their design implications:

- In the set of heating tests conducted on the FRCM coupons, the thickness of the mortar layer provided between each layer of fabric showed a significant insulation effect on transferring the heat. As a result, the cementitious matrix played a key role concerning maintaining the integrity of FRCM coupons.
- In the loading tests conducted on the specimens, FRCM composite systems proved to show a promising behaviour when exposed to fire. This result was obtained from

monitoring two key mechanical outcomes (ultimate strength, cracked elastic modulus) that define the material's resistance. FRCM showed a pronounced reduction in strength at high temperatures but maintained approximately 50% of their tensile capacity at temperatures as high as 300°C under steady state conditions. This suggests that FRCM strengthening systems could continue to contribute to load resistance for a certain period of time during a fire event (although further testing on bond capacity and full-scale structural members is needed to verify this point). The transient state tests confirmed that by increasing the thickness of the mortar layer (using a 15 mm cover rather than 10 mm), the performance of the system improved, since 50% load capacity corresponded to a temperature of roughly 375°C.

- Increasing the number of layers showed a decrease in mechanical properties and efficiency of fabric, even though the ultimate force capacity increased. Moreover, by comparing different fabric configurations (unidirectional, bidirectional), FRCM showed that retained mechanical behaviour of carbon FRCM at high temperatures was nearly similar for the materials considered in this study.

By comparing the data from 84 tests on FRCM specimens, this material demonstrated a relatively good performance at elevated temperatures compared to composites made with polymeric resins. The promising behaviour of the fabric in retaining the capacity of the material accompanied with the insulation effect provided by the cementitious matrix can lead to more effective strengthening solutions for structures that must consider fire safety.

4.6 Interpretation of the findings in practice

The performance of structural members and their degradation in potential fire scenarios is an important consideration for design. One of the most significant aspects of FRCM research is its broad suitability to various types of applications. Even though this research provided a scientific approach towards the subject of FRCM composite systems, the investigation outcomes can be interpreted in more practical applications. It is important to note, however, that any quantitative findings of this study should not be generalized to all FRCM systems or configurations and should be considered relevant only for the specific material types and layer thicknesses considered in this work. It is recommended that any FRCM system that is used for structural strengthening be first tested on large-scale structural members under standard fire conditions, or if no data is available its contribution in a fire scenario should be neglected. Nevertheless, some qualitative observations and trends may be applicable and can be used to provide some preliminary recommendations for design. All of the following preliminary recommendations should be verified through large scale testing.

It is likely that the tensile strength reductions observed in this research study are more severe than would be observed in practice with the same material and thicknesses. In these tests, the heat was applied uniformly from all exposed surfaces due to the wrapping configuration of the

heating tape. In real strengthening applications, heat exposure would occur from only one side and therefore inner layers of fabric would benefit from a greater degree of insulation compared to the coupons tested in this project. Hence, applying the results of this study to structural strengthening applications is expected to yield conservative results if the failure mode is governed by the tensile strength of the FRCM; however, other possible failure modes (such as anchorage failure) are outside the scope of this thesis.

It is clear from the test results that an important aspect affecting the behaviour of FRCM at high temperatures is the amount of insulation provided by the cementitious matrix. The greater the thickness of the matrix, the higher amount of time is required for the inner fabric to degrade. Hence, design provisions should specify minimum thicknesses for FRCM systems. The results of this research showed that FRCM can lose up to 50% of its tensile strength when the fabric reaches a temperature of 300°C. Therefore, for structures that may be exposed to fire, it is recommended to a) limit stresses in the FRCM to no more than 40% of their nominal ultimate strength under unfactored service loads (assuming an acceptably low probability of simultaneous overloading and fire) and b) provide sufficient thickness of the outer mortar layer to ensure that the structure can be evacuated before the outer fabric layer reaches the critical temperature of 300°C (15 mm for the outer layer is recommended as a minimum thickness for preliminary design purposes, although thermal modelling or experimental testing using standard fire time-temperature curves is required to verify this value). If either of these design conditions cannot be met, it should be assumed that the FRCM fabric will not contribute to load resistance during a fire but may provide benefit as an insulating layer to protect the internal reinforcement in the concrete member.

4.7 **Limitations of the study**

The current study focused exclusively on tensile properties of a commercially available carbon FRCM system with different number of fabric layers. This is an important preliminary step towards the eventual development of rational design guidelines. However, considering the intended scope of this research, the following limitations should be noted:

- The findings of this study should not be generalized to other FRCM systems or layer thicknesses;
- Failure modes governed by bond or shear have not been considered. Furthermore, additional crack openings caused by bending, which could possibly accelerate heat penetration, were not a factor in this study;
- Non-standard test and heating setups were used in this study. Therefore, the data cannot be used to estimate fire ratings for design purposes. All design recommendations should be understood as preliminary and should be verified with large-scale testing.

5 CONCLUSIONS

The experimental investigation explained in this thesis focused on the effectiveness of fabric-reinforced cementitious matrix (FRCM) at elevated temperature in order to provide a more comprehensive behaviour in fire scenarios of this innovative material for designers and engineers.

As a result, 84 specimens were tested to identify their performance. Nine specimens were heated to realize the temperature gradient inside the specimen; theses specimens were not loaded and only the temperature propagation was observed and quantified. Sixty specimens were tested under a steady-state condition, and the effects number of layers, orientation, and temperatures were studied. The remaining 24 specimens were tested under a transient-state condition.. Moreover, Several cubic samples of the cementitious matrix were fabricated to provide an understanding of the compressive behaviour. Based on the analyses in mechanical behaviour, the following conclusions were drawn:

- Under the heating setup used in this research, the heating tests demonstrated that the soak time required for the inner fabric to reach a relatively stable temperature was approximately 45 minutes for all specimens. As a result, this additional time was taken into account for tests conducted at the steady-state conditions to provide a consistent behaviour.
- With regards to the steady-state condition, the ultimate tensile strength and cracked elastic modulus were investigated as two prominent representatives of the mechanical behaviour of the FRCM. The FRCM system used in this research showed a linear reduction in tensile capacity with increasing temperature and retained 50% of its tensile capacity at temperatures as high as 300°C, regardless of number of layers or fabric orientation. The cracked elastic modulus at high temperatures varied according to the number of fabric layers, ranging from about 40 to 60% of their original room temperature values at 400°C. In terms of orientation effects, bidirectional specimens showed a higher ultimate strength value. For example, in room temperature bidirectional specimens failed at 882 MPa compared to 791 MPa recorded in unidirectional specimens. However, regarding the cracked elastic modulus bidirectional specimens showed a slightly less value as 59500 MPa, while unidirectional specimens resulted in 60200 MPa value in ambient temperature. At 400°C, unidirectional and bidirectional specimens resulted in 295 and 276 MPa as peak strength. The corresponding elastic modulus for unidirectional and bidirectional specimens was 24700 and 24800 MPa. This performance was due to the carbon transversal fibres anchoring the main longitudinal fabric in place more effectively and a more effective bond transfer mechanism with the cementitious matrix. Regardless of the specimen type, failure occurred by fabric slippage for all specimens; this could be attributed to the clevis-grip loading mechanism utilized in this research.

- Transient-state specimens had only one fabric layer with a total thickness of either 20 mm or 30 mm. In this condition, the insulation effect was observed, with a significant increase in the external temperature at failure for the thicker samples. The critical temperature corresponding to a 50% load level increased from 300°C in the 20 mm specimens to approximately 375°C in the 30 mm samples. In all the specimens, the main failure mode was slippage of fabric within the matrix; however, the critical temperature at failure increased with a decrease in the sustained load level.

6 RECOMMENDATIONS FOR FUTURE STUDIES

This thesis presented a preliminary study on the unknown tensile behaviour of FRCM at elevated temperatures. There remain several related subjects with respect to FRCM systems that require further investigation. These areas of research include:

1. It is recommended to study the bond performance of FRCM at high temperatures to determine critical parameters in anchorage regions.
2. The fire performance of large-scale FRCM-strengthened structural members is needed to verify the findings of this study and lead to the development of rational design guidelines.
3. Investigations of other FRCM systems considering different material types, fabric spacing, surface treatments, and other parameters are essential to extract general trends that can be used in design.
4. The residual performance of this material in the post-fire stage should be studied to understand the safety of strengthened structures following fire exposure. This will provide better knowledge for FRCM performance in the applications in which members were already exposed to high temperatures.
5. A detailed finite element investigation regarding high temperature is highly recommended due to the lack of studies to model this behaviour numerically.
6. Studies focusing on FRCM reinforced with prestressed fabric are also an area of investigation that has not been studied sufficiently. Therefore, research on this subject is also encouraged.
7. Different loading conditions, including the cyclic behaviour of FRCM, are also recommended to provide a better understanding of different load combinations in real applications.
8. Tensile tests investigations focusing on Digital Image Correlate (DIC) as a new non-contact technique to measure stress concentration and crack pattern more precisely also could be an interesting subject. This was not possible in the current study due to the presence of the heating tape which obscured the test specimens from view during the tests.

7 REFERENCES

Akbari Hadad, H., and A. Nanni. 2020. “Fatigue Behavior of FRCM-Strengthened RC Beams.” *J. Compos. Constr.,* 24 (6): 04020074. American Society of Civil Engineers. https://doi.org/10.1061/(ASCE)CC.1943-5614.0001084.

Alabdulhady, M. Y., and L. H. Sneed. 2018. “A study of the effect of fiber orientation on the torsional behavior of RC beams strengthened with PBO-FRCM composite.” *Constr. Build. Mater.,* 166: 839–854. https://doi.org/10.1016/j.conbuildmat.2018.02.004.

Alabdulhady, M. Y., L. H. Sneed, and C. Carloni. 2017. “Torsional behavior of RC beams strengthened with PBO-FRCM composite – An experimental study.” *Eng. Struct.,* 136: 393–405. https://doi.org/10.1016/j.engstruct.2017.01.044.

Aljazaeri, Z. R., M. A. Janke, and J. J. Myers. 2019. “A novel and effective anchorage system for enhancing the flexural capacity of RC beams strengthened with FRCM composites.” *Compos. Struct.,* 210: 20–28. https://doi.org/10.1016/j.compstruct.2018.10.110.

Aljazaeri, Z. R., and J. J. Myers. 2017. “Strengthening of Reinforced-Concrete Beams in Shear with a Fabric-Reinforced Cementitious Matrix.” *J. Compos. Constr.,* 21 (5): 04017041. American Society of Civil Engineers. https://doi.org/10.1061/(ASCE)CC.1943-5614.0000822.

Aljazaeri, Z. R., and J. J. Myers. 2018. “Flexure Performance of RC One-Way Slabs Strengthened with Composite Materials.” *J. Mater. Civ. Eng.,* 30 (7): 04018120. American Society of Civil Engineers. https://doi.org/10.1061/(ASCE)MT.1943-5533.0002299.

Al-Salloum, Y. A., and T. H. Almusallam. 2003. “Rehabilitation of the Infrastructure Using Composite Materials: Overview and Applications.” *J. King Saud Univ. - Eng. Sci.,* 16 (1): 1–20. https://doi.org/10.1016/S1018-3639(18)30777-3.

Al-Salloum, Y. A., T. H. Almusallam, H. M. Elsanadedy, and R. A. Iqbal. 2016. “Effect of elevated temperature environments on the residual axial capacity of RC columns strengthened with different techniques.” *Constr. Build. Mater.,* 115: 345–361. https://doi.org/10.1016/j.conbuildmat.2016.04.041.

Al-Salloum, Y. A., H. M. Elsanadedy, and A. A. Abadel. 2011a. “Behavior of FRP-confined concrete after high temperature exposure.” *Constr. Build. Mater.,* 25 (2): 838–850. https://doi.org/10.1016/j.conbuildmat.2010.06.103.

Al-Salloum, Y. A., H. M. Elsanadedy, and A. A. Abadel. 2011b. “Behavior of FRP-confined concrete after high temperature exposure.” *Constr. Build. Mater.,* Composite Materials and Adhesive Bonding Technology, 25 (2): 838–850. https://doi.org/10.1016/j.conbuildmat.2010.06.103.

Arboleda, D., F. G. Carozzi, A. Nanni, and C. Poggi. 2016. “Testing Procedures for the Uniaxial Tensile Characterization of Fabric-Reinforced Cementitious Matrix Composites.” *J. Compos. Constr.,* 20 (3): 04015063. https://doi.org/10.1061/(ASCE)CC.1943-5614.0000626.

Ascione, L., F. G. Carozzi, T. D’Antino, and C. Poggi. 2018. “New Italian guidelines for design of externally bonded Fabric-Reinforced Cementitious Matrix (FRCM) systems for repair and strengthening of masonry and concrete structures.” *Procedia Struct. Integr.,* 11: 202–209. https://doi.org/10.1016/j.prostr.2018.11.027.

Ascione, L., G. de Felice, and S. De Santis. 2015. “A qualification method for externally bonded Fibre Reinforced Cementitious Matrix (FRCM) strengthening systems.” *Compos. Part B Eng.*, 78: 497–506. https://doi.org/10.1016/j.compositesb.2015.03.079.

Azam, R., and K. Soudki. 2014. “FRCM Strengthening of Shear-Critical RC Beams.” *J. Compos. Constr.*, 18 (5): 04014012. American Society of Civil Engineers. https://doi.org/10.1061/(ASCE)CC.1943-5614.0000464.

Babaeidarabad, S., G. Loreto, D. Arboleda, and A. Nanni. 2014a. *Flexural Behavior of RC Beams Strengthened with Fabric-reinforced-cementitious-matrix (FRCM) Composite*. *Proc. 7th Int. Conf. FRP Compos. Civ. Eng. CICE 2014*.

Babaeidarabad, S., G. Loreto, and A. Nanni. 2014b. “Flexural Strengthening of RC Beams with an Externally Bonded Fabric-Reinforced Cementitious Matrix.” *J. Compos. Constr.*, 18 (5): 04014009. American Society of Civil Engineers. https://doi.org/10.1061/(ASCE)CC.1943-5614.0000473.

Bellini, A., M. Bovo, and C. Mazzotti. 2019a. “Experimental and numerical evaluation of fiber-matrix interface behaviour of different FRCM systems.” *Compos. Part B Eng.*, 161: 411–426. https://doi.org/10.1016/j.compositesb.2018.12.115.

Bellini, A., S. K. Shahreza, and C. Mazzotti. 2019b. “Cyclic bond behavior of FRCM composites applied on masonry substrate.” *Compos. Part B Eng.*, 169: 189–199. https://doi.org/10.1016/j.compositesb.2019.04.009.

Bernat-Maso, E., L. Gil, L. Mercedes, and C. Escrig. 2018. “Mechanical properties of pre-stressed fabric-reinforced cementitious matrix composite (PFRCM).” *Constr. Build. Mater.*, 191: 228–242. Elsevier B.V. https://doi.org/10.1016/j.conbuildmat.2018.09.210.

Bilotta, A., F. Ceroni, G. P. Lignola, and A. Prota. 2017a. “Use of DIC technique for investigating the behaviour of FRCM materials for strengthening masonry elements.” *Compos. Part B Eng.*, 129: 251–270. https://doi.org/10.1016/j.compositesb.2017.05.075.

Bilotta, A., F. Ceroni, E. Nigro, and M. Pecce. 2017b. “Experimental tests on FRCM strengthening systems for tuff masonry elements.” *Constr. Build. Mater.*, 138: 114–134. Elsevier B.V. https://doi.org/10.1016/j.conbuildmat.2017.01.124.

Bisby, L. 2016. “7 - Fire resistance of textile fiber composites used in civil engineering.” *Text. Fibre Compos. Civ. Eng.*, T. Triantafillou, ed., 169–185. Woodhead Publishing.

Bisby, L. A., T. J. Stratford, E. C. Roy, and M. Ward. 2009. “Fibre Reinforced Cementitious Matrix Systems for Fire-Safe Flexural Strengthening of Concrete: Pilot Testing at Ambient Temperatures.” *Adv. Compos. Constr. ACIC 2009 Conf. Proc.*, 449–460. NetComposites Ltd.

Bisby, L., T. Stratford, C. Hart, and S. Farren. 2013. “Fire performance of well-anchored TRM, FRCM and FRP flexural strengthening systems.” *Adv. Compos. Constr. 2013 ACIC 2013 - Conf. Proc.*

Borwankar, A. n.d. “FRCM is in the same family as FRP, but it differs in how it’s installed and how it benefits certain applications.” 36.

Caggegi, C., F. G. Carozzi, S. De Santis, F. Fabbrocino, F. Focacci, Ł. Hojdys, E. Lanoye, and L. Zuccarino. 2017a. “Experimental analysis on tensile and bond properties of PBO and aramid fabric reinforced cementitious matrix for strengthening masonry structures.” *Compos. Part B Eng.*, 127: 175–195. https://doi.org/10.1016/j.compositesb.2017.05.048.

Caggegi, C., E. Lanoye, K. Djama, A. Bassil, and A. Gabor. 2017b. “Tensile behaviour of a basalt TRM strengthening system: Influence of mortar and reinforcing textile ratios.” *Compos. Part B Eng.*, 130: 90–102. https://doi.org/10.1016/j.compositesb.2017.07.027.

Calabrese, A. S., T. D'Antino, C. Poggi, P. Colombi, G. Fava, and M. A. Pisani. 2020. "Application of Externally Bonded Inorganic-Matrix Composites to Existing Masonry Structures." *Build. Educ. Multidiscip. Overv. Des. Sch. Build.*, Research for Development, S. Della Torre, M. Bocciarelli, L. Daglio, and R. Neri, eds., 283–292. Cham: Springer International Publishing.

Carozzi, F. G., A. Bellini, T. D'Antino, G. de Felice, F. Focacci, Ł. Hojdys, L. Laghi, E. Lanoye, F. Micelli, M. Panizza, and C. Poggi. 2017a. "Experimental investigation of tensile and bond properties of Carbon-FRCM composites for strengthening masonry elements." *Compos. Part B Eng.*, 128: 100–119. https://doi.org/10.1016/j.compositesb.2017.06.018.

Carozzi, F. G., A. Bellini, T. D'Antino, G. de Felice, F. Focacci, Ł. Hojdys, L. Laghi, E. Lanoye, F. Micelli, M. Panizza, and C. Poggi. 2017b. "Experimental investigation of tensile and bond properties of Carbon-FRCM composites for strengthening masonry elements." *Compos. Part B Eng.*, 128: 100–119. https://doi.org/10.1016/j.compositesb.2017.06.018.

Carozzi, F. G., and C. Poggi. 2015. "Mechanical properties and debonding strength of Fabric Reinforced Cementitious Matrix (FRCM) systems for masonry strengthening." *Compos. Part B Eng.*, 70: 215–230. https://doi.org/10.1016/j.compositesb.2014.10.056.

de Carvalho Bello, C. B., I. Boem, A. Cecchi, N. Gattesco, and D. V. Oliveira. 2019. "Experimental tests for the characterization of sisal fiber reinforced cementitious matrix for strengthening masonry structures." *Constr. Build. Mater.*, 219: 44–55. https://doi.org/10.1016/j.conbuildmat.2019.05.168.

Cascardi, A., F. Micelli, and M. A. Aiello. 2018. "FRCM-confined masonry columns: experimental investigation on the effect of the inorganic matrix properties." *Constr. Build. Mater.*, 186: 811–825. https://doi.org/10.1016/j.conbuildmat.2018.08.020.

Cerniauskas, G., Z. Tetta, D. Bournas, and L. Bisby. 2016. "Textile reinforced mortar versus FRP for confined concrete: Behaviour at elevated temperatures." *8th Int. Conf. Fibre-Reinf. Polym. FRP Compos. Civ. Eng. CICE 2016*.

Chowdhury, E. U., L. A. Bisby, M. F. Green, and V. K. R. Kodur. 2007. "Investigation of insulated FRP-wrapped reinforced concrete columns in fire." *Fire Saf. J.*, Structures in Fire, 42 (6): 452–460. https://doi.org/10.1016/j.firesaf.2006.10.007.

Codispoti, R., D. Oliveira, R. Olivito, P. Lourenco, and R. Fangueiro. 2015. "Mechanical performance of natural fiber-reinforced composites for the strengthening of masonry." *Compos. Part B Eng.*, 77. https://doi.org/10.1016/j.compositesb.2015.03.021.

Colombo, I., M. Colombo, A. Magri, G. Zani, and M. di Prisco. 2011. "Textile Reinforced Mortar at High Temperatures." *Appl. Mech. Mater.* Trans Tech Publications Ltd. Accessed July 6, 2020. /AMM.82.202.

Crisci, G., G. Ramaglia, G. P. Lignola, F. Fabbrocino, and A. Prota. 2020. "Effects of the Mortar Matrix on the Flexural Capacity of Masonry Cross Sections Strengthened with FRCM Materials." *Appl. Sci.*, 10 (21): 7908. Multidisciplinary Digital Publishing Institute. https://doi.org/10.3390/app10217908.

D'Ambrisi, A., L. Feo, and F. Focacci. 2013. "Experimental and analytical investigation on bond between Carbon-FRCM materials and masonry." *Compos. Part B Eng.*, 46: 15–20. https://doi.org/10.1016/j.compositesb.2012.10.018.

D&amp, J., apos, Anna, G. Amato, J. Chen, G. Minafo, and L. L. Mendola. 2020. "Effects of Different Test Setups on the Experimental Tensile Behaviour of Basalt Fibre Bidirectional Grids for FRCM Composites." *Fibers*, 8 (11): 1a–1a. MDPI AG. https://doi.org/10.3390/fib8110068.

D'Anna, J., G. Amato, J. F. Chen, G. Minafò, and L. La Mendola. 2021. "Experimental application of digital image correlation for the tensile characterization of basalt FRCM composites." *Constr. Build. Mater.*, 271: 121770. https://doi.org/10.1016/j.conbuildmat.2020.121770.

D'Antino, T., and C. (Corina) Papanicolaou. 2018. "Comparison between different tensile test set-ups for the mechanical characterization of inorganic-matrix composites." *Constr. Build. Mater.*, 171: 140–151. https://doi.org/10.1016/j.conbuildmat.2018.03.041.

De Santis, S., H. A. Hadad, F. De Caso y Basalo, G. de Felice, and A. Nanni. 2018. "Acceptance Criteria for Tensile Characterization of Fabric-Reinforced Cementitious Matrix Systems for Concrete and Masonry Repair." *J. Compos. Constr.*, 22 (6): 04018048. American Society of Civil Engineers. https://doi.org/10.1061/(ASCE)CC.1943-5614.0000886.

De Santis Stefano, Hadad Houman A., De Caso y Basalo Francisco, de Felice Gianmarco, and Nanni Antonio. 2018. "Acceptance Criteria for Tensile Characterization of Fabric-Reinforced Cementitious Matrix Systems for Concrete and Masonry Repair." *J. Compos. Constr.*, 22 (6): 04018048. American Society of Civil Engineers. https://doi.org/10.1061/(ASCE)CC.1943-5614.0000886.

Dong, J., Q. Wang, and Z. Guan. 2013. "Structural behaviour of RC beams with external flexural and flexural–shear strengthening by FRP sheets." *Compos. Part B Eng.*, 44 (1): 604–612. https://doi.org/10.1016/j.compositesb.2012.02.018.

Donnini, J., F. Bompadre, and V. Corinaldesi. 2020. "Tensile Behavior of a Glass FRCM System after Different Environmental Exposures." *Processes*, 8 (9): 1074. Multidisciplinary Digital Publishing Institute. https://doi.org/10.3390/pr8091074.

Donnini, J., G. Chiappini, G. Lancioni, and V. Corinaldesi. 2019a. "Tensile behaviour of glass FRCM systems with fabrics' overlap: Experimental results and numerical modeling." *Compos. Struct.*, 212: 398–411. https://doi.org/10.1016/j.compstruct.2019.01.053.

Donnini, J., and V. Corinaldesi. 2017a. "Mechanical characterization of different FRCM systems for structural reinforcement." https://doi.org/10.1016/J.CONBUILDMAT.2017.04.051.

Donnini, J., and V. Corinaldesi. 2017b. "Mechanical characterization of different FRCM systems for structural reinforcement." *Constr. Build. Mater.*, 145: 565–575. https://doi.org/10.1016/j.conbuildmat.2017.04.051.

Donnini, J., F. De Caso y Basalo, V. Corinaldesi, G. Lancioni, and A. Nanni. 2017. "Fabric-reinforced cementitious matrix behavior at high-temperature: Experimental and numerical results." *Compos. Part B Eng.*, 108: 108–121. https://doi.org/10.1016/j.compositesb.2016.10.004.

Donnini, J., S. Spagnuolo, and V. Corinaldesi. 2019b. "A comparison between the use of FRP, FRCM and HPM for concrete confinement." *Compos. Part B Eng.*, 160: 586–594. https://doi.org/10.1016/j.compositesb.2018.12.111.

Ehlig, D., and S. Hothan. 2011. "REINFORCED CONCRETE SLABS STRENGTHENED WITH TEXTILE REINFORCED CONCRETE SUBJECTED TO FIRE." Accessed October 31, 2021. https://www.semanticscholar.org/paper/REINFORCED-CONCRETE-SLABS-STRENGTHENED-WITH-TEXTILE-Ehlig-Hothan/af259761755668c3f61304cdf607a513ef80a6f8.

El Maaddawy, T., and A. El Refai. 2015. *Rehabilitation of corrosion-aged concrete T-girders with textile-reinforced mortar*.

Elghazy, M. 2018. "FRCM Composites For Strengthening Corrosion-Damaged Structures: Experimental & Numerical Investigations."

El-Maaddawy, T., and A. El Refai. 2016. “Innovative Repair of Severely Corroded T-Beams Using Fabric-Reinforced Cementitious Matrix.” *J. Compos. Constr.*, 20 (3): 04015073. American Society of Civil Engineers. https://doi.org/10.1061/(ASCE)CC.1943-5614.0000641.

Escrig, C., L. Gil, and E. Bernat. 2017. “Experimental comparison of reinforced concrete beams strengthened against bending with different types of cementitious-matrix composite materials.” *Constr. Build. Mater.*, 137: 317–329. https://doi.org/10.1016/j.conbuildmat.2017.01.106.

Feng, R., Y. Liu, J.-H. Zhu, and F. Xing. 2020a. “Flexural behaviour of C-FRCM strengthened corroded RC continuous beams.” *Compos. Struct.*, 245: 112200. https://doi.org/10.1016/j.compstruct.2020.112200.

Feng, R., J. Zhang, J.-H. Zhu, and F. Xing. 2020b. “Experimental study on the behavior of carbon-fabric reinforced cementitious matrix composites in impressed current cathodic protection.” *Constr. Build. Mater.*, 264: 120655. https://doi.org/10.1016/j.conbuildmat.2020.120655.

Firmo, J. P., J. R. Correia, and L. A. Bisby. 2015. “Fire behaviour of FRP-strengthened reinforced concrete structural elements: A state-of-the-art review.” *Compos. Part B Eng.*, 80: 198–216. https://doi.org/10.1016/j.compositesb.2015.05.045.

Focacci, F., T. D’Antino, and C. Carloni. 2020. “The role of the fiber–matrix interfacial properties on the tensile behavior of FRCM coupons.” *Constr. Build. Mater.*, 265: 120263. https://doi.org/10.1016/j.conbuildmat.2020.120263.

Gonzalez-Libreros, J. H., L. H. Sneed, T. D’Antino, and C. Pellegrino. 2017. “Behavior of RC beams strengthened in shear with FRP and FRCM composites.” *Eng. Struct.*, 150: 830–842. https://doi.org/10.1016/j.engstruct.2017.07.084.

Górszczyk, J., K. Malicki, and T. Zych. 2019. “Application of Digital Image Correlation (DIC) Method for Road Material Testing.” *Materials*, 12 (15). https://doi.org/10.3390/ma12152349.

Green, M. F., L. A. Bisby, A. Z. Fam, and V. K. R. Kodur. 2006. “FRP confined concrete columns: Behaviour under extreme conditions.” *Cem. Concr. Compos.*, Durability and Ductility of FRP Strengthened Beams, Slabs and Columns, 28 (10): 928–937. https://doi.org/10.1016/j.cemconcomp.2006.07.008.

Grzymski, F., T. Trapko, and M. Musiał. 2019. “Performance of GFRP bar anchored PBO-FRCM composite on one-way RC slabs under flexure.” *IOP Conf. Ser. Mater. Sci. Eng.*, 652: 012020. https://doi.org/10.1088/1757-899X/652/1/012020.

Hojdys, Ł., and P. Krajewski. 2021. “Tensile Behaviour of FRCM Composites for Strengthening of Masonry Structures—An Experimental Investigation.” *Materials*, 14 (13): 3626. Multidisciplinary Digital Publishing Institute. https://doi.org/10.3390/ma14133626.

Iorfida, A., S. Candamano, F. Crea, L. Ombres, S. Verre, and P. Fazio. 2019. “Bond Behaviour of FRCM Composites: Effects of High Temperature.” *Key Eng. Mater.*, 817: 161–166. https://doi.org/10.4028/www.scientific.net/KEM.817.161.

Ismail, N., T. El Maaddawy, N. Khattak, and N. Amanullah. 2018a. “In-Plane Shear Strength Improvement of Hollow Concrete Masonry Panels Using a Fabric-Reinforced Cementitious Matrix.” *J. Compos. Constr.*, 22. https://doi.org/10.1061/(ASCE)CC.1943-5614.0000835.

Ismail, N., T. El-Maaddawy, N. Khattak, and A. Najmal. 2018b. “In-Plane Shear Strength Improvement of Hollow Concrete Masonry Panels Using a Fabric-Reinforced

Cementitious Matrix." *J. Compos. Constr.*, 22 (2): 04018004. American Society of Civil Engineers. https://doi.org/10.1061/(ASCE)CC.1943-5614.0000835.
Jabr, A., A. El-Ragaby, and F. Ghrib. 2017a. "Effect of the Fiber Type and Axial Stiffness of FRCM on the Flexural Strengthening of RC Beams." https://doi.org/10.3390/FIB5010002.
Jabr, A., A. El-Ragaby, and F. Ghrib. 2017b. "Effect of the Fiber Type and Axial Stiffness of FRCM on the Flexural Strengthening of RC Beams." *Fibers*, 5: 2. https://doi.org/10.3390/fib5010002.
Jung, H. 2020. "Blast Retrofit of Unreinforced Masonry Walls Using Fabric Reinforced Cementitious Matrix (FRCM) Composites." Thesis. Université d'Ottawa / University of Ottawa.
Kashwani, G. A., and A. K. Al-Tamimi. 2014. "Evaluation of FRP Bars Performance under High Temperature." *Phys. Procedia*, 8th International Conference on Material Sciences, CSM8-ISM5, 55: 296–300. https://doi.org/10.1016/j.phpro.2014.07.043.
Koutas, L. N., and D. A. Bournas. 2017. "Flexural Strengthening of Two-Way RC Slabs with Textile-Reinforced Mortar: Experimental Investigation and Design Equations." *J. Compos. Constr.*, 21 (1): 04016065. American Society of Civil Engineers. https://doi.org/10.1061/(ASCE)CC.1943-5614.0000713.
Koutas, L. N., Z. Tetta, D. A. Bournas, and T. C. Triantafillou. 2019. "Strengthening of Concrete Structures with Textile Reinforced Mortars: State-of-the-Art Review." *J. Compos. Constr.*, 23 (1): 03118001. American Society of Civil Engineers. https://doi.org/10.1061/(ASCE)CC.1943-5614.0000882.
Koutas Lampros N., Tetta Zoi, Bournas Dionysios A., and Triantafillou Thanasis C. 2019. "Strengthening of Concrete Structures with Textile Reinforced Mortars: State-of-the-Art Review." *J. Compos. Constr.*, 23 (1): 03118001. American Society of Civil Engineers. https://doi.org/10.1061/(ASCE)CC.1943-5614.0000882.
LaHood, F. T. S. R. n.d. "10 Years After Bridge Collapse, America Is Still Crumbling." *NPR.org*. Accessed January 25, 2021. https://www.npr.org/2017/08/01/540669701/10-years-after-bridge-collapse-america-is-still-crumbling.
Larbi, A. S., R. Contamine, E. Ferrier, and P. Hamelin. 2010. "Shear strengthening of RC beams with textile reinforced concrete (TRC) plate." *Constr. Build. Mater.*, 24 (10): 1928–1937. Elsevier B.V. https://doi.org/10.1016/j.conbuildmat.2010.04.008.
Lee, S., K. Hong, Y. Yeon, and K. Jung. 2018. "Flexural Behavior of RC Slabs Strengthened in Flexure with Basalt Fabric-Reinforced Cementitious Matrix." *Adv. Mater. Sci. Eng.*, 2018. Hindawi Limited. https://doi.org/10.1155/2018/2982784.
Loreto, G., S. Babaeidarabad, L. Leardini, and A. Nanni. 2015. "RC beams shear-strengthened with fabric-reinforced-cementitious-matrix (FRCM) composite." *Int. J. Adv. Struct. Eng. IJASE*, 7 (4): 341–352. https://doi.org/10.1007/s40091-015-0102-9.
Loreto, G., L. Leardini, D. Arboleda, and A. Nanni. 2014. "Performance of RC Slab-Type Elements Strengthened with Fabric-Reinforced Cementitious-Matrix Composites." *J. Compos. Constr.*, 18 (3): A4013003. American Society of Civil Engineers. https://doi.org/10.1061/(ASCE)CC.1943-5614.0000415.
Ma, C.-K., N. M. Apandi, C. S. Y. Sofrie, J. H. Ng, W. H. Lo, A. Z. Awang, and W. Omar. 2017. "Repair and rehabilitation of concrete structures using confinement: A review." *Constr. Build. Mater.*, 133: 502–515. https://doi.org/10.1016/j.conbuildmat.2016.12.100.

Marcinczak, D., T. Trapko, and M. Musiał. 2019. “Shear strengthening of reinforced concrete beams with PBO-FRCM composites with anchorage.” *Compos. Part B Eng.*, 158: 149–161. https://doi.org/10.1016/j.compositesb.2018.09.061.

Maroudas, S. R., and C. C. G. Papanicolaou. 2017. “Effect of High Temperatures on the TRM-to-Masonry Bond.” *Key Eng. Mater.*, 747: 533–541. https://doi.org/10.4028/www.scientific.net/KEM.747.533.

Mercedes, L., E. Bernat-Maso, and L. Gil. 2021. “Flexural failure of fabric reinforced cementitious mortar (FRCM) plates under punctual loads: Experimental test, analytical approach and numerical simulation.” *Constr. Build. Mater.*, 272: 121651. https://doi.org/10.1016/j.conbuildmat.2020.121651.

Michels, J., and M. Motavalli. 2013. “Strength evolution after high temperature exposure of coated carbon fiber rovings used for a fiber-reinforced cementitious matrix (FRCM).” (6 pp.).

Michels, J., D. Zwicky, J. Scherer, Y. Harmanci, and M. Motavalli. 2014. “Structural Strengthening of Concrete with Fiber Reinforced Cementitious Matrix (FRCM) at Ambient and Elevated Temperature – Recent Investigations in Switzerland.” *Adv. Struct. Eng.*, 17. https://doi.org/10.1260/1369-4332.17.12.1785.

Nanni, A. n.d. “A New Tool for Concrete and Masonry Repair.” 8.

Napoli, A., and R. Realfonzo. 2020. “Compressive strength of concrete confined with fabric reinforced cementitious matrix (FRCM): Analytical models.” *Compos. Part C Open Access*, 2: 100032. https://doi.org/10.1016/j.jcomc.2020.100032.

Narayanan, S. 2008. “I-35W Mississippi river bridge failure - Is it a wake up call?” 82: 29–38.

Ombres, L., P. Mazzuca, and S. Verre. 2022. “Effects of Thermal Conditioning at High Temperatures on the Response of Concrete Elements Confined with a PBO-FRCM Composite System.” *J. Mater. Civ. Eng.*, 34 (1): 04021413. American Society of Civil Engineers. https://doi.org/10.1061/(ASCE)MT.1943-5533.0004053.

Ombres, L., and S. Verre. 2015. “Structural behaviour of fabric reinforced cementitious matrix (FRCM) strengthened concrete columns under eccentric loading.” *Compos. Part B Eng.*, 75: 235–249. https://doi.org/10.1016/j.compositesb.2015.01.042.

Palmieri, A., S. Matthys, and L. Taerwe. 2013. “Fire Endurance and Residual Strength of Insulated Concrete Beams Strengthened with Near-Surface Mounted Reinforcement.” *J. Compos. Constr.*, 17 (4): 454–462. American Society of Civil Engineers. https://doi.org/10.1061/(ASCE)CC.1943-5614.0000338.

Pantelides, C. P., Y. Okahashi, and L. D. Reaveley. 2008. “Seismic Rehabilitation of Reinforced Concrete Frame Interior Beam-Column Joints with FRP Composites.” *J. Compos. Constr.*, 12 (4): 435–445. American Society of Civil Engineers. https://doi.org/10.1061/(ASCE)1090-0268(2008)12:4(435).

Parisi, F., C. Menna, and A. Prota. 2019. “10 - Fabric-Reinforced Cementitious Matrix (FRCM) composites: Mechanical behavior and application to masonry walls.” *Fail. Anal. Biocomposites Fibre-Reinf. Compos. Hybrid Compos.*, Woodhead Publishing Series in Composites Science and Engineering, M. Jawaid, M. Thariq, and N. Saba, eds., 199–227. Woodhead Publishing.

Park, S.-H., N. H. Dinh, J.-W. Um, and K.-K. Choi. 2021. “Experimental study on the seismic performance of RC columns retrofitted by lap-spliced textile-reinforced mortar jackets after high-temperature exposure.” *Compos. Struct.*, 256: 113108. https://doi.org/10.1016/j.compstruct.2020.113108.

Peled, A. 2007. “Pre-tensioning of fabrics in cement-based composites.” *Cem. Concr. Res.*, 37 (5): 805–813. https://doi.org/10.1016/j.cemconres.2007.02.010.
Peled, A., and A. Bentur. 2000. “Geometrical characteristics and efficiency of textile fabrics for reinforcing cement composites.” *Cem. Concr. Res.*, 30 (5): 781–790. https://doi.org/10.1016/S0008-8846(00)00239-8.
Peled, A., A. Bentur, and D. Yankelevsky. 1998. “Effects of Woven Fabric Geometry on the Bonding Performance of Cementitious Composites: Mechanical Performance.” *Adv. Cem. Based Mater.*, 7 (1): 20–27. https://doi.org/10.1016/S1065-7355(97)00012-6.
Pino, V., H. Akbari Hadad, F. De Caso y Basalo, A. Nanni, U. Ali Ebead, and A. El Refai. 2017. “Performance of FRCM-Strengthened RC Beams Subject to Fatigue.” *J. Bridge Eng.*, 22 (10): 04017079. American Society of Civil Engineers. https://doi.org/10.1061/(ASCE)BE.1943-5592.0001107.
Pohoryles, D. A., J. Melo, T. Rossetto, M. Fabian, C. McCague, K. Stavrianaki, B. Lishman, and B. Sargeant. 2017. “Use of DIC and AE for Monitoring Effective Strain and Debonding in FRP and FRCM-Retrofitted RC Beams.” *J. Compos. Constr.*, 21 (1): 04016057. American Society of Civil Engineers. https://doi.org/10.1061/(ASCE)CC.1943-5614.0000715.
Raoof, S. M., and D. A. Bournas. 2017a. “Bond between TRM versus FRP composites and concrete at high temperatures.” *Compos. Part B Eng.*, 127: 150–165. https://doi.org/10.1016/j.compositesb.2017.05.064.
Raoof, S. M., and D. A. Bournas. 2017b. “TRM versus FRP in flexural strengthening of RC beams: Behaviour at high temperatures.” *Constr. Build. Mater.*, 154: 424–437. https://doi.org/10.1016/j.conbuildmat.2017.07.195.
Spagnuolo, S., A. Meda, Z. Rinaldi, and A. Nanni. 2018. *Residual behaviour of glass FRP bars subjected to high temperatures. Compos. Struct.*
Sui, Z.-A., K. Dong, J. Jiang, S. Yang, and K. Hu. 2020. “Flexural Behavior of Fire-Damaged Prefabricated RC Hollow Slabs Strengthened with CFRP versus TRM.” *Materials*, 13 (11): 2556. Multidisciplinary Digital Publishing Institute. https://doi.org/10.3390/ma13112556.
Team, A. T. S.-T. B. 2018. “Five FRP Advantages for Contractors and Structure Owners.” *Build. Strong*. Accessed May 19, 2021. https://blog.strongtie.com/five-frp-advantages-contractors-structure-owners/.
Team, A. T. S.-T. B. 2019. “FRCM – An Alternative to Shotcrete for Structural Repair and Strengthening of Concrete.” *Build. Strong*. Accessed May 19, 2021. https://blog.strongtie.com/frcm-an-alternative-to-shotcrete-for-structural-repair-and-strengthening-of-concrete/.
Tello, N., Y. Alhoubi, F. Abed, A. El Refai, and T. El-Maaddawy. 2021. “Circular and square columns strengthened with FRCM under concentric load.” *Compos. Struct.*, 255: 113000. https://doi.org/10.1016/j.compstruct.2020.113000.
Tetta, Z. C., and D. A. Bournas. 2016. “TRM vs FRP jacketing in shear strengthening of concrete members subjected to high temperatures.” *Compos. Part B Eng.*, 106: 190–205. https://doi.org/10.1016/j.compositesb.2016.09.026.
Toska, K., F. Faleschini, M. A. Zanini, L. Hofer, and C. Pellegrino. 2021. “Repair of severely damaged RC columns through FRCM composites.” *Constr. Build. Mater.*, 273: 121739. https://doi.org/10.1016/j.conbuildmat.2020.121739.

Tran, M. T., X. H. Vu, and E. Ferrier. 2020. “Mesoscale numerical modeling and characterization of the effect of reinforcement textile on the elevated temperature and tensile behaviour of carbon textile-reinforced concrete composite.” *Fire Saf. J.*, 116: 103186. https://doi.org/10.1016/j.firesaf.2020.103186.

Trapko, T. 2013. “The effect of high temperature on the performance of CFRP and FRCM confined concrete elements.” *Compos. Part B Eng.*, 54: 138–145. https://doi.org/10.1016/j.compositesb.2013.05.016.

Trapko, T., D. Urbańska, and M. Kamiński. 2015. “Shear strengthening of reinforced concrete beams with PBO-FRCM composites.” *Compos. Part B Eng.*, 80: 63–72. https://doi.org/10.1016/j.compositesb.2015.05.024.

Truong, G. T., S.-H. Park, and K.-K. Choi. 2019. “Tensile Behaviors of Lap-Spliced Carbon Fiber-Textile Reinforced Mortar Composites Exposed to High Temperature.” *Materials*, 12 (9): 1512. Multidisciplinary Digital Publishing Institute. https://doi.org/10.3390/ma12091512.

Tsesarsky, M., A. Peled, A. Katz, and I. Anteby. 2013. “Strengthening concrete elements by confinement within textile reinforced concrete (TRC) shells – Static and impact properties.” *Constr. Build. Mater.*, 44: 514–523. https://doi.org/10.1016/j.conbuildmat.2013.03.031.

User, S. n.d. “Fire Damage of Concrete Structures – Assessment and Repair.” Accessed May 19, 2021. https://www.nbmcw.com/product-solutions/concrete-chemicals-waterproofing-repairs/repairs-rehabilitation/fire-damage-of-concrete-structures-assessment-and-repair.html.

Wakjira, T. G., M. Afzal, and U. Ebead. 2018. “Efficacy of FRCM systems in flexural strengthening of RC T-beams.” *IOP Conf. Ser. Mater. Sci. Eng.*, 431: 072007. https://doi.org/10.1088/1757-899X/431/7/072007.

Wakjira, T. G., and U. Ebead. 2018. “Hybrid NSE/EB technique for shear strengthening of reinforced concrete beams using FRCM: Experimental study.” *Constr. Build. Mater.*, 164: 164–177. https://doi.org/10.1016/j.conbuildmat.2017.12.224.

Wakjira, T. G., and U. Ebead. 2019. “Internal transverse reinforcement configuration effect of EB/NSE-FRCM shear strengthening of RC deep beams.” *Compos. Part B Eng.*, 166: 758–772. https://doi.org/10.1016/j.compositesb.2019.03.004.

Wang, X., C. C. Lam, B. C. Sun, T. Noguchi, and V. P. Iu. 2020. “Effect of curing environment on the tensile behaviour of FRCM composites.” *Constr. Build. Mater.*, 238: 117729. https://doi.org/10.1016/j.conbuildmat.2019.117729.

Wei, L.-L., J.-H. Zhu, T. Ueda, M.-N. Su, J. Liu, W. Liu, L.-P. Tang, and F. Xing. 2020. “Tensile behaviour of carbon fabric reinforced cementitious matrix composites as both strengthening and anode materials.” *Compos. Struct.*, 234: 111675. https://doi.org/10.1016/j.compstruct.2019.111675.

Xu, S., L. Shen, J. Wang, and Y. Fu. 2014. “High temperature mechanical performance and micro interfacial adhesive failure of textile reinforced concrete thin-plate.” *J. Zhejiang Univ. Sci. A*, 15: 31–38. https://doi.org/10.1631/jzus.A1300150.

Yaqub, M., and C. G. Bailey. 2011. “Repair of fire damaged circular reinforced concrete columns with FRP composites.” *Constr. Build. Mater.*, 25 (1): 359–370. https://doi.org/10.1016/j.conbuildmat.2010.06.017.

Younis, A., and U. Ebead. 2018. “Characterization and application of FRCM as a strengthening material for shear-critical RC beams.” *MATEC Web Conf.*, (M. G. Alexander, H.

Beushausen, F. Dehn, and P. Moyo, eds.), 199: 09004. https://doi.org/10.1051/matecconf/201819909004.
Younis, A., U. Ebead, and K. Shrestha. 2020. “Tensile characterization of multi-ply fabric-reinforced cementitious matrix strengthening systems.” *Struct. Concr.*, 21 (2): 713–723. https://doi.org/10.1002/suco.201900076.
Younis, A., U. Ebead, and K. C. Shrestha. 2017. “Different FRCM systems for shear-strengthening of reinforced concrete beams.” *Constr. Build. Mater.*, 153: 514–526. https://doi.org/10.1016/j.conbuildmat.2017.07.132.
https://www.ruregold.com/product/c-mesh-182/

https://www.sandberg.co.uk/site/inspection/fire-damaged-concrete/

https://www.sika.com/en/construction/structural-strengthening.html

https://www.strongtie.com/

ACI 549.4R-20

https://www.astm.org/

8 APPENDIX

In this section the stress-strain curves of specimens are demonstrated. Each type of test based on the variables was conducted with three repetitions. In this section, all three curves are demonstrated in a graph for 60 specimens.

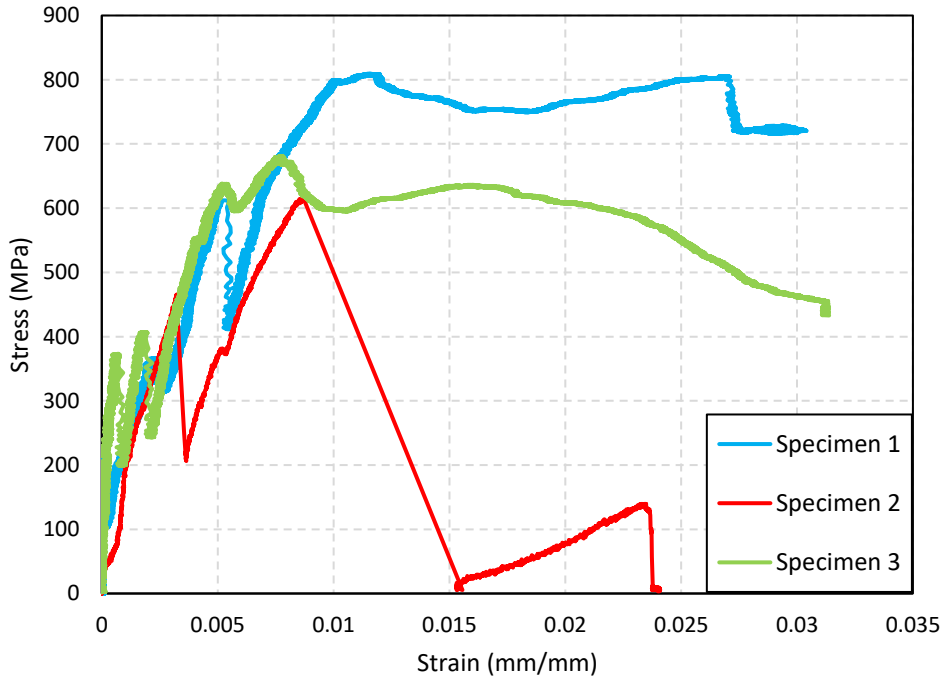

Figure 8-1: Stress-strain diagram for unidirectional one-layered specimens at ambient temperature.

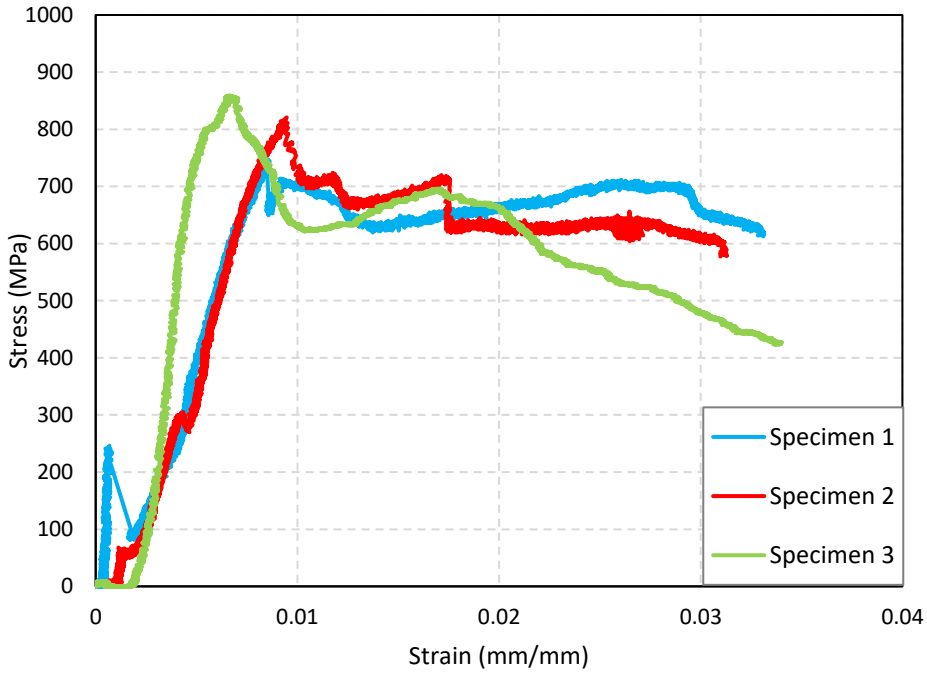

Figure 8-2: Stress-strain diagram for unidirectional one-layered specimens at 100°C temperature.

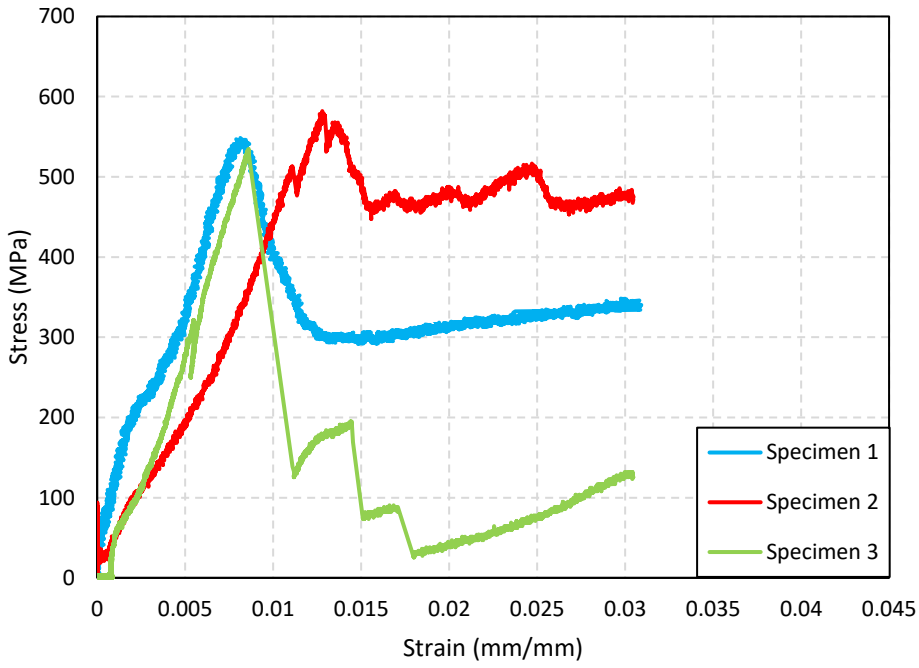

Figure 8-3: Stress-strain diagram for unidirectional one-layered specimens at 200°C temperature.

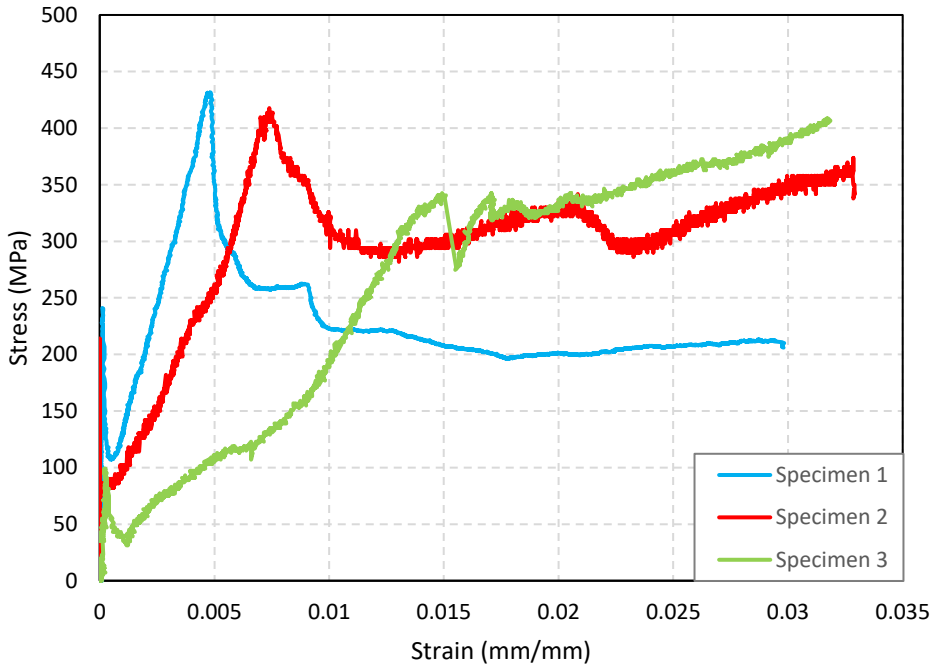

Figure 8-4: Stress-strain diagram for unidirectional one-layered specimens at 300°C temperature.

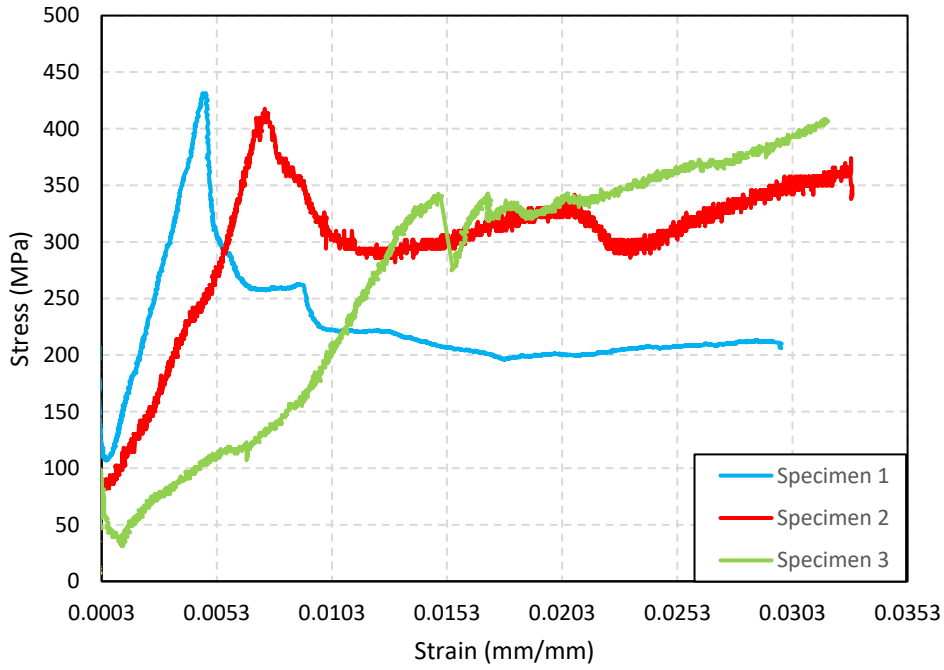

Figure 8-5: Stress-strain diagram for unidirectional one-layered specimens at 400°C temperature.

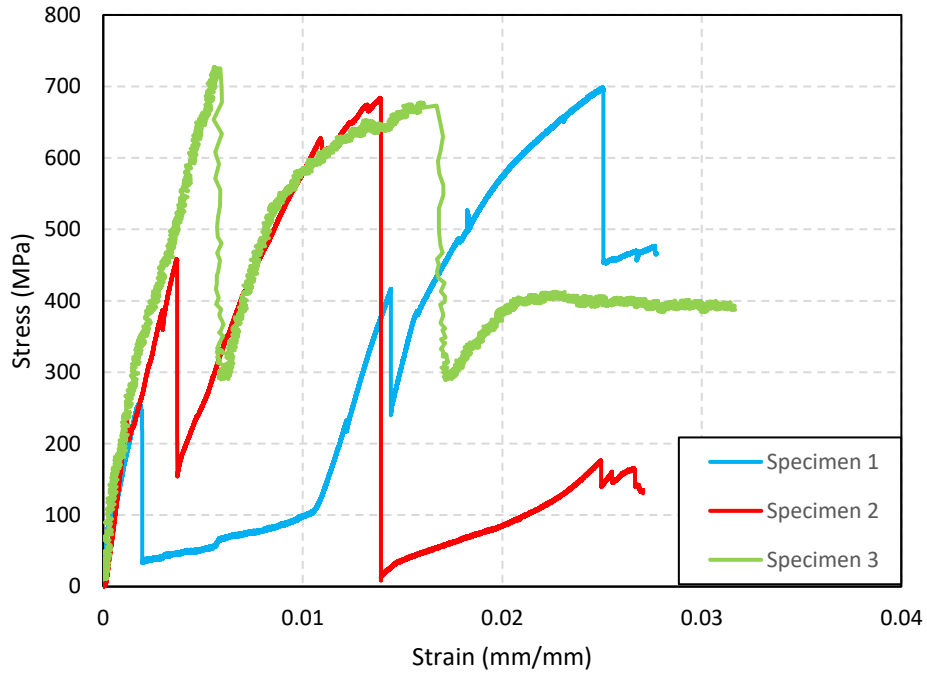

Figure 8-6: Stress-strain diagram for unidirectional two-layered specimens at ambient temperature.

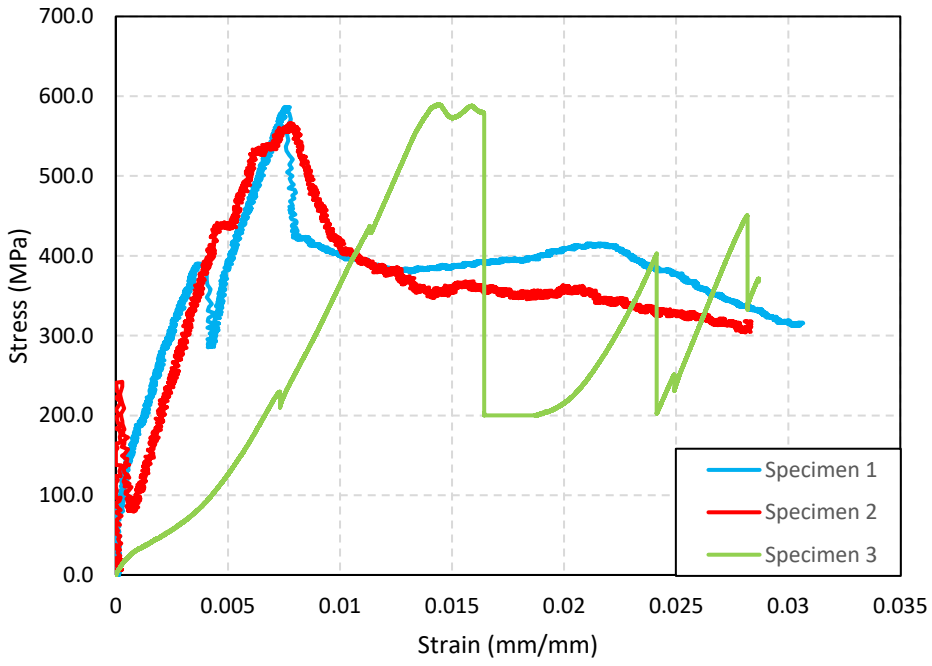

Figure 8-7: Stress-strain diagram for unidirectional two-layered specimens at 100°C temperature.

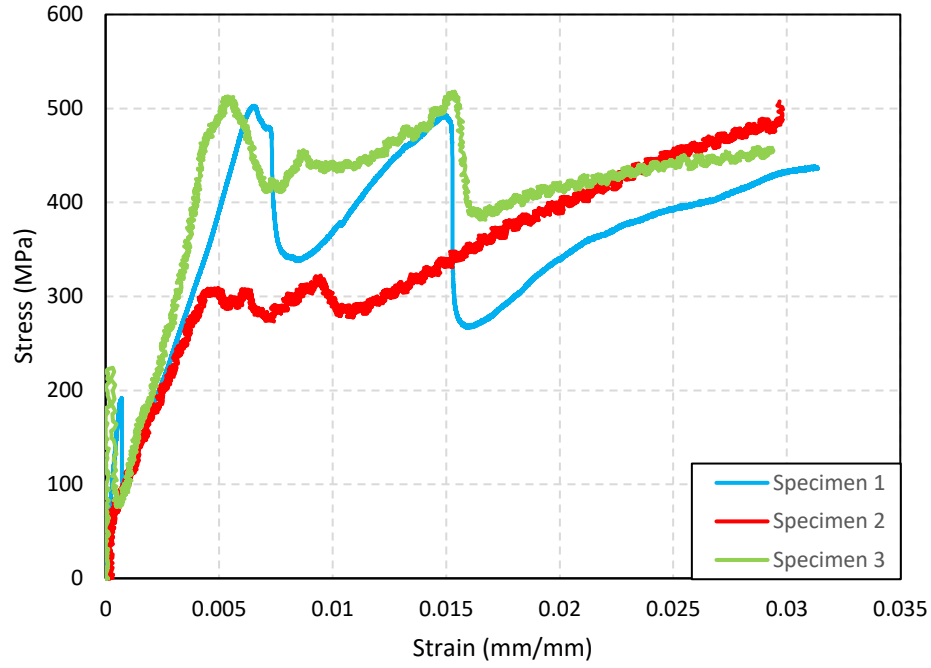

Figure 8-8: Stress-strain diagram for unidirectional two-layered specimens at 200°C temperature.

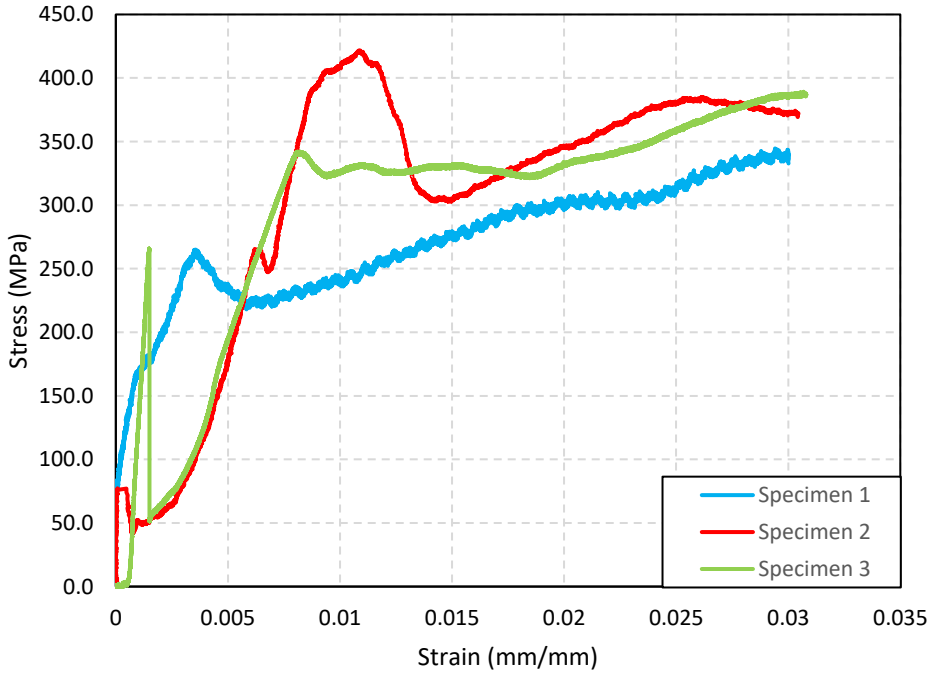

Figure 8-9: Stress-strain diagram for unidirectional two-layered specimens at 300°C temperature.

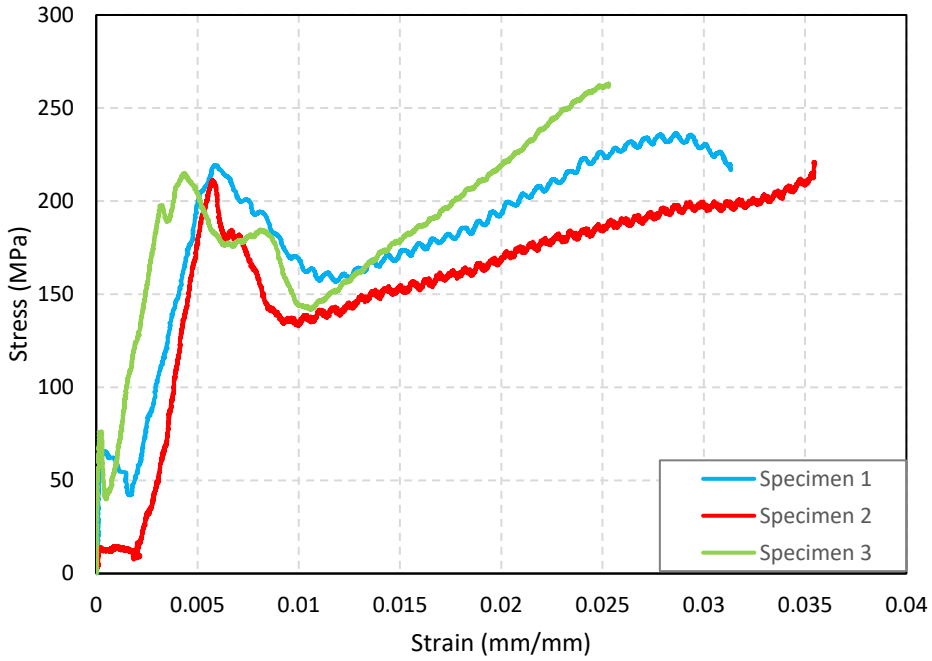

Figure 8-10: Stress-strain diagram for unidirectional two-layered specimens at 400°C temperature.

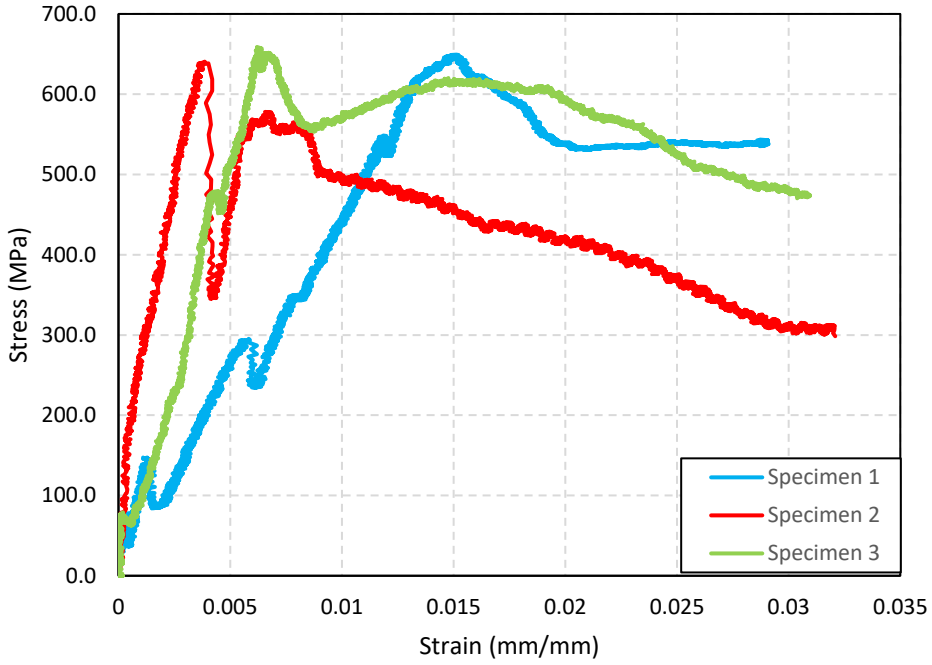

Figure 8-11: Stress-strain diagram for unidirectional three-layered specimens at ambient temperature.

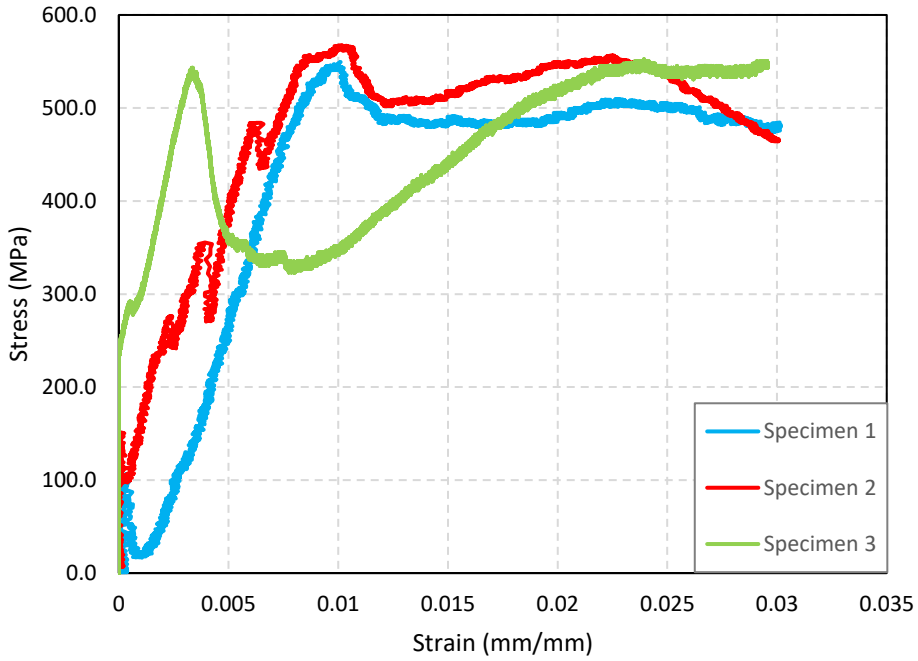

Figure 8-12: Stress-strain diagram for unidirectional three-layered specimens at 100°C temperature.

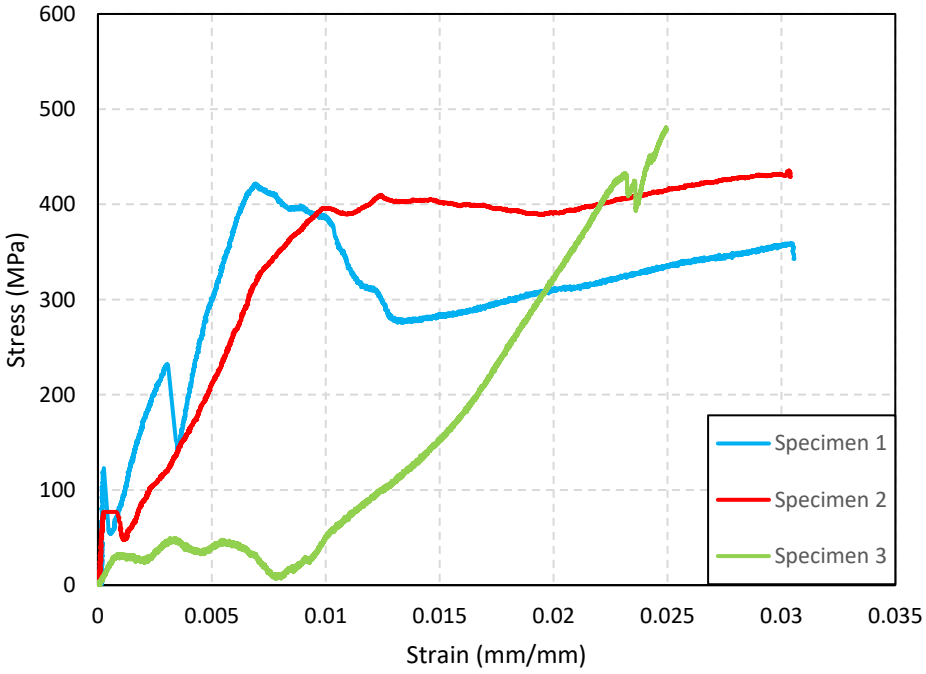

Figure 8-13: Stress-strain diagram for unidirectional three-layered specimens at 200°C temperature.

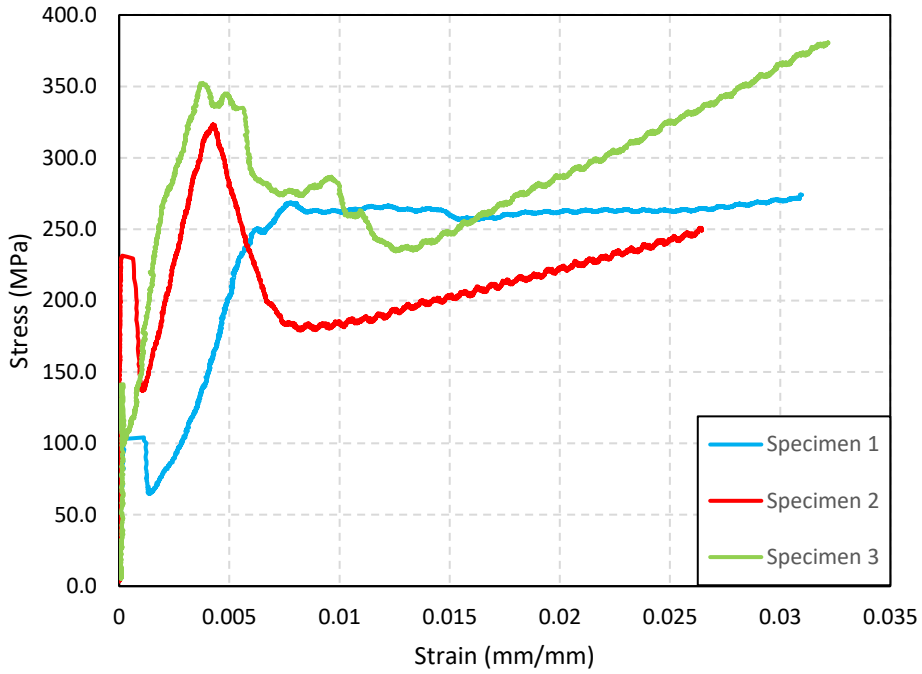

Figure 8-14: Stress-strain diagram for unidirectional three-layered specimens at 300°C temperature.

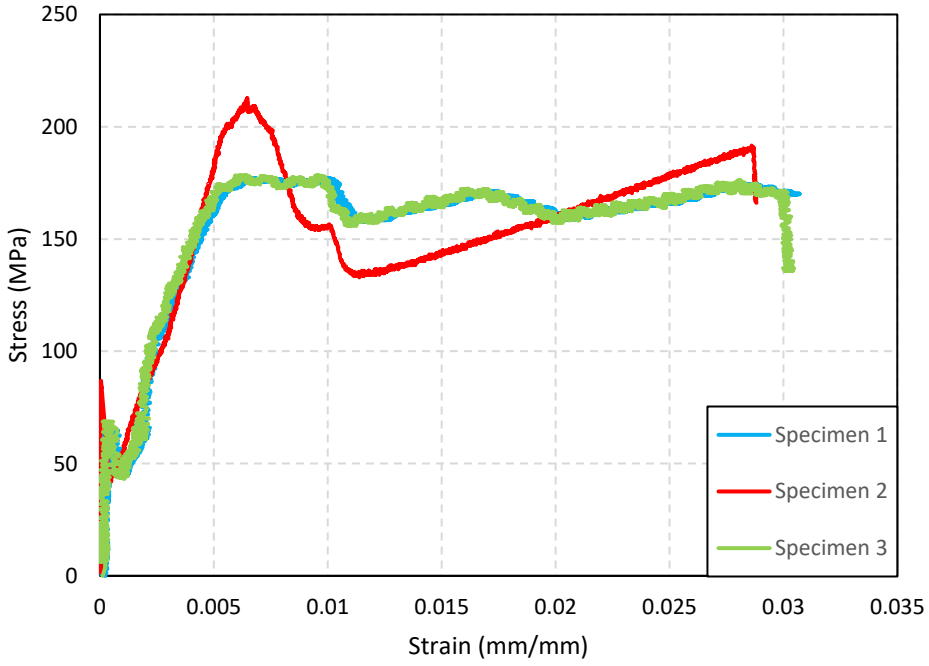

Figure 8-15: Stress-strain diagram for unidirectional three-layered specimens at 400°C temperature.

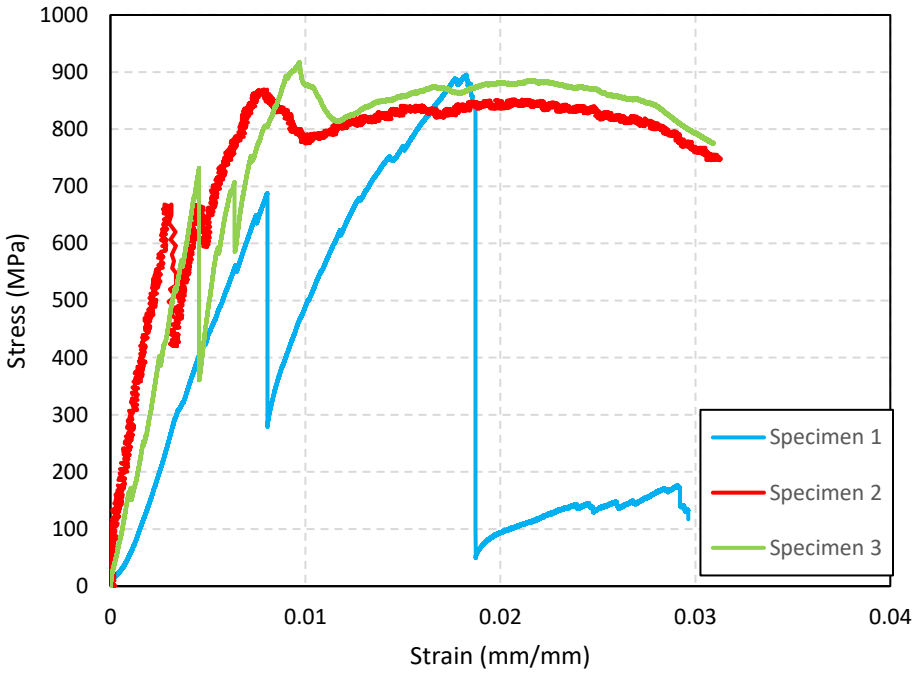

Figure 8-16: Stress-strain diagram for bidirectional one-layered specimens at ambient temperature.

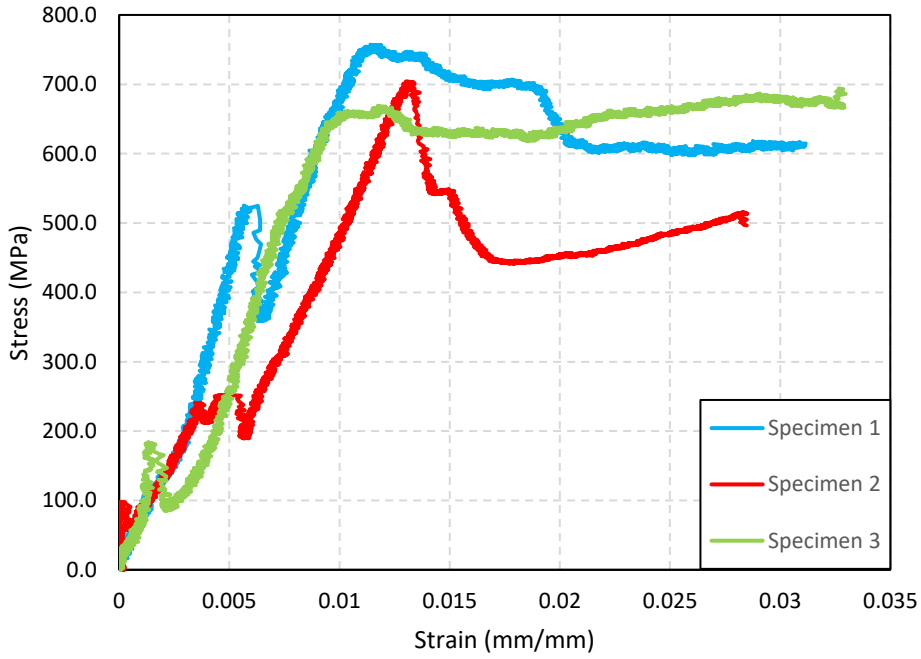

Figure 8-17: Stress-strain diagram for bidirectional one-layered specimens at 100°C temperature.

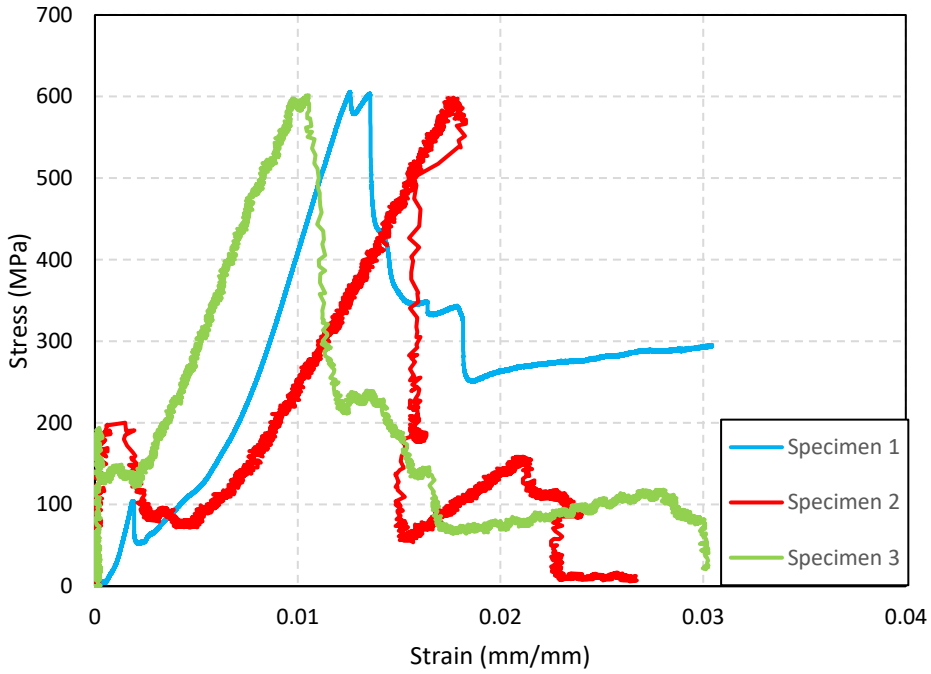

Figure 8-18: Stress-strain diagram for bidirectional one-layered specimens at 200°C temperature.

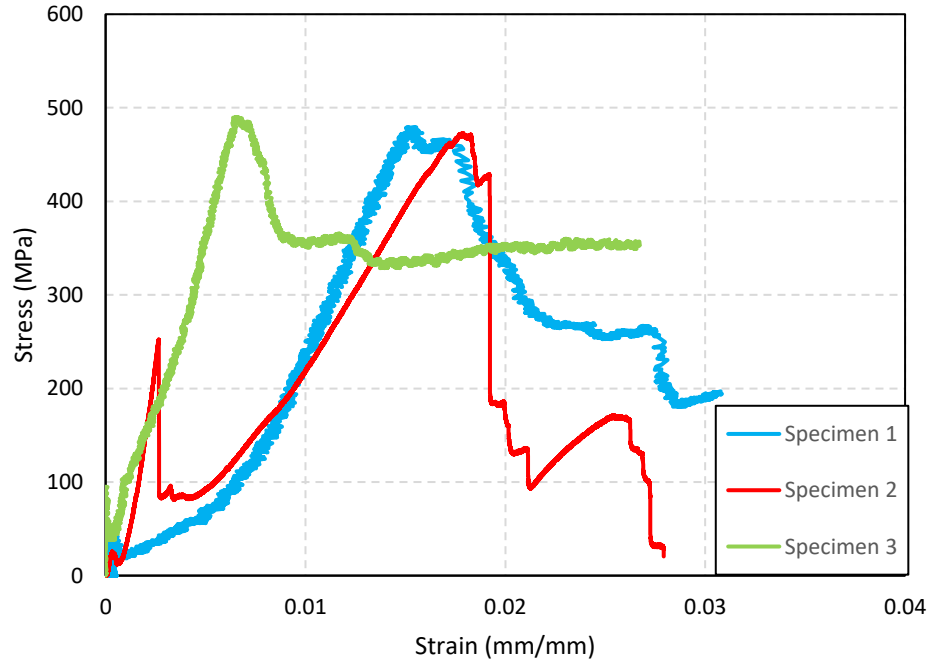

Figure 8-19: Stress-strain diagram for bidirectional one-layered specimens at 300°C temperature.

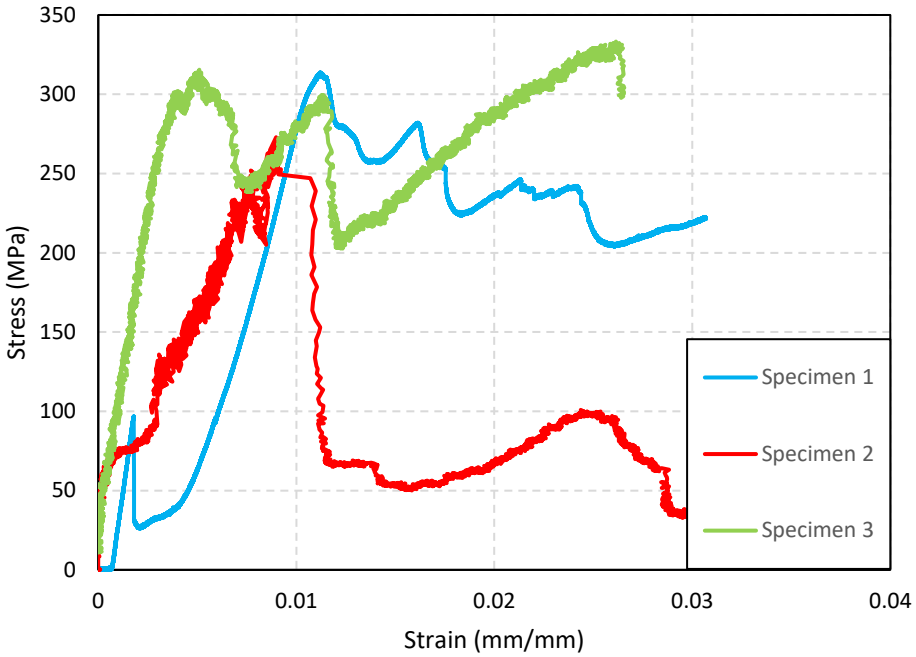

Figure 8-20: Stress-strain diagram for bidirectional one-layered specimens at 400°C temperature.

The failure modes that specimens experienced are also shown in the following figures:

Figure 8-21: Failure modes of specimens, from left to right: slippage of fabric and debonding at fabric and matrix interface.